High-Throughput Manufacturing of Portable Plastic Pneumatic Logic Circuits for Integrated Microfluidic Control

Vidhya Balaji

A thesis submitted in partial fulfillment of the requirements for the degree of

Master of Science in Electrical Engineering

University of Washington

2017

Committee:

Albert Folch

Karl F. Bohringer

Program Authorized to Offer Degree:

Electrical Engineering

University of Washington
Abstract

High-Throughput Manufacturing of Portable Plastic Pneumatic Logic Circuits for Integrated Microfluidic Control

Vidhya Balaji

Chair of the Supervisory Committee:
Associate Professor Dr. Albert Folch
Bioengineering

Microfluidic technology has advanced biological research and medical diagnostics by enabling large-scale parallelization and integration of multiple processes within small areas. Active microfluidic circuits have components such as valves and pumps which need to function in a highly integrated manner in full analytical systems. However, there exists a limitation in size and functionality caused by the complexity and cost of external hardware control. Autonomous microfluidic systems aim to deliver the results of complex multi-step bioassays without external controls or energy input. Embedded control enables the devices to autonomously execute pre-programmed operations and makes scalability of design easier.

Analogous to the electronic microprocessor, microfluidic control consists of components that execute combinational logic such as multiplexers and sequential logic such as counters. Synchronization between these blocks is achieved by a timing reference such as an oscillator that generates a clock at a specific frequency. This research examines the manufacturing of a pneumatic oscillator in a ring configuration using a popular family of plastics used in microfluidics, acrylics. PMMA is one such acrylic with amenable properties available in varying thicknesses and used to fabricate microfluidic devices for various applications. The first part of the research explores the different techniques used to manufacture single pneumatic membrane

valves and oscillator circuits made from them. Limitations and challenges faced with two specific methods, hot embossing and CNC milling are explained.

The second part of the research focusses on the third manufacturing technique, laser engraving, which successfully produced functional devices. The development of a bonding technique of the membrane material, poly-dimethyl siloxane (PDMS) with PMMA is also discussed as part of the assembly process. Test results with a portable pneumatic source, a syringe, showed the utility of the device for portable microfluidics. Circuits made with valves driven using the oscillator output as a control signal demonstrated the repeatability and scalability of the device fabrication process.

Manufacturing microfluidic logic circuits in a large scale requires techniques that can reduce the turnaround time between prototype and production. This research develops such a fabrication process, from manufacturing of layers to assembly, to produce functional devices that are useful for portable microfluidic applications.

Acknowledgements

"Arise, Awake and Stop not until the goal is reached." (Swami Vivekananda) – the motto responsible for the successful completion of this research. There are so many people I need to thank for guiding and supporting me to achieve my objectives. I am thankful to Prof. Albert Folch for introducing me to the beauty of microfluidics and encouraging me to excel. This work is a product of his vision. I am greatly indebted to Dr. Karl F. Bohringer for his guidance and support. Dr. Nirveek Bhattacharjee has been a valuable mentor and a huge resource for ideas. I acknowledge Dr. Cesar Parra's guidance in introducing me to 3D printing in the lab. I am thankful to Kurt Castro for laser engraving designs. Yuan-Sheng and Yong-Tae Kim have helped me in 3D printing and suggestions for valve functionality respectively. The discussions I had with Lisa Horowitz, Adan Rodriguez and Alex Kuo have been of assistance in my work. I also cannot forget Amit Karkamkar's help in learning Inventor and other tips.

The use of WNF and MAF for profilometer measurements are acknowledged. Prof. Sawyer Fuller's AIR lab has also provided immense help for my hot embossing experiments. I thank him and his students for their assistance. Makerspace personnel have helped me in CNC milling. The financial support through research and teaching assistantship from University of Washington is also acknowledged as well as the encouragement and guidance received from graduate advising.

I wouldn't have completed this project without the source of my strength and motivation, my dear 6-year-old son. I thank my wonderful husband for his belief in me and support. My parents have always encouraged me to keep learning for which I am indebted to them. Above all, I am grateful to Eeshwar, for His benevolent grace!

Table of Contents

List of Figures

List of Tables

List of Nomenclature

Symbol	Section first used in	Description
ELISA	1.2	Enzyme-linked immunosorbent assay
MOSFET	1.2	Metal oxide semiconductor field effect transistor
NC	1.2	Normally closed
PDMS	1.3	Poly-dimethyl siloxane
T_g	1.3.2	Glass transition temperature
PMMA	1.5.2	Polymethyl methacrylate
APTES	2.3	Aminopropyltriethoxysilane
IPA	3.4	Isopropyl alcohol
T_D	5.1	Time delay of each stage in a ring oscillator
Rp	5.4.1	Pull-up fluidic resistance
τ	5.4.1	Time period of oscillations

1. Microfluidic devices for integrated digital control logic

1.1 Introduction

Microfluidic devices that are used for different functionalities analogous to macroscale fluidic counterparts include valves, pumps and mixers. These devices have been developed both as passive and active devices. For example, there are passive microvalves that are operated using the pressure of the fluid for activation. An active valve is excited using an external signal which gives it the advantage of being independently controlled. Considerable research effort has been invested in integrating a large number of active microfluidic components on a smaller area, thus enabling multiple analysis to be performed on a single chip[1].

The drawback of the high degree of parallelism that has been achieved is the large increase in the number of external connections associated with the control operations of the numerous valves. Integration of self-driven control elements on-chip obviates the need for external control, thereby making portable microfluidic devices a possibility. Microfluidic logic circuits and quasi-processors have been demonstrated using valves and channels. However, it is challenging to manufacture larger circuits both in terms of time and process complexity. Therefore, the current need is to focus on manufacturing techniques that will make the process of creating devices more economic and simpler.

1.2 Pneumatic circuits for digital logic control operations

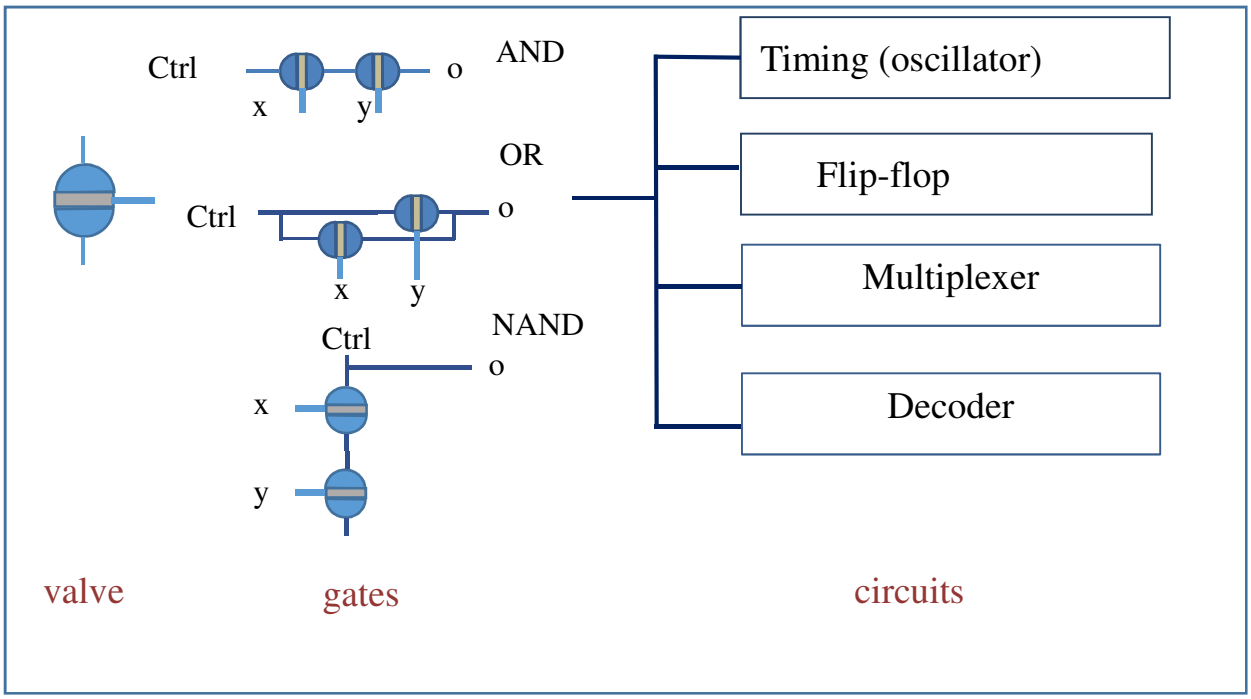

Figure 1: Overview of digital microfluidic logic components

A microfluidic diagnostic assay like the enzyme-linked immunosorbent assay (ELISA) is carried out in microwell plates wherein a number of steps are carried out before the outcome of the test is

obtained. Execution of the steps correspond to control operations performed either off-chip or manually. These include several washing steps with detergent and timed switching between buffers/reagents. An on-chip timer, the main control operation in this process, can be implemented with a clock signal generator and a counter. These circuits, in turn, are implemented using a network of gates connected in a specific combination. The gates can consist of microvalves, analogous to electronic transistors constituting the basic building blocks of digital logic. In effect, similar to having a microprocessor executing commands for an electronic system, a "valve-based processor" executes commands for a microfluidic system.

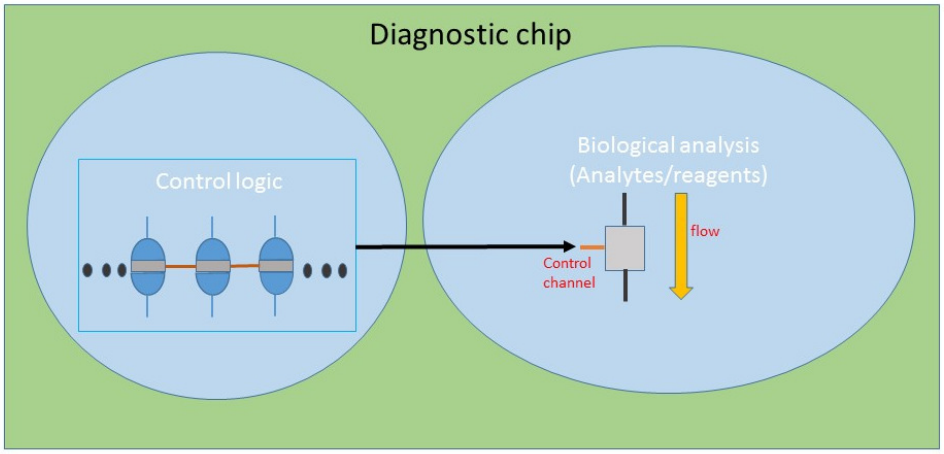

Figure 2: Block diagram of a microfluidic chip with control logic section and fluidic section

Both hydraulic and pneumatic actuation for the valves have been demonstrated. The advantage of the hydraulic system over the pneumatic system is that it prevents potential bubble formation due to the lack of a vacuum line and latching times can be permanent. However, the viscosity of water is two orders of magnitude greater than that of air. The hydraulic resistance is correspondingly higher leading to significant pressure drops when cascading gates. As a result, time delays are longer and the operating pressures are higher.

The basic component of microfluidic pneumatic logic is a normally closed (NC) valve with three terminals analogous to an n-type metal oxide semiconductor field effect transistor (MOSFET). The NC valve is on (air flows) only when the source minus gate pressure is greater than a threshold pressure (by applying a vacuum at the gate)[2]. As shown in Fig.1, the valves can be connected to implement the Boolean functions such as AND, OR, NAND, which, in turn, are the building blocks for more complex logic (counters, shift registers, etc.)

1.3 Fabrication of device prototypes using soft lithography

Soft lithography encompasses a suite of techniques wherein features on a master template are transferred to a soft material, usually an elastomeric polymer such as polydimethylsiloxane

(PDMS) or a thermoplastic. With respect to PDMS-based stamps, four sub-categories are replica molding, microtransfer molding, micromolding in capillaries and solvent-assisted micromolding.

Molding of thermoplastics using hot embossing is also considered a form of soft lithography. In hot embossing, patterns are imprinted on a thermoplastic from a micromachined quartz, metal master or polymeric stamp.

1.3.1 PDMS Molding

PDMS is the most common material used in soft lithography due to three properties:

i) It is elastic and has low surface energy enabling it to make reversible conformal contact with non-planar substrates. Irreversible bonds to other surfaces (eg. glass) can be formed by treating the surface with oxygen plasma, making it easier to form microfluidic features such as channels.
ii) It is transparent down to wavelengths of 280 nm allowing for integration of optical elements into the device.
iii) It is commercially available at moderate prices (~\$100 kg^{-1}).

However, PDMS has disadvantages as well. It is not the best material for high aspect-ratio structures. Multi-layer devices need to be replica-molded layer-by-layer and assembled which eliminates the possibility of complex devices being manufactured with this technique.

Replica Molding with PDMS: Replica molding (REM) with PDMS creates microfluidic devices by replicating the shape and structure of a mold called a master. The master pattern is first prepared on a silicon wafer by spin-coating photoresist[3]. Photolithography with a plastic or glass mask containing the device features and then development leads to the features being imprinted on the photoresist as shown in Fig. 3.

Before the PDMS is poured onto the master, the master needs treatment by applying a chemical such as a trichlorosilane, which makes the surface hydrophobic and prevents the PDMS from sticking to the wafer. The PDMS prepolymer is then mixed to uniform consistency, poured onto the master and allowed to set and cure at a temperature of 60°C-70°C for 1-2 hours. The PDMS is then peeled away from the master and contains a negative embossed image of the master.

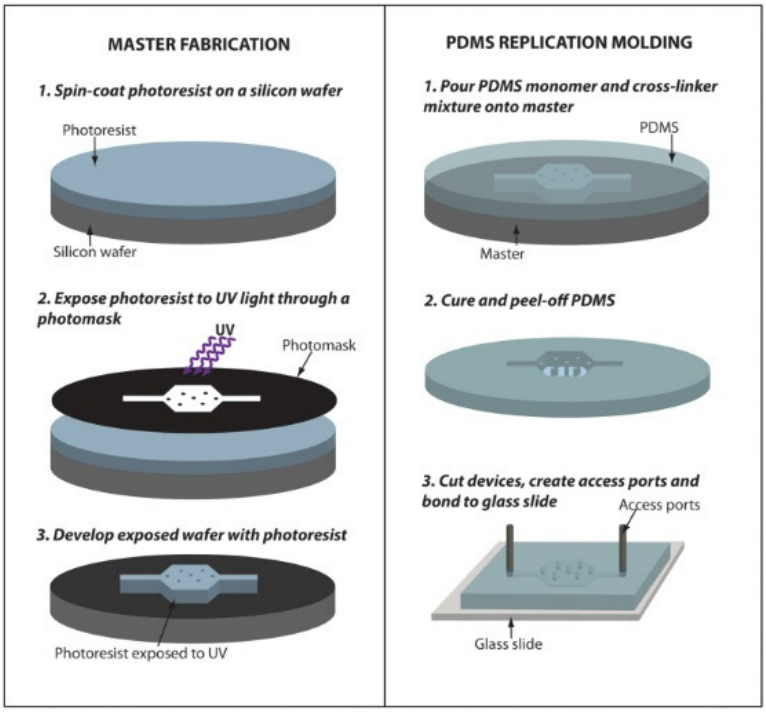

Figure 3: PDMS molding soft lithography process - Image reproduced from Ref 4

1.3.2 Hot embossing

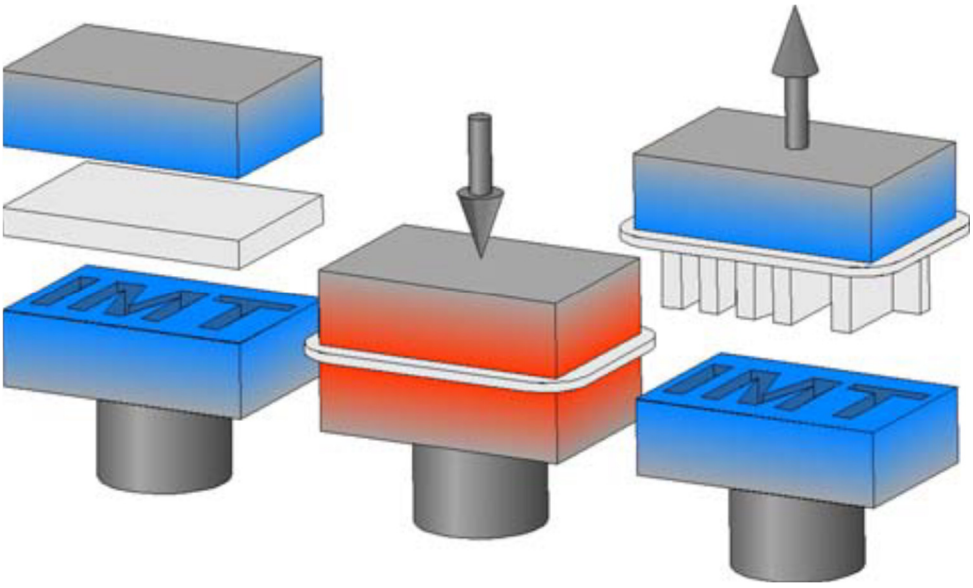

Figure 4: The hot embossing process: heating, molding, and demolding are the characteristic process steps - Image reproduced from Ref 5 with permission from Springer

Hot embossing is the technique of simultaneously using pressure and temperature to stamp patterns into a polymer substrate. In this process, the glass transition property of thermoplastic polymers is utilized. The glass transition temperature (*Tg*) is one of the most important thermo-physical properties of amorphous polymers. Polymeric materials are soft and rubbery above *Tg* allowing

them to be deformed. The reshaping upon heating and preservation of chemical and physical properties after cooling down is an important feature of these polymers that makes them suitable for imprinting.

The steps in hot embossing are:

1. The mold and polymer substrate are heated above the glass transition temperature of the polymer material.
2. Mold and substrate are pressed against each other (1 mm/min) until the required maximum embossing force/pressure is achieved.
3. The force/pressure is held constant for a holding time. At this stage, the relative movement between the mold and substrate has to be controlled to ensure a constant force. The force is kept constant over an additional time period called the packing time corresponding to the reduction of the residual layer under constant acting force.
4. Finally, the system is cooled down below the transition point of the substrate. The lower temperature at which the pressure is removed and mold/substrate separation can take place is called the deembossing temperature. At this stage, the desired features on the substrate can be observed.

Table 1: Glass transition temperature of some common polymers

Polymer	T*g* (℃)
Polypropylene (PP)	-13.15
Polyethylene (HDPE)	-125.15
Polystyrene (PS)	99.85
Polymethylmethacrylate(PMMA)	105
Polyvinylchloride (PVC)	81

Considerations in hot embossing[6]:

The structural/geometrical properties of the mold influence the process parameters. Ratio of area occupied by small structures versus the large structures, shapes of the structures (curved vs. linear), etc. have a bearing on the embossing temperature, deembossing temperature and hold time of the process.

In general, the degree to which the embossing is isothermal plays a role in the completeness of replication. Demolding is a critical step as the destruction of the mold structures or non-release of the substrate (due to tight sticking together of mold and replica) is possible.

In addition, for high-aspect-ratio structures, more considerations are involved:

1. Sidewall surface properties of master mold: Frictional forces between the embossing tool and substrate play a role in obtaining an intact replica. Low surface roughness of the master is important for minimizing the frictional force. SU-8 structures with average roughness of less than 5 nm are very suitable for high-aspect-ratio features (>0.5).

Vertical sidewalls increase the frictional force and the more the deviation from the vertical, the less problematic the deembossing.

2. Chemical interface between master mold and substrate: The stiction force is another force that contributes to problems during deembossing. Surface bonding sites enabled by the chemical interaction of the substrate and mold material should be minimized.
3. Temperature coefficient of materials: A large difference in temperature coefficient of the tool and substrate can lead to formation of irregular structures on the substrate during the cooling.

By optimizing the mold surface parameters, process thermal cycle and pressure application, high quality replicas can be produced using the hot embossing technique which make it a suitable for manufacturing microfluidics.

1.4 Stereolithography for manufacturing active microfluidic devices

Standard microfabrication methods typically lead to the production of open channels on the surface of a substrate. For creating an enclosed microfluidic channel, an additional layer is required, which implies a multistep procedure. Stereolithography (SL) is a 3D printing technique simplifying the process for creating such closed features and has emerged as an important rapid prototyping technique for microfluidic devices. SL involves building an object layer by layer from a photocurable liquid polymer resin using a UV light source[7]. Depending on the curing method and the orientation of the light source, two different configurations are possible. Figure 5 depicts the bath and the layer configuration. In the bath setup, the device is built from the bottom up, with the z-stage moving down into the resin vat after each layer has been cured to start building the next layer. In the layer configuration, the movable platform is suspended above the resin reservoir and the light source is located beneath an optically clear bottomed vat. The material in the vat between the light source and the platform is polymerized for a single layer. A whole layer can be cured at one step. This setup has the advantage of consuming lower volumes of resin, being able to print unrestricted heights and the layer thickness can be more readily controlled by the z-stage positioning. After the first layer cures, the z-stage moves upwards producing a print that is upside down at the end of the process.

SL to manufacture microfluidic devices has been gaining popularity in recent years with 3D flow channels easily being fabricated for generating emulsions[9] and helical microchannels to detect pathogens[10].

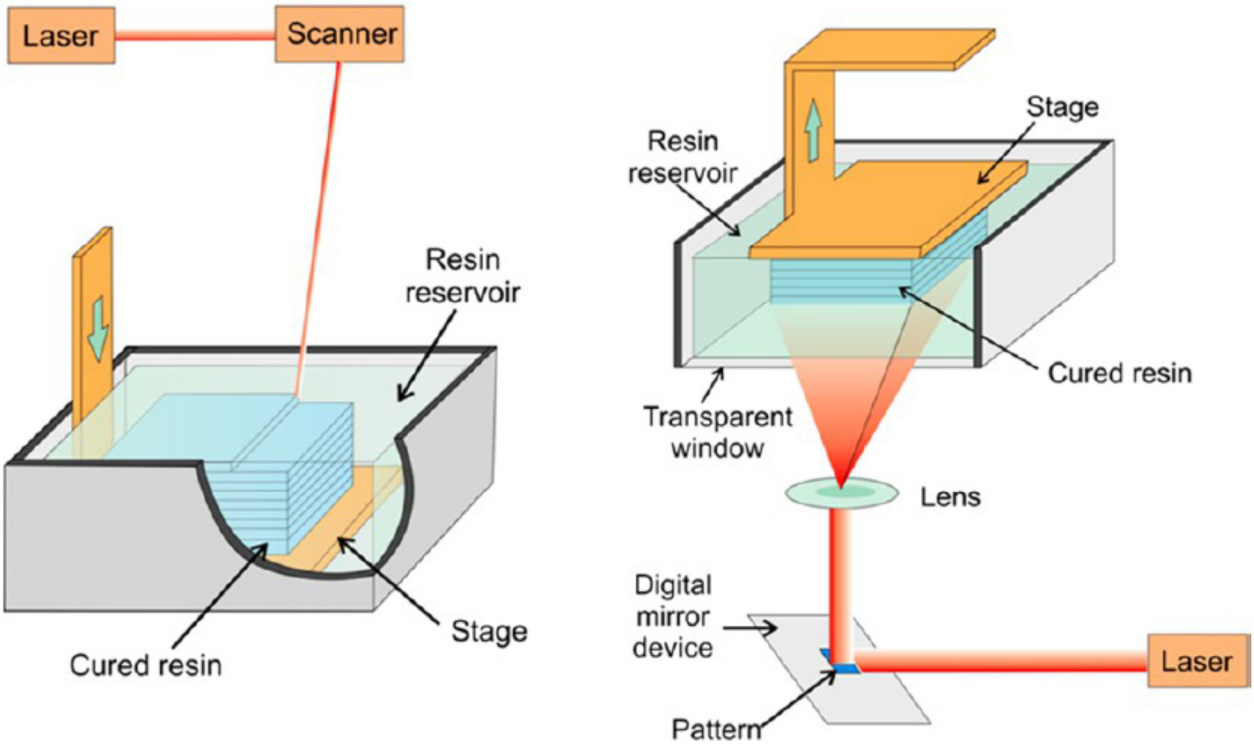

Figure 5: Schematic (left) of a bath configuration SLA printer with a direct write curing process where the stage is just below the surface of the liquid resin. (Right) Schematic of an SLA printer with a projection based curing process. – Image reproduced from Ref 8 with the permission from American Chemical Society

1.5 Large scale manufacturing of microfluidic devices

In order to manufacture microfluidic devices in a high-volume, a high-quality master mold from which a large number of replicas can be made is a requirement. Injection molding is one technique that is commonly used for hard plastic microfluidics where the liquid polymer is injected into the mold cavity and solidifies in the shape of the mold. CNC milling is another technique that can be applied for micro-component mold manufacturing.

1.5.1 Micro-injection molding with plastics

Microinjection molding involves the production of an initial mold and then mass-producing replicas. This is one of the main techniques to produce polymer microfluidic devices such as micropumps, mixers and other structures. The main processes involved in sequence are: plasticizing granular resin, metering molten material, injecting melt into the cavity, packing the melt for shrink compensation, cooling the molded product and finally demolding (Fig. 6). Precision molding of micro-components takes into account some specific factors in comparison to conventional injection molding: tiny cavities place more constraints on mold temperature, thorough venting is very important, increased influence of microscale viscosity and surface tension.

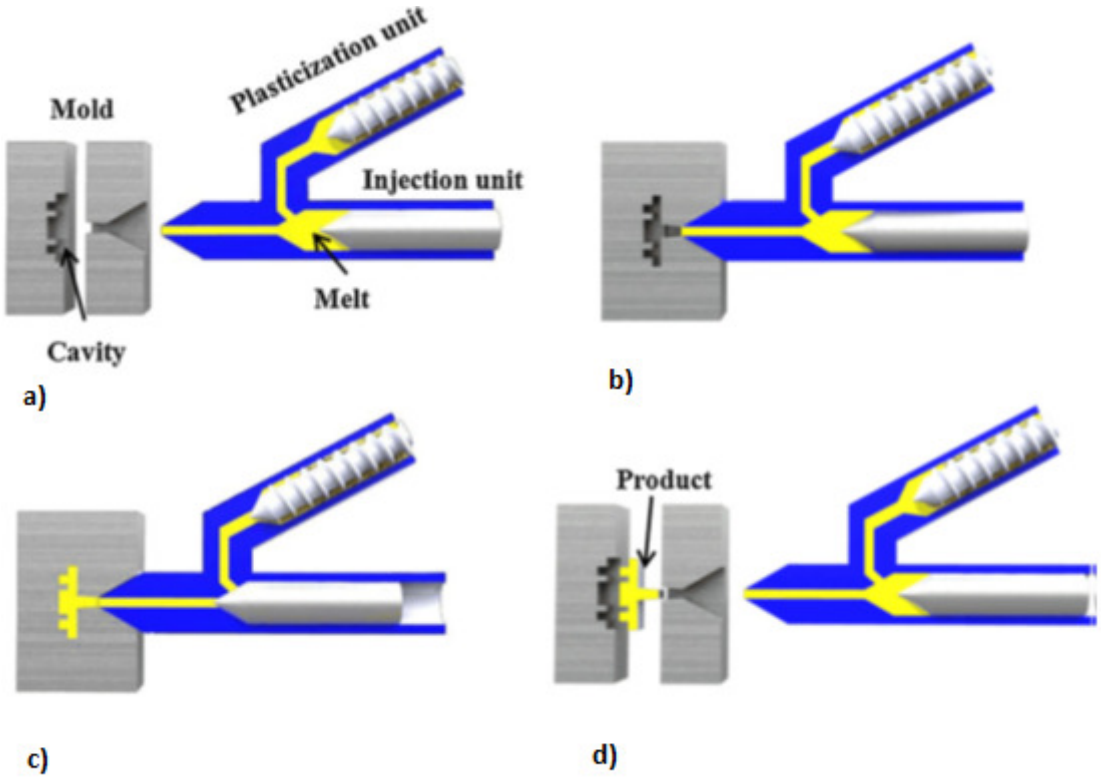

Figure 6: Microinjection molding process (a) plasticization, (b) mold closing, (c) injection, packing and cooling and (d) demolding and replasticization – Image reproduced from Ref 11 with the permission from Institute of Physics Publishing

This increases the challenges associated with developing smaller polymer micro-components although development has taken place in machine development, mold tool fabrication and expanding capabilities over the last few decades.

1.5.2 CNC milling with plastics

Micromilling is a fabrication technique that creates microscale features on a material via cutting tools. Microfluidic devices such as oil and aqueous interfaces for cell capture and RNA,DNA isolation have been created using this method. Despite research demonstrating the usefulness of micromilling for the fabrication of devices, it has not attained the popularity of methods such as hot embossing and injection molding due to:

1. High costs involved in setting up good precision mills
2. Unique technical expertise required

There are two ways micromilling can be used for microfluidic applications: (1) Machining the master mold used for subsequent fabrication (2) machining features directly into the part which will become the final device. In the second case, turnaround time from design to prototype can be as low as 30 minutes for simple designs, offering an important advantage.

Technical capabilities:

In terms of materials, milling can be used for metals, polymers and brittle material such as glass. The degree of difficulty varies with the material, metals being more easily milled. Glass and polymer milling can result in chipping /cracking and difficulty in material removal due to elastic deformation respectively. Table 2 lists some of the differences in the different manufacturing techniques in terms of features produced and capabilities[12].

Table 2: Comparison of feature production/capabilities of different manufacturing techniques

Categories	Milling	Embossing	Stereolithography	Injection Molding
Height and aspect ratio	Higher heights and aspect ratio(8:1)	Lower heights and aspect ratio(2:1)	limited by method	Higher aspect ratio(8:1) are possible
3D feature contouring	continuous	layered	layered	continuous
Corners and rounding	Special tools required	Depends on mold	Depends on pixel resolution	Depends on mold
Surface roughness	Depends on material and tool	Depends on mold	Depends on pixel size of projector	Depends on mold

Mill cost and equipment:

CNC mills are available in a wide range of configurations that vary in technical specifications and cost. Specifications that affect the accuracy of the machining and cost are feed rate (translational speed of the stage) and spindle speed (rotational speed of the spindle that holds the cutting tool). A basic CNC mill with an accuracy around 25um can cost anywhere between $10,000-$20,000 whereas one with automated tool alignment (accuracy <5um) can cost between $100000-$200000.

The tool used for milling is called an endmill. Endmills are available in various sizes, shapes and materials. Carbide is the most common material for micro-endmills with a square profile used for flat channels of the type found in microfluidic devices.

The following chapter focuses on using polymethyl methacrylate (PMMA) to manufacture microfluidic devices, particularly pneumatic valves and logic circuits which enable microfluidic automation.

2. PMMA microfluidic devices

2.1 PMMA as a preferred material for microfluidics

PMMA, polycarbonate(PC),polystyrene(PS),polyvinyl chloride(PVC) and the family of cyclic olefin polymers belong to a class of synthetic polymers that are widely used for manufacturing microfluidic devices called thermoplastics. Thermoplastics have several properties amenable to microfluidic applications:

1. Biocompatibility
2. Mechanical stability
3. Impermeability to water
4. Organic solvent and acid/base resistivity
5. Ease of fabrication and adaptation to mass manufacturing

Thermoplastics overcome the drawbacks of PDMS-based microfluidic fabrication such as channel deformation, sample absorption and leaching. In addition to the above mentioned properties, PMMA, in particular is widely available at a low price and has excellent transparency to visible light.

PMMA Chemical Structure and Properties[13]

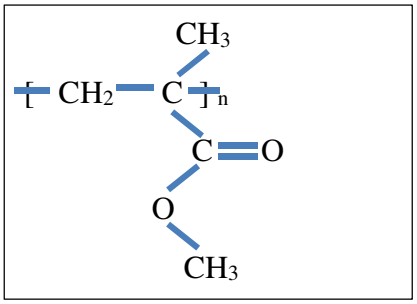

Figure 7: Chemical structure of PMMA

Table 3: Important properties of PMMA

Property	Value
Density	1.15-1.19 g/cm^3
Water Absorption	0.3-2%
Hardness,Rockwell M	63-97
Tensile Strength,Ultimate	47-79 MPa
Thermal Conductivity	0.19-0.24 W/m.K
Glass Temperature	100-110°C
Transmission,visible	80-93%

As can be deduced from table 3, PMMA has high mechanical strength and exhibits good dimensional stability due to low water absorbing capacity. It also has a fairly good resistance to temperature changes. All of these factors make it suitable for microfluidic device manufacturing.

A variety of techniques have been used to fabricate PMMA devices including injection molding, hot embossing, laser cutting and solvent etching. In terms of reliability and replication fidelity, injection molding and hot embossing are the best approaches. For prototyping purposes, laser cutting and micro-milling are suitable techniques for fast turnovers and quick development cycles.

Table 4: Comparison between hot embossing, micro-milling and laser cutting

		Hot embossing	Micro-milling	Laser cutting
Aspects of technique	Replica mold fabrication	Requires sturdy master mold	Mask/mold free	Mask/mold free
	Mass production	Not suitable for mass production due to degradation of mold after 10-20 runs	For devices with features <100 um, not suitable due to high rate of breakage of endmills; more suitable for making master molds	Suitable for mass production
	Precision	Depends on precision of mold	High precision possible when using small-sized endmills	High precision possible
	Surface properties	Low roughness but slight unevenness of features can be caused by reflow during application of heat	Low roughness when small-sized endmills are used	Channel surfaces are rough; they are uneven for wide cuts (>100um)
	Manufacturing time	Total time 1-2 hours (excluding mold fabrication time)	30 minutes-2 hours per chip depending on chip complexity and feature depths	10-30 minutes depending on complexity of design

2.2 Fabrication of PMMA-PDMS hybrid microfluidic devices

Pneumatic valves and pumps have been assembled by sandwiching a PDMS membrane between PMMA microfluidic channels[14]. These devices combine the advantages of both materials, the PMMA being hydrophobic and versatile and PDMS being elastomeric and hence suitable for

fluid actuation. PMMA-PDMS hybrid structures have been used for applications such as PCR amplification and show potential for utility in portable and disposable microfluidic devices. The primary steps involved in the fabrication of such a device are:

1. Creating the channel/features on PMMA through a suitable technique: hot embossing, micro-milling, laser ablation, etc.
2. Bonding of the PDMS membrane to the PMMA layers for a robust structure capable of withstanding higher fluidic pressures.

The bonding aspect is addressed in the following sections. Experimentation on PMMA-PDMS bonding and the development of the successful protocol are explained.

2.3 Bonding PMMA to PDMS

Microfluidic devices performing various functionalities are often multi-layered devices wherein several polymeric layers are aligned and bonded together. Accordingly, a polymer bonding process is required. Several bonding techniques have been reported using heat, pressure, adhesive or solvent[15].Channel deformation or clogging is a drawback of using thermal, pressure and solvent bonding. A robust bonding process should preserve feature structure and offer high bonding strength.

Bonding two homogeneous substrates is an easy task as surface properties are the same. Direct thermal bonding and solvent bonding are the most common approaches for bonding two PMMA substrates[16].Chlorocarbon solvents such as chloroform have often been used, but require more care as they dissolve PMMA. The strength of thermally bonded PMMA depends on the temperature of the process and this factor is balanced against the requirement of low geometric deformation. On the other hand, for permanently bonding two PDMS pieces, O_2 plasma treatment of the two surfaces is a standard procedure that has been followed successfully.

Direct bonding between PMMA and PDMS is challenging as the surfaces are different. Oxygen plasma treatment alone will not create an irreversible bond. Different techniques to bond the two materials have been developed including surface modification of PMMA by chemical vapor deposition (CVD), silane and adhesive coating. One such PMMA-adhesive-PDMS structure which is easy to implement and cost-effective is illustrated in Fig.8. The membrane is a hybrid consisting of an adhesive and PDMS.

The method of silanization involves creating a self-assembled layer, essentially a silane matrix similar to glass. Subsequently, it can be treated with oxygen plasma and bonded to plasma treated PDMS. For creating the self-assembled layer, various materials have been used. Silica gel spin coated on PMMA, PMMA surface treated with bis-trimethoxy-silyl-propyl-amine, tetraethyl orthosilicate(TEOS) or aminopropyltriethoxysilane(APTES) are some of the approaches demonstrated. APTES, in particular, has been reported with a high bonding quality by many groups (Vlachopoulou, Kim,etc.)

After considering these options, the self-assembled layer method using APTES was chosen for my devices.

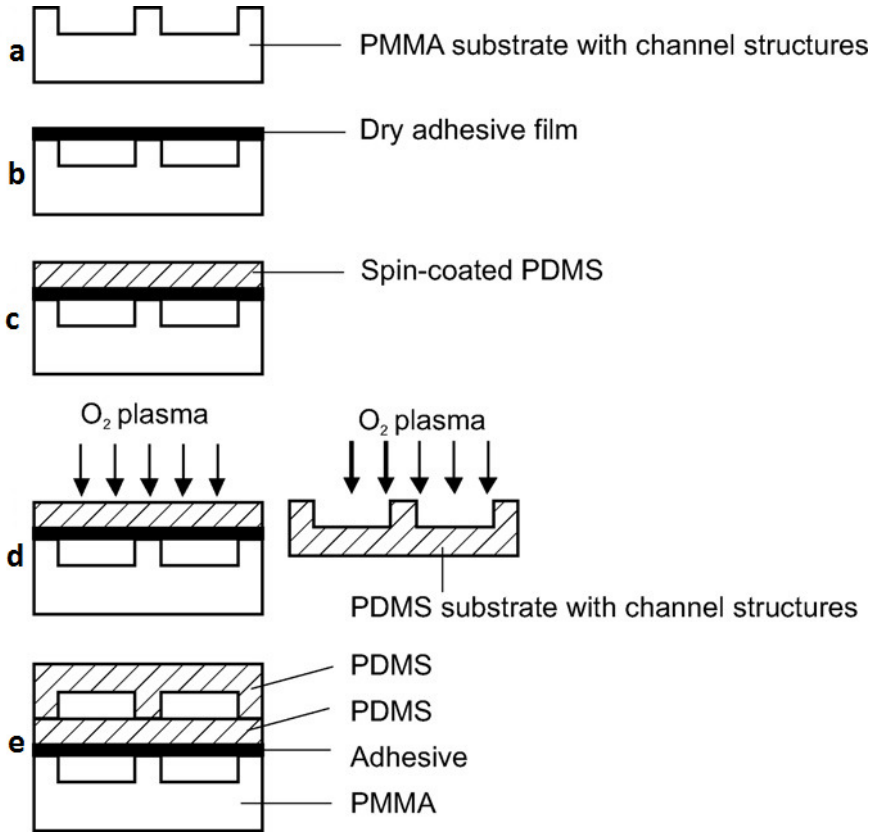

Figure 8: A PMMA-adhesive-PDMS peristaltic micropump fabrication process: a) PMMA substrate with chambers; b) dry adhesive film laminated onto the PMMA; c) PDMS spin coated onto the PMMA wafer covered by the adhesive; d) PMMA substrate with the adhesive/PDMS membrane and PDMS substrate are treated in oxygen plasma; e) treated surfaces are bonded together to form the micropump - Image reproduced from Ref 16 with the permission from Elsevier

2.3.1 APTES treatment of PMMA for surface activation

Need for surface activation of polymers

The specific energy of a polymer determines the bond strength with another polymer. Hydrophobic polymers, such as PMMA and PDMS, typically have low specific energy leading to low bond strength. In order to increase surface energy, plasma activation is a commonly used technique. Energetic photons, ions and electrons in the plasma break chemical bonds on the polymer surface to produce highly reactive free radicals on the surface. The hydrophilicity and wettability of the surface is also increased. Kim et al[17] reported a decrease in contact angle of the PMMA surface by an order of 15° which further reduced to below 10° after APTES treatment. Generating polar functional groups on the surface allows for strong hydrogen or covalent bonds to be formed across the interface of the two surfaces in contact.

Varying the experimental parameters of APTES treatment

The basic process for APTES treatment of PMMA is explained below:

Step 1: PMMA surface modification through oxygen plasma treatment – The creation of reactive hydroxyl groups on the PMMA surface assists in the formation of bonds in the next step.

Step 2: Treatment of surface-modified PMMA with 3-APTES (Aminopropyltriethoxysilane)- The silicon-amino group forms a bond with the oxygen atoms of the hydroxyl group to anchor on the substrate.

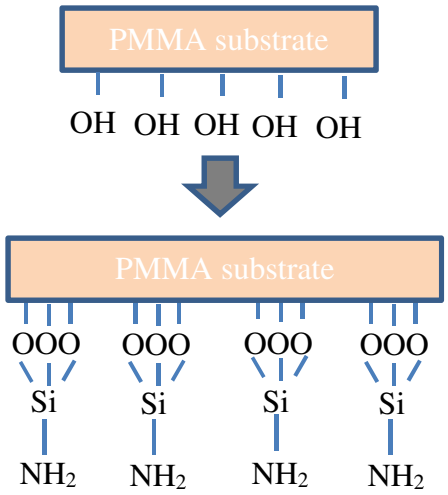

Figure 9: The two step process where hydroxylation of PMMA surface and subsequent formation of amino-silicon-oxygen bond takes place

Next, the PDMS membrane is treated with oxygen plasma for 1.5 minutes and then bonded to the PMMA.

In this process, there are two parameters that may be varied: (1) time duration of oxygen plasma treatment for PMMA and (2) concentration of APTES solution used.

Experiments with different concentrations of APTES solution ranging from 1%-5% have been carried out[18] at room temperature and with heating. I carried out bonding using the same method as described above in Fig. 9. For oxygen plasma, I used the Diener Zepto plasma surface technology equipment with an oxygen pressure of 660mTorr. With 1% APTES concentration at room temperature, I obtained limited success with PMMA-PDMS bonding. After increasing the APTES (Aldrich 440140, 99%) concentration to 5% with heating to 85°C, the number of trials that resulted in successful bonding became higher. In order to evaluate the outcomes under different times of oxygen plasma treatment, a set of trials were carried out with and without heating of the PMMA-PDMS after conformal contact. Table 5 shows the results indicating that higher time period of oxygen plasma treatment tends to be advantageous.

Table 5: Plasma treatment outcome under different time durations

Heating	2.5 min	3.5 min	4.5 min	5 min
None	none/complete	partial	partial	Not done
At 65°C	partial	complete	Complete/partial	partial

In the next sections, techniques to pattern features on PMMA are discussed starting with solvent embossing and then laser cutting.

2.4 Solvent embossing on PMMA

Solvent-based polymer imprinting is a technique that has been used to pattern microdevices within a short period of time in comparison to approaches like hot-embossing and machining which take a few hours to complete[19]. This approach involves the application of a solvent on the surface of hard polymers to soften it for pattern transfer.

Acetone and acetonitrile are two solvents that have been used for solvent imprinting. Acetonitrile is more suitable for relatively softer plastics like PMMA due to the lower rates of solubility. A schematic of the process followed is shown in Fig. 10.

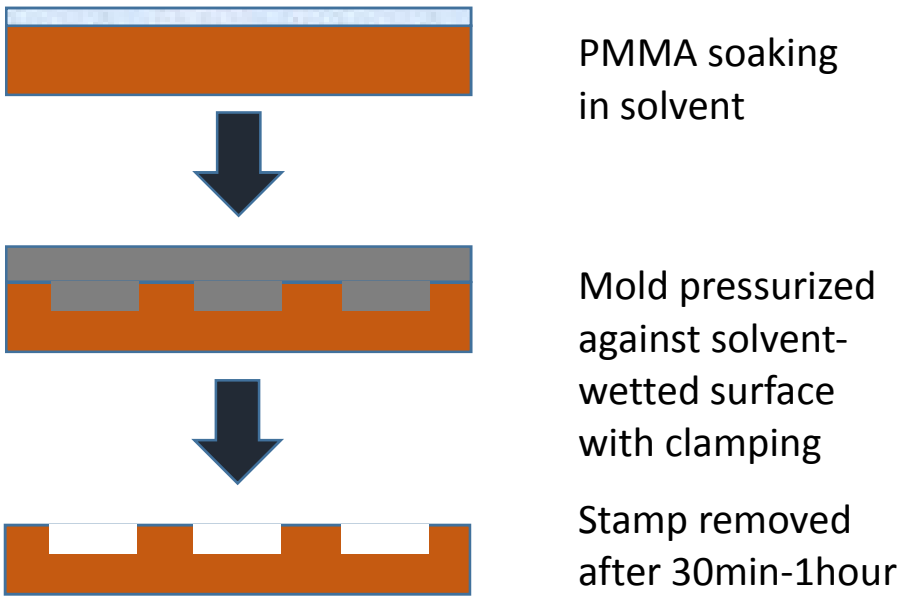

Figure 10: Solvent soaking process with PMMA

First, cut pieces of PMMA of approximately 4cmx2.5cmx0.3cm were cleaned with soap, DI water and then dried with a nitrogen gun. Next, a uniform layer of acetonitrile [500uL-1mL] was applied to the surface of the pieces and allowed to soak for a period ranging from 30 sec-2 minutes. The mold consisting of SU-8 patterned wafers was pressed against the solvent-wetted PMMA surface and a C-clamp used to apply pressure for a period of 20 minutes-1 hour. A C-clamp was estimated to be sufficient to apply pressure evenly over the small area of 1 inch^2.

Initial results with a penny as a mold with varying solvent soaking and clamping times are shown in Fig.11. Some of the outlines of the rectangular areas can be clearly seen on the PMMA but finer details such as the sitting Lincoln did not form any imprint. We can see that increased soaking time degrades the surface. The optimal soaking time was 1 minute and a clamping

period between 30 minutes-1 hour produced similar results. An SU-8 template with a cubic structure (Fig. 12) produced an imprint that was approximately reproduced in the x-y plane but was 1/30 times the actual dimension in depth.

As the results demonstrate, even the imprints with the least degradation were not good replicas of the mold, both in terms of surface roughness and aspect ratio of features. If areas less than 1inch^2 cannot be replicated uniformly on the PMMA, larger area microfluidic logic circuits are more problematic. Hence solvent imprinting was not pursued further for fabricating devices from PMMA.

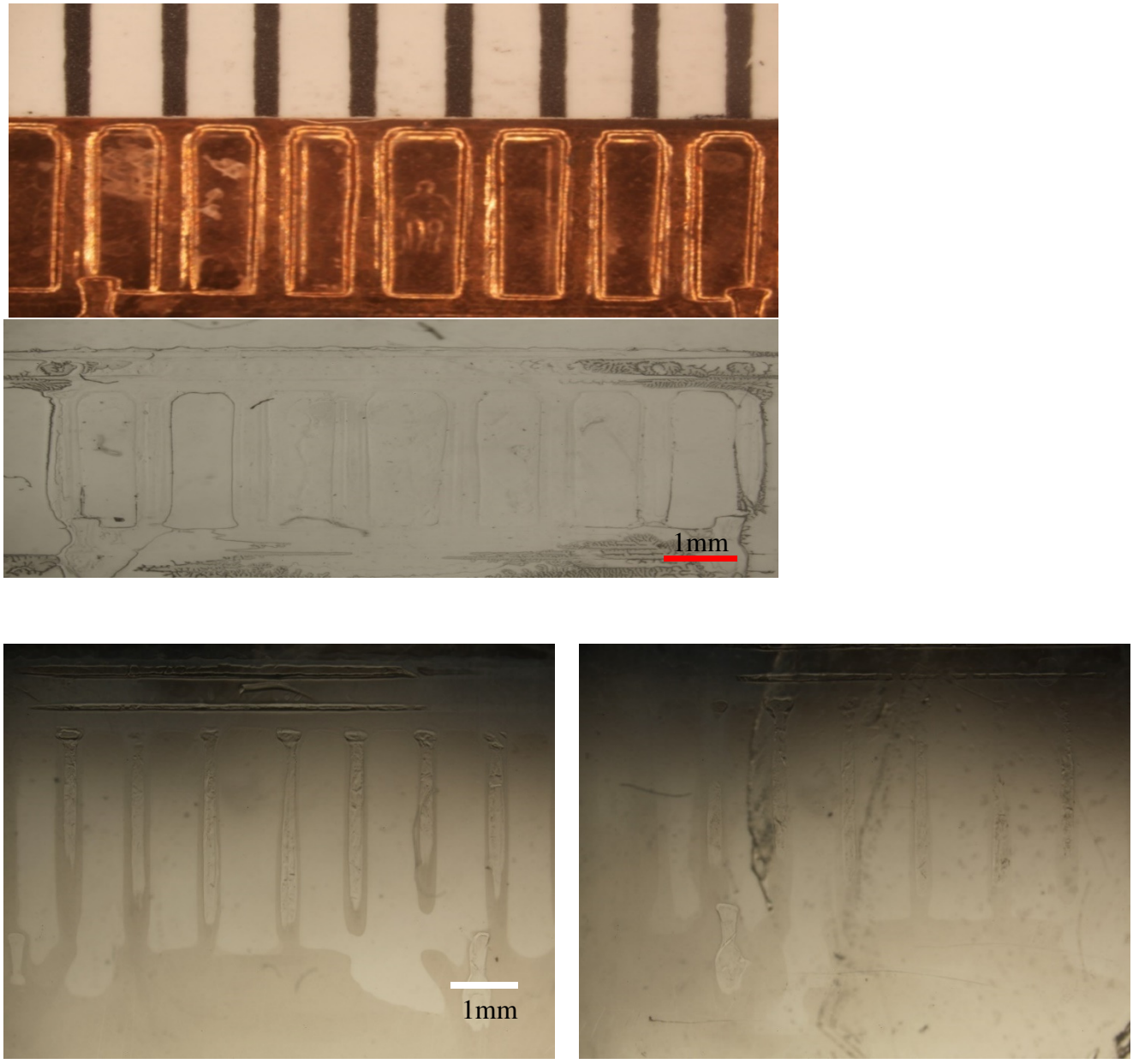

Figure 11: PMMA embossed with a penny as a mold (top);1 minute soaking time with 30 minutes clamping (bottom left); 2 minutes soaking time with 20 minutes clamping(bottom right)

Figure 12: Cubic structures on SU-8 300um tall (left) and corresponding imprint on PMMA (right)

2.5 Laser engraving technique for manufacturing PMMA devices

Laser cutting/engraving of microfluidic structures have many advantages over comparable techniques as described in table 4. Two of the main advantages are manufacturing time and high precision. Additionally, while CNC machining depends on the quality, size and geometry of the tools used, there is no dependency on additional tools for laser cutting. A wide range of polymers (from PDMS to PMMA) can be processed by the laser cutter. However, manufacturing defects in the form of non-uniform channel walls and floors are an issue. Surface roughness in particular affects the optical transparency of the channels and eventually fluid flow in the complete device[20].

Fabrication with PMMA:

The designs for the logic circuits were first created using Autodesk Inventor Professional 2017 and then translated into a line diagram in Autodesk AutoCAD. The translation is performed by identifying the center lines of symmetry of the channels. The 2D .dwg file is used directly as input to the laser's proprietary software.

Acrycast cell cast PMMA sheets (Astari Niagara) of thickness 1/8" and a commercial CO_2 laser system, VersaLaser 3.60, were used in my experiments. The laser operates at 10.2 um wavelength and a power range of 10-60 W with two modes, vector and raster for the cuts. The top raster speed is 1270 mm/s and vector speed is 254 mm/s. Through experimentation, it was determined that higher power and slower speeds produce deeper cuts while lower power and higher speeds produce shallower cuts.

Figure 13 shows the channel aspect ratio of different combinations of speed and power for vector cuts on PMMA. In general, lower powers produce higher aspect ratios for each speed. At higher powers, the aspect ratio can reduce by as much as 4 times (speed 20%).

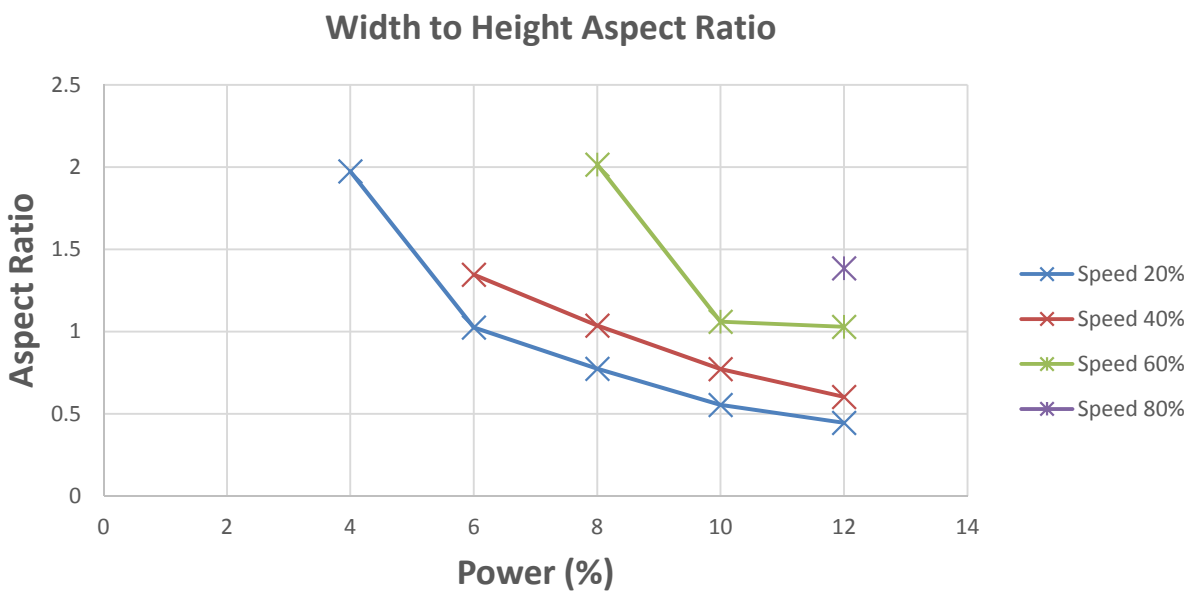

Figure 13: Aspect ratio of laser cuts plotted against power for different speeds (ref. Kurt Castro)

As a first step, the PMMA sheet was placed onto a *z*-axis adjustable stage and moved into focus with the laser head. A desired depth of engraving is achieved using suitable adjustments of the laser duty cycle, speed and power which are calibrated with sample pieces before the actual device layers are fabricated.

Color coding for depths: A maximum of 6 settings for depth are allowed which are distinguished by the color allotted to each setting. The widths of the lines correspond to the channel widths that are desired. The actual width of the channel differs by +/- 20-50 um depending on the speed and power used. Figure 14 shows a section of a dwg file drawn in AutoCAD with features of different colors indicating different depths of cut.

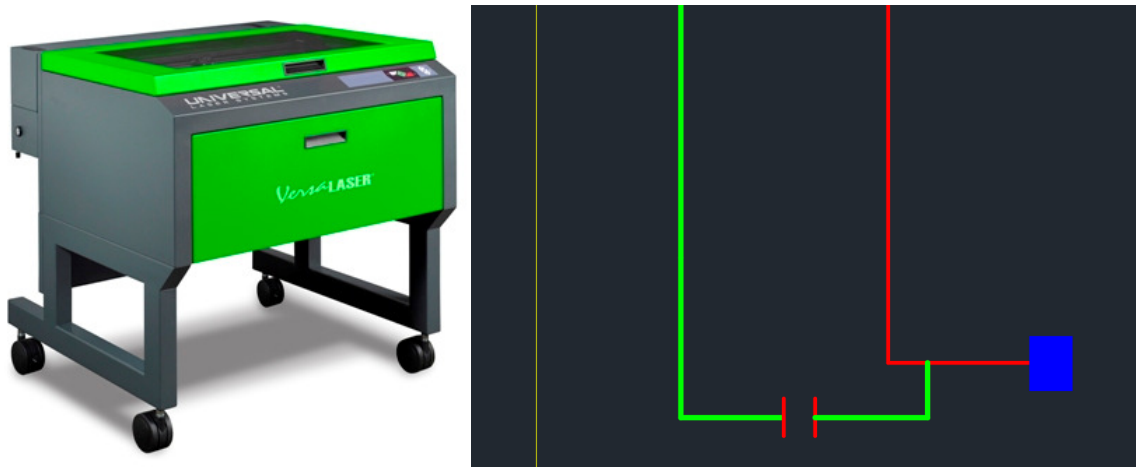

Figure 14: The VersaLaser apparatus (left) and color-coded drawing in AutoCAD (right)

The number of passes of the laser affects defect formation at larger depths (>300um) with a single pass resulting in larger volume of residual material from which defects can form. Multiple passes can reduce the extent of defect but can take more time. In our case, as the designed depths were restricted to below 100 um, this was not an issue.

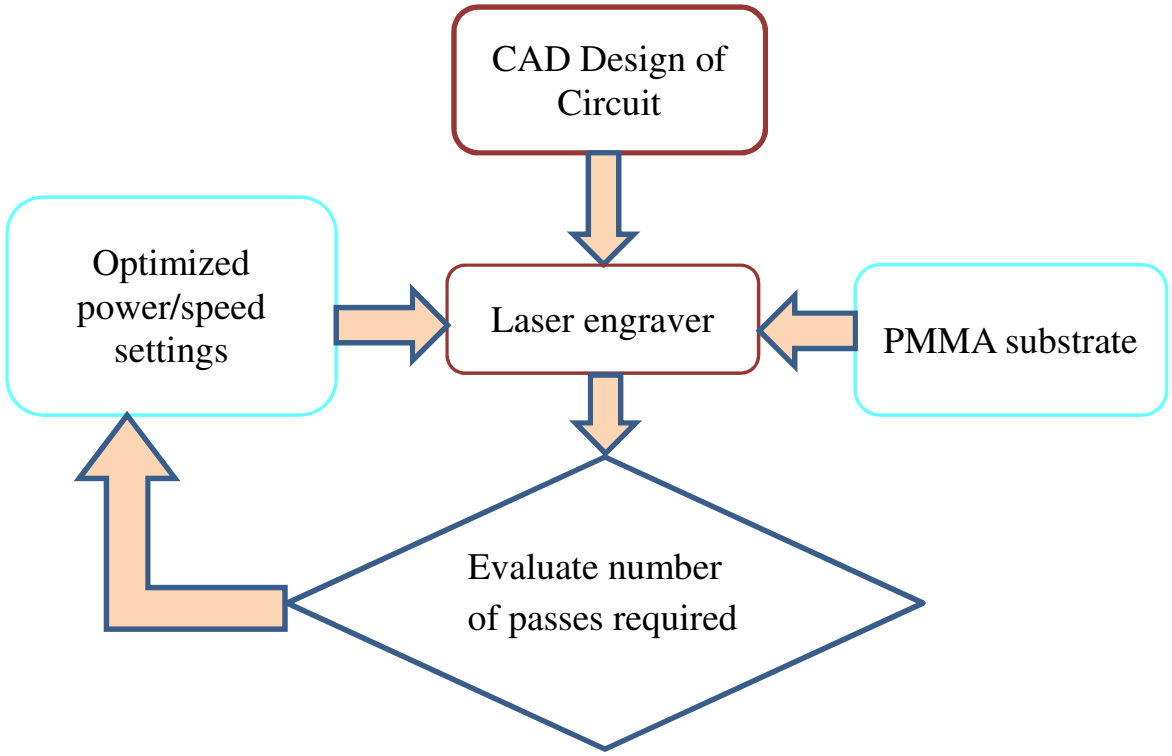

Figure 15: Procedure for optimizing number of passes

In the next chapter, experiments with hot embossing for creating features on PMMA and the results are discussed. As hot embossing is a well-documented technique with numerous studies examining the process parameters, it was chosen to fabricate devices for initial performance analysis.

3. Hot embossing experiments with silicon wafer molds

Before proceeding to fabricate PMMA devices with the hot embossing procedure, a procedure to identify the optimal parameters needed to be carried out. The primary requirement was a compressive set-up that could apply pressure in the appropriate range and also be temperature-controlled. A number of high precision hot embossing machines/presses are available commercially. Table 6 shows two of them along with their key properties.

Table 6: Commercially available machines for hot embossing

	Temperature(C)	Force	Pressure
EVG 520	Max. 550	200-20kN	1-10e-5 bar
Tetrahedron MTP-8	Max. 454	Max. 49kN	7.65e-3 bar

While these are suitable for large-scale manufacturing using the hot embossing technique, for initial experimentation and feasibility studies with different substrates, less expensive options were explored.

3.1 Custom-made compressive systems – background

Custom-made embossing structures are more common than commercially available equipment. Many researchers have developed the components of such a system and constructed the complete set-up. Becker and Heim were one of the first groups to demonstrate hot embossing as a method to generate microstructures on polymer substrates. The schematic of their machine is shown in Fig. 16 along with a PMMA mold and corresponding PMMA replica of a groove from the structure.

The force frame which delivers the compressive force via a spindle and T-bar and heating plates containing cooling channels are the primary components. A vacuum chamber contains both the tool and the substrate. In addition, a feedback mechanism exists for the control of force applied to the tool-substrate sandwich. Typically, during the process, the thermal cycle is restricted to a narrow range of temperatures so as to minimize thermally induced stresses in the material.

Another system was designed with CAD for the structural body and compressive system. A heating component along with control electronics for the temperature regulation constitute the remaining parts of the device. Similar to Becker and Heim's set-up, this system also has a working stage and mold holder with the heating mechanism built-in. Hydraulic pistons are used for compressing the substrate and the mold. Pressure is applied after heating the substrate to soften it. Using an aluminum micro-mold and experimenting with the embossing temperature and times, channels were replicated on PMMA with depth errors as low as 2%.

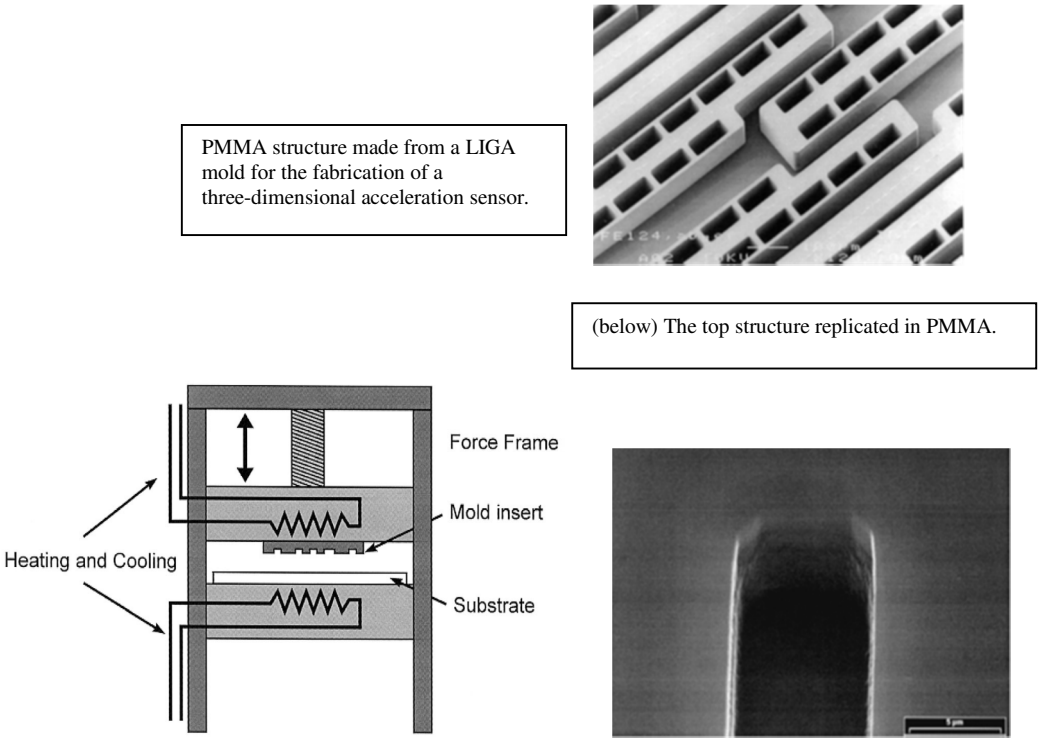

Figure 16: The PMMA mold (top) and hot embossed replica (bottom right) along with apparatus (bottom left) for embossing- Image reproduced from Ref 6 with the permission from Elsevier

3.2 Carver hydraulic press for hot embossing

For my initial experimentation with hot embossing of PMMA, the Carver hydraulic manually operated press (series no. 4386), a benchtop apparatus with a simple operation procedure was found to be suitable. Its important parameters are listed in table 7.

Table 7: Parameters of the Carver Hydraulic Manually-operated Press (series no. 4386)

Parameter	Value
Clamping Force	12 tons
Temperature range	Upto 650 °F
Pressure Gauge range	0-24000 lb
Dimensions	19”L-Rx16”F-Bx39”H
Weight	300 lbs

The press (Fig.17) consists of two heated platens each having a digital temperature controller for separate regulation. Ramp rates for heating the top and bottom platens can be set individually. A manually-operated lever applies the compressive force which is displayed on a digital pressure gauge.

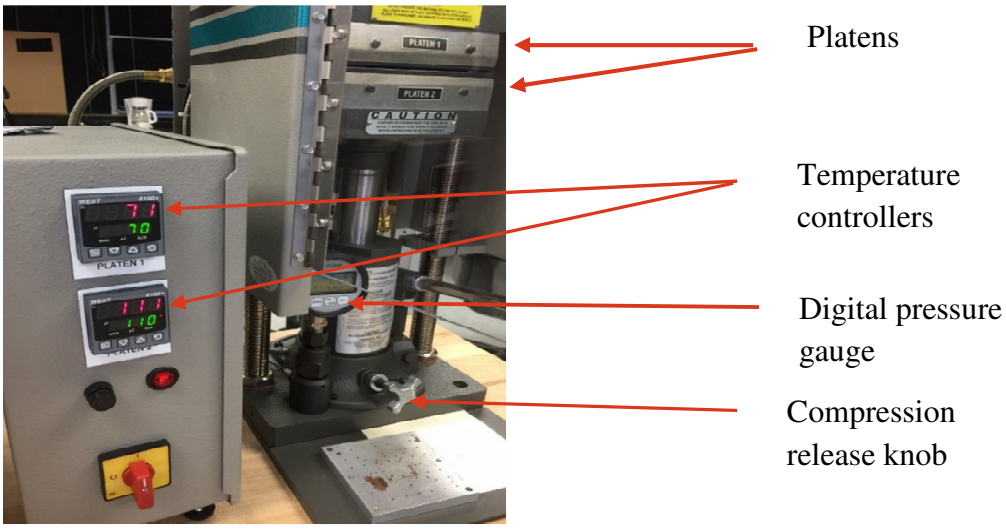

Figure 17: Carver Hydraulic Manually-operated Press

3.3 Deciding the range of process parameters

Two primary parameters influencing the outcome of the hot embossing procedure are temperature and pressure of the substrate-mold sandwich. These parameters, in turn, depend on the master and substrate material. Accordingly, based on the hardness of the material used to make the mold, there are soft and hard molds. Silicon and metals belong to the category of hard molds whereas polymers such as SU-8 belong to the soft mold category.

3.3.1 SU-8 as a soft mold

Soft molds have the advantage of higher tolerance of pressure, mechanical stability and lower frangibility when compared to hard molds such as silicon. Additionally, SU-8 in particular has good coating, planarization and surface roughness properties. Various heights of SU-8 patterns can be made by controlling the spinning speed, which makes it useful for developing a wide array of features. Its high glass transition temperature T_g of approximately 200 °C makes it suitable for use with a large number of substrates including PMMA.

SU-8 structures can be built on glass or silicon as a substrate. Using glass has the advantage of being able to use higher embossing temperatures but the low adhesion between SU-8 and glass is a limitation. SU-8 on silicon has the advantage of stability of the SU-8 structure and hence higher lifetime of master. In my embossing experiments, I chose this type of master mold for initial trials.

As a starting point for my PMMA-SU-8 embossing experiments, I referred to the embossing procedure followed by Shamsi et al. in their studies[21]. Figure 18 shows the variation of temperature and pressure over a total embossing duration of 90 minutes. The process uses a peak temperature of 160°C for an approximate duration of 20 minutes. T_g of PMMA and SU-8 considered here are 105 and 240 °C respectively.

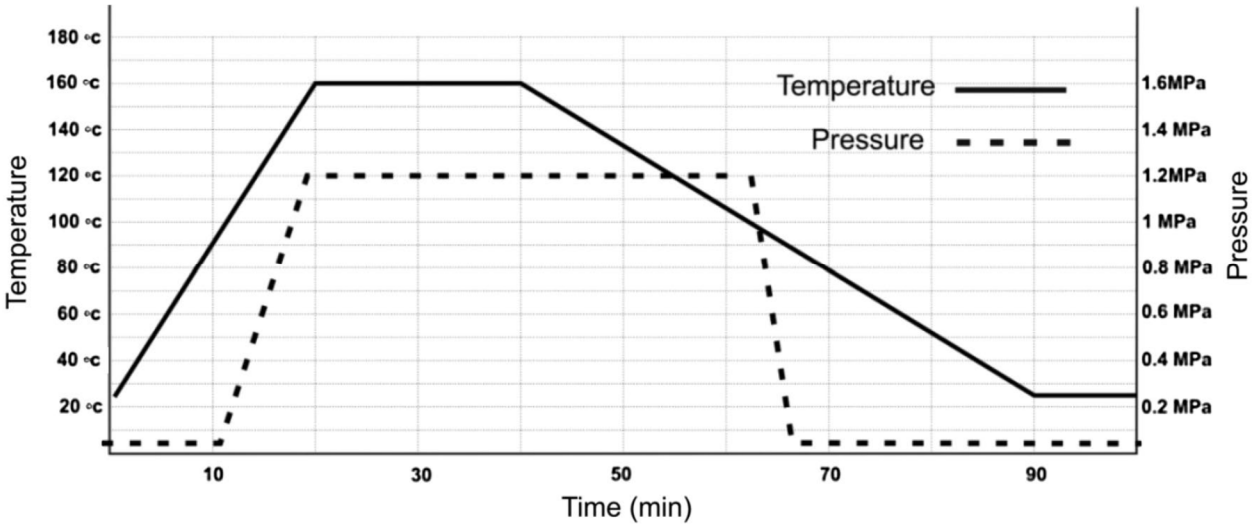

Figure 18: Variation of Temperature and Pressure in Hot Embossing Procedure for PMMA with SU-8 master mold- Image reproduced from Ref 21 with the permission from Springer

In general, PMMA can have a T_g in the range of 95-120°C depending on the manufacturer. The peak temperature of the process varies accordingly. De-embossing is performed at a temperature of 90 °C. In this particular study, the temperature is raised to a value much higher than T_g of PMMA in order to apply lower pressure thereby reducing master wear.

Other studies have used temperatures up to 10 degrees higher than the nominal 105°C and a time duration between 5-10 minutes for a total cycle time of between 20-35 minutes[22]. A force in the range of 1kN-15kN (224 lbs-3372 lbs) has been applied.

Taking into consideration the outcomes of these studies, a peak temperature range of 105-130°C and a force range of 170-250 lbs was set for the initial trials.

3.4 Hot embossing procedure with the Carver press

SU-8 structures on silicon wafer with varying aspect ratios and density of features were chosen as the first molds to carry out the embossing procedure. Figure 19 shows one of four 100 um tall structures equidistant from the center of a 3 inch silicon wafer.

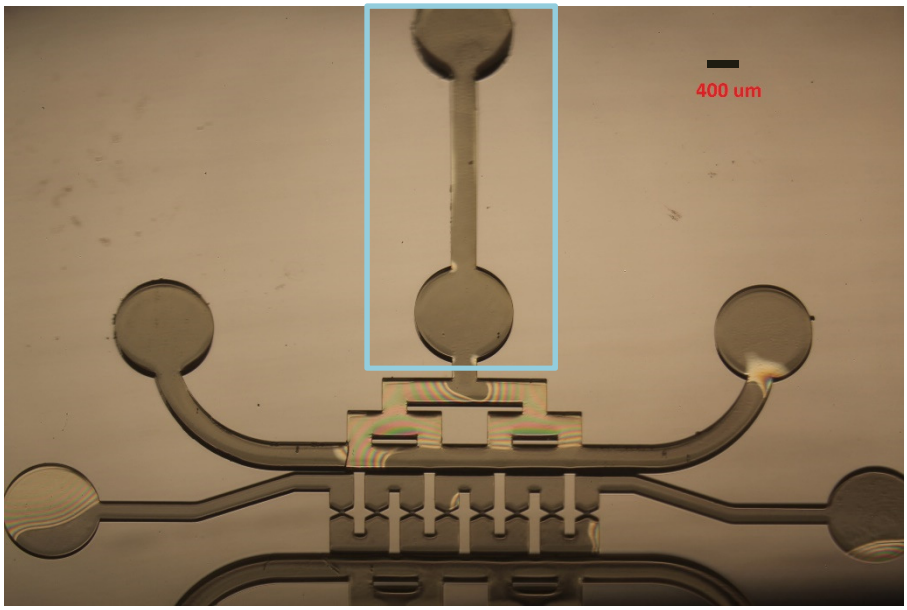

Figure 19: SU-8 master mold with 100um tall structures

The procedure followed with the Carver press was as follows:

Step 1: Clean the PMMA substrate with Isopropyl alcohol(IPA).

Step 2: Center the silicon wafer with SU-8 mold on the lower platen and place the PMMA substrate on top of it.

Step 3: Place a sheet of Teflon (of 50um thickness) on top of the PMMA. (This is to protect the surface of the PMMA in contact with the heated platen and reduce surface roughness at the end of the procedure.)

Step 4: Set the upper platen temperature to 100 °C (ramp rate can be set to any value).

Step 5: Lower platen temperature setting-The ramping to T_g of PMMA is done in two stages:

a. Set the temperature of the lower platen to 70 °C (ramp rate can be set to any value)
b. Once the platen reaches 70 °C, set the temperature to the peak value 110°C with a ramp of 170 °C/hr.

Step 6: After the temperature of the lower platen reaches 90 °C, compress the platens by applying force with the hand lever. The ramping of the force from 0 lbs to 240 lbs over a temperature range of 20 °C (until the temperature reaches the set 110 °C) is done gradually.

Step 7: The temperature is maintained at 110 °C for 5-10 minutes.

Step 8: A rampdown of the two platen temperatures is initiated with a final set temperature of 40 °C.

Step 9: Deembossing (releasing the compression of the platens) is performed at 70 °C and the substrates removed.

Initial Observations:

Trials demonstrated that the temperature of the top platen did not have a significant influence on the outcome of the embossing process within a range of 70-110°C. Heating it beyond 100°C did not provide any advantage. In fact, lower temperatures produced less surface roughness. A Teflon sheet was later placed on the top PMMA surface to further minimize the roughness.

Ramp rate depends on the mold used. For SU-8, it was found that beyond 70°C, the adhesion of the SU-8 structures to the silicon wafer is degraded if the ramp rate is above 170°C/hr.

Compression ramping cannot be precisely controlled as it is dependent on the force applied with the hand on the lever. To establish a satisfactory level of consistency, repeated trials on the press were helpful. Two types of ramping were performed in order to test the effect on feature replication:

1. Application of force commenced after the lower platen reached 105°C in order to ensure that the PMMA substrate was sufficiently moldable.
2. In the first stage, the force was ramped to 100 lbs as the temperature also ramped to 95°C and in the second stage, the remainder of the force was applied as the temperature reached the final peak temperature.

Feature replication/distortion was not sensitive to the type of force ramping as differences were not observed.

Reflow on PMMA: Lower platen temperatures higher than 115°C produced a noticeable "reflow" of the PMMA both around the features and on featureless areas. Figure 21 illustrates this effect on the PMMA replica of the channel in the blue rectangle of Fig.19. Figure 20 shows the SU-8 channel profile where the height and width are found to be 100um and 400 um respectively.

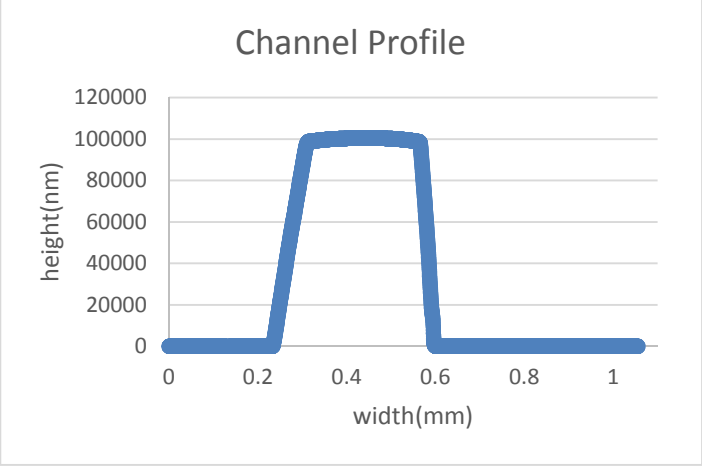

Figure 20: Profile of 100um tall channel marked by the blue rectangle of Fig. 19

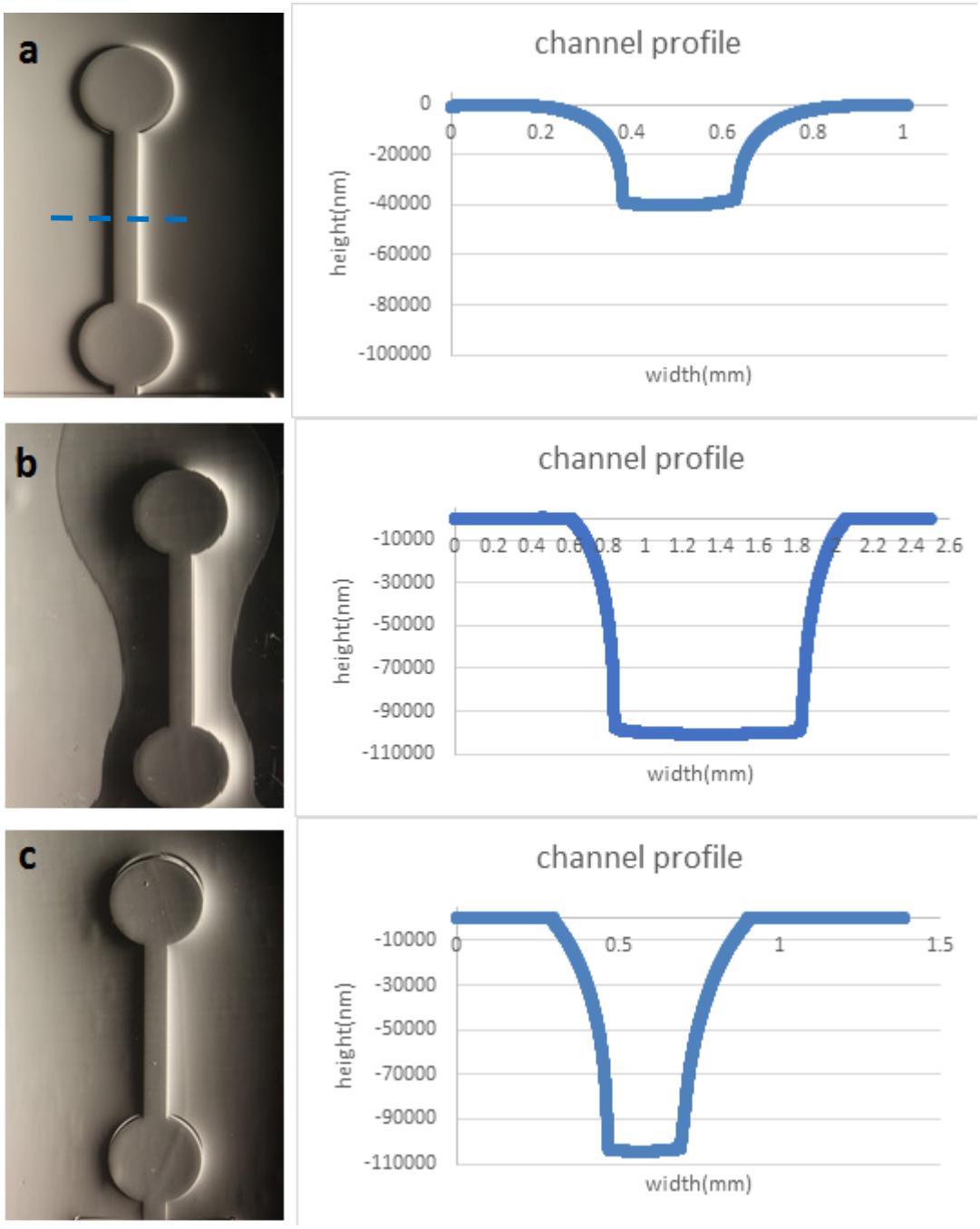

Figure 21: PMMA replica of mold at (a) 115 °C and force of 230 lbs (channel height 40um) (b) 120 °C and force of 210 lbs with reflow (channel height 100um) (c) another section of the same PMMA piece without reflow(channel height 104um).

At 115°C, the height of the PMMA channel is 40 um whereas at 120°C, it is exactly reproduced with 100 um height. But the reflow distorted the channel edges and therefore the width. Interestingly, another section on the same PMMA piece which did not have visible reflow had a

channel of height 104um. This may have been caused by decrease in PMMA height locally due to uneven reflow.

A temperature of 110°C and a force between 220-250 lbs is a reasonable compromise between fidelity of replication, surface roughness and master wear. An embossed PMMA piece without any reflow and minimal roughness is shown in Fig. 22.

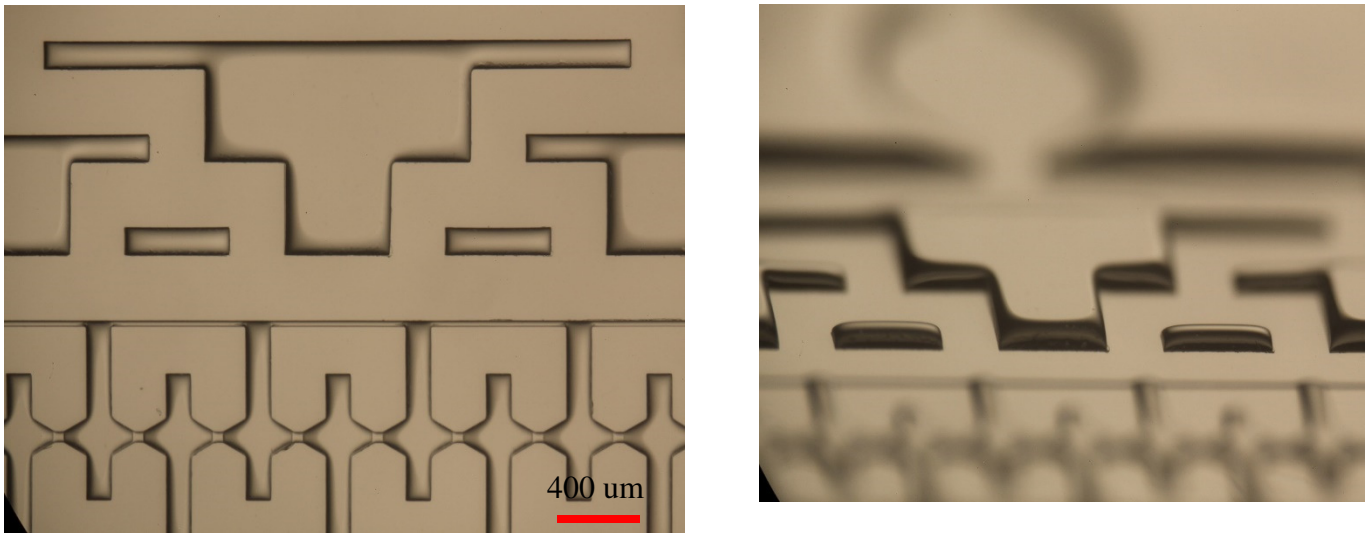

Figure 22: Mold (left) and corresponding pattern (right) produced on PMMA with hot embossing at a temperature of 110 °C and force of 220 lbs

3.5 AZ-50XT as a mold

PMMA embossing of the Quake valve flow channel molds created from AZ-50XT resist on a 3 inch silicon wafer (pattern shown in Fig.26) was carried out using the same process as described in the previous section. As seen from Fig.23, the height of the mold channel is 52 um and the height of the corresponding embossed PMMA channel is 44 um which represents a feature reproduction of 85%. The edges of the PMMA channel are not sharp but display a slope that increases the width and affect the surrounding area.

AZ-50XT exhibited more robustness as a mold since the adhesion to the silicon wafer was not affected by higher ramp rates of temperature. A ramp rate of up to 250°C/hr was used without any apparent effect (molds did not peel off wafer upon deembossing). Higher force of compression (up to 400 lbs) could also be applied for AZ as compared to SU-8. This may imply a higher compressibility of AZ hard baked photoresist.

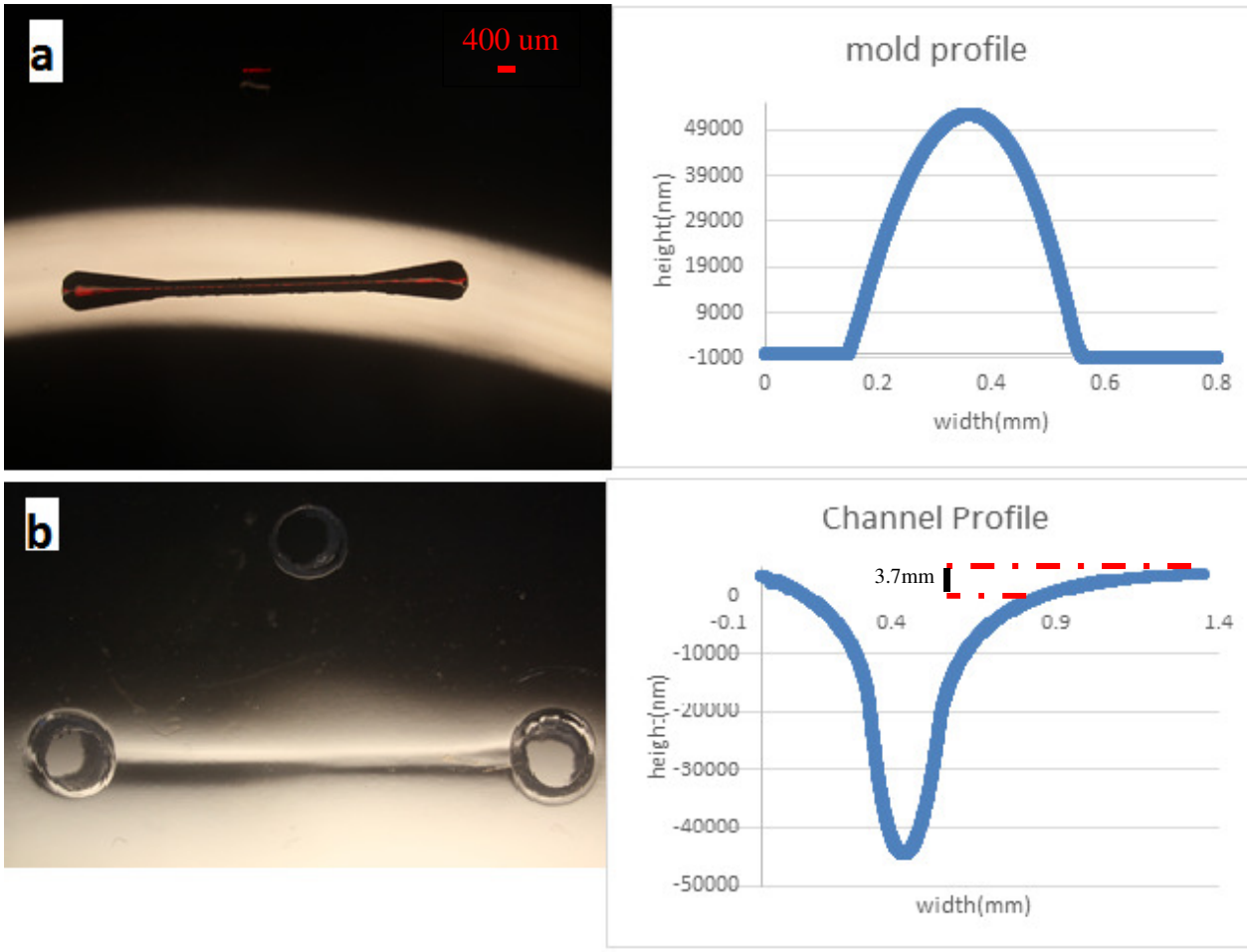

Figure 23: a) AZ-50XT mold of 400um wide channel and corresponding profile. The rounding can be clearly seen. b) PMMA channel embossed at 112°C and force of 240lbs with holes drilled for inlets. Although the rounding has been reproduced, the edges are not sharp and are raised by approximately 3.7mm from the surface.

The pressure and temperature of different embossing trials were plotted against the replication ratio (embossed PMMA height/mold height) as illustrated in Fig.24. For the AZ molds, pressure was not a significant factor in better replication as even lower pressures produced channel heights that were closer to the mold heights as compared to higher pressures. Although the SU-8 plot shows that a temperature of 120°C produced the best height replication, these trials were associated with reflow as depicted in Fig.21. Taking into account fidelity of feature reproduction and PMMA surface distortion at edges/surrounding the channels, temperatures between 110°C-112°C and force between 210-230 lbs offer the best embossing outcomes.

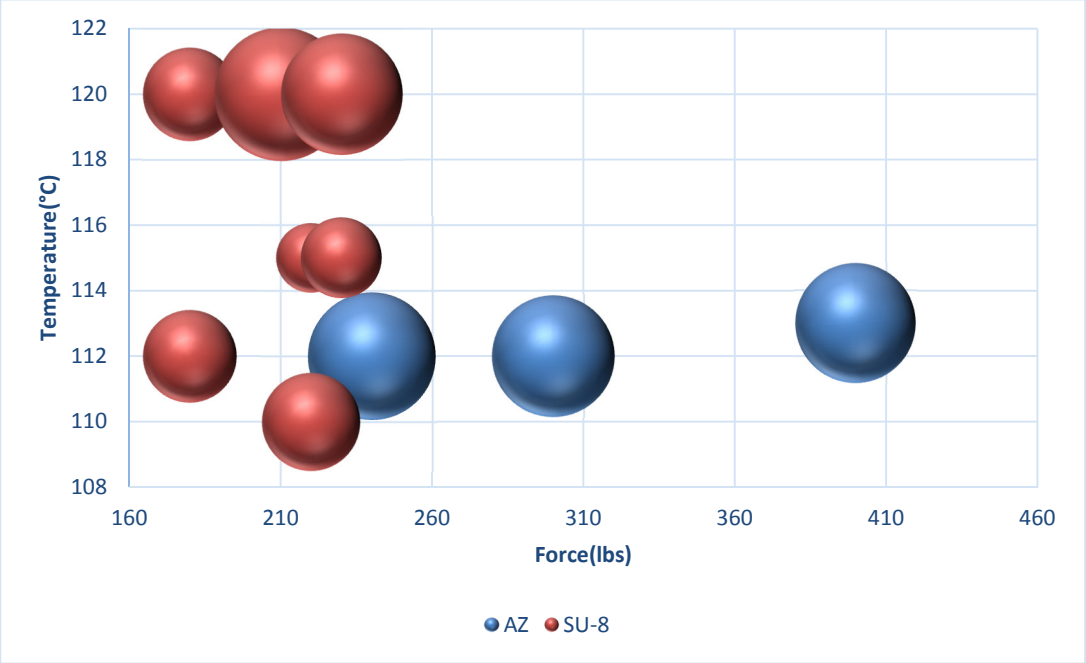

Figure 24: Replication ratio for AZ-50XT and SU-8 molds plotted against temperature and force of the process. Size of bubble indicates how close the replicated feature heights are to the mold heights.

In the next chapter, the application of hot embossing and laser engraving to fabricate two types of pneumatic valves are explored.

4. Single pneumatic valve fabrication and characterization

In order to construct larger circuits using pneumatic valves, the characteristics of a single valve need to be analyzed and optimized. There are two types of valves depending on mode of operation: normally opened and normally closed. The normally opened Quake valve is examined first followed by the normally-closed valve.

4.1 Design of open-at-rest valve based on Quake architecture

An open-at-rest or normally opened valve is a 3-layer device consisting of a rounded channel layer, an orthogonal channel layer to apply pressure control and a membrane layer separating them. The structure is shown in figure 25. These valves were first produced by Dr. Stephen Quake at Caltech using PDMS as the material and soft-lithography as the fabrication process.

The Quake valve was the first demonstration of round cross section channels using soft lithography. A specific category of photoresists capable of reflow during the hard bake step of mold fabrication is utilized. In the paper published in Science Reports titled "Monolithic Microfabricated Valves and Pumps by Multilayer Soft Lithography" by Dr. Quake, the Shipley SJR 5740 photoresist is used in the process. It is spun at 2000 RPM and patterned with a high resolution mask to produce channels of 10 µm in height. When baked at 200 ^{0}C after the development step, photoresist reflow causes the rounding of the inverse channels. The valves were stated to completely close at 5.8 psi (40 kPa) applied pressure in the control channel.

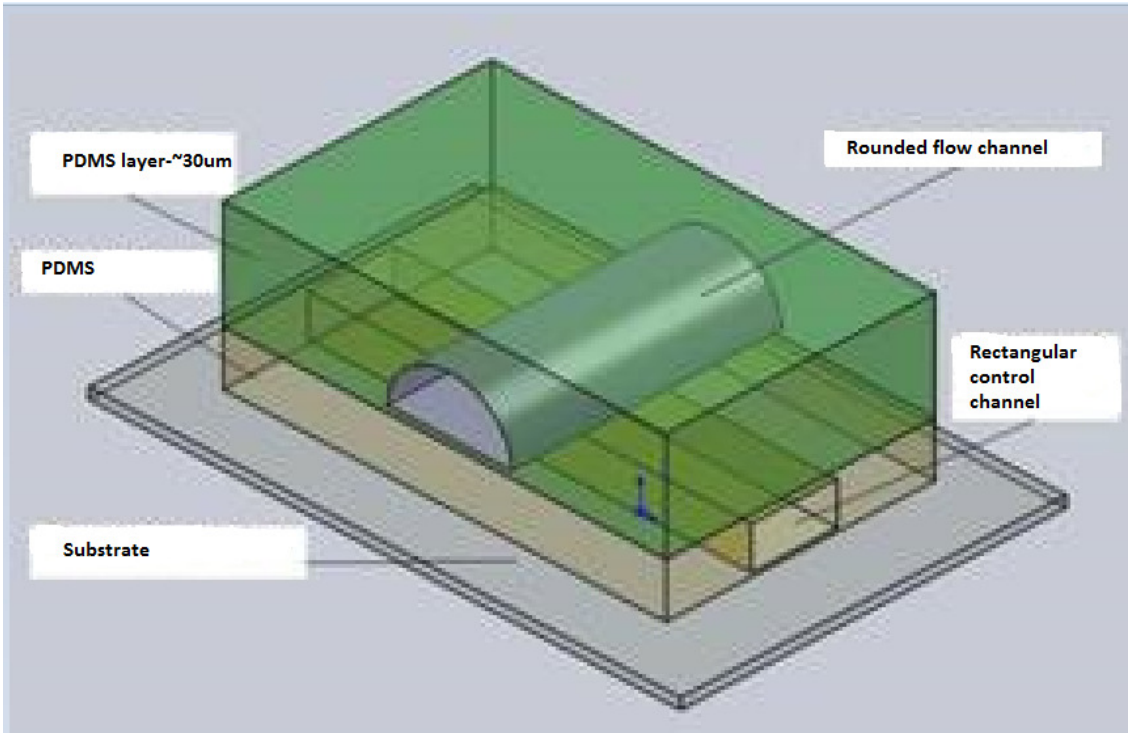

Figure 25: Manufacturing steps of Quake valve - Image reproduced from https://stanford.ilabsolutions.com/service_center/show_external/22/microfluidics-foundry

4.1.1 CAD design of valve layers

The flow and control layers designed using AutoCAD are cross-channel structures of different dimensions as shown in figures 26 and 27.

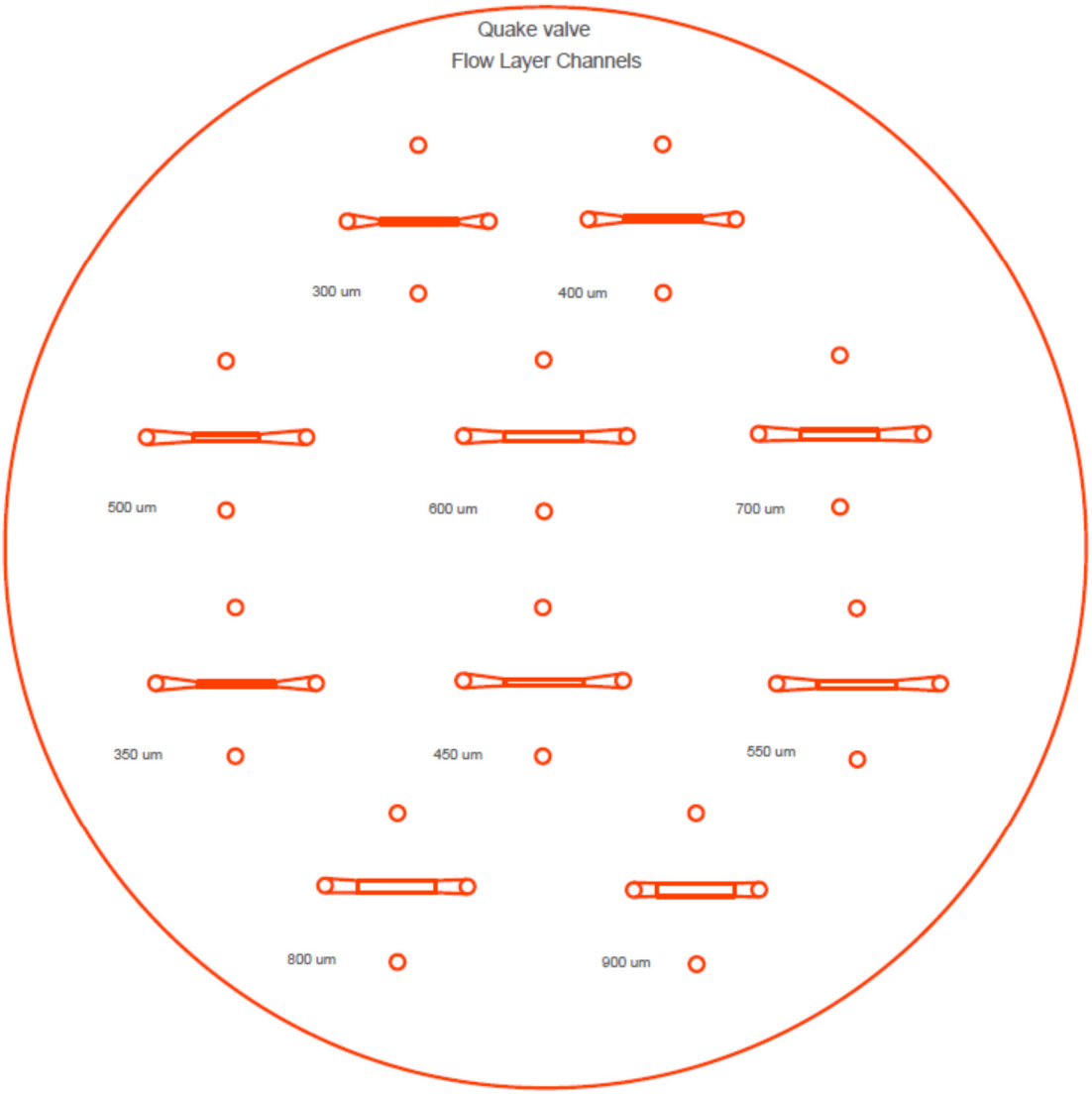

Figure 26: AutoCAD drawing of flow layer channel of Quake valve of widths ranging from 300um-900um

This array of channels ranging from a width of 300um-900um was designed with the intention of evaluating the resistance offered by the valve and the longer-length channels from which they are formed. Although these dimensions are feasible for valves, they are not typical Quake valves and are not desirable for high density microfluidic structures.

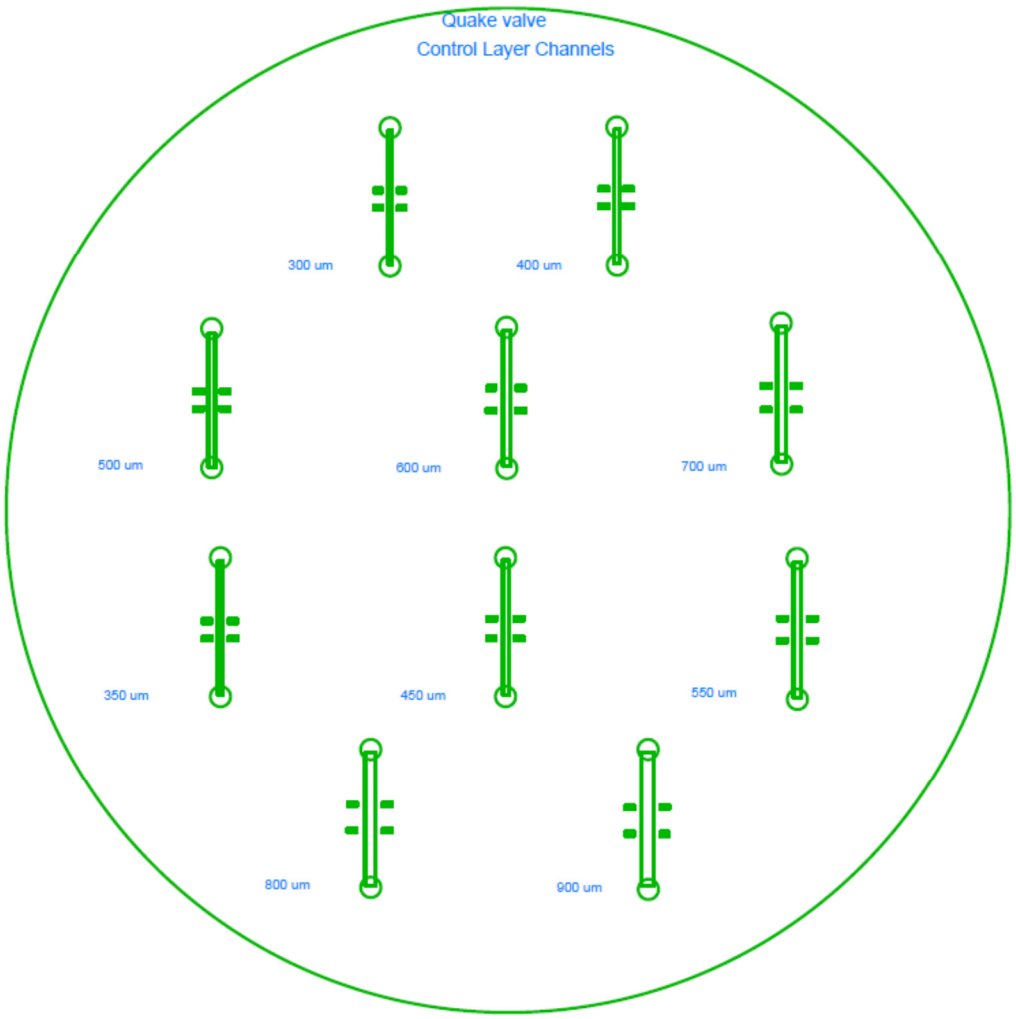

Figure 27: AutoCAD drawing of control layer channel of Quake valve of widths ranging from 300um-900um.

4.1.2 Fabrication of flow and control layer molds on silicon wafer

Master molds for Quake valve layers are required both for soft lithography and hot embossing process. For the control layer, SU-8 2075 resist was used to create the different-dimensioned channels. The flow layer requires a resist capable of reflow upon hard bake. AZ-50XT was identified for this purpose. The important properties of AZ-50XT are outlined below:

- Positive resist with 50-80um single coat capability and 120um double coat capability
- 3 to 1 aspect ratio with good sidewall profiles
- Compatible with existing thick film processes
- Used with inorganic developers such as AZ421K or AZ 400K (1:3)

As a first step, the CAD files described in the previous section were translated to masks on a transparent sheet (CAD/Art Services Inc.).

The procedure for mold fabrication for the two resists are outlined below:

a. SU-8 Mold

Steps:

I. Photoresist spinning and baking

1. Pour a small amount of SU-8 2075 resist on the wafer and spin-coat using the recipe corresponding to the thickness of the feature desired.
2. Soft bake for a duration corresponding to the thickness of the resist and allow to cool.

II. Photolithography

1. Expose to UV radiation for a time period $T=\frac{\frac{mJ}{cm^2}\ mentioned\ in\ datasheet}{power\ of\ radiation}$
2. Develop in SU-8 developer solution (Propylene glycol monomethyl ether acetate)
3. Final rinse with IPA and nitrogen gun for drying

III. Post-development hard bake at 200 °C for 3 hours with a ramp from room temperature at 60°C/hr

b. AZ mold[23]

Steps:

I. Photoresist spinning and baking

1. Prebake 3 inch silicon wafer for 5 minutes at 110°C on hotplate and allow to cool.
2. Pour small amount of AZ 50XT resist on the wafer and spincoat using the following recipe:
   a. 200 rpm for 5 sec @ 200 rpm/s
   b. 750 rpm for 30 sec @ 110 rpm/s
   c. 2750 rpm for 1 sec @2000 rpm/s
3. Wait for 10 minutes for the resist to stabilize
4. Soft bake on hot plate: room temperature to 65 °C with a ramp @ 350 °C/hr, 65-112°C with a ramp @ 240 °C/hr for 25 min and then back to room temperature
5. Rehydrate overnight

II. Photolithography

1. Expose to UV for 113 sec three times (4.75W is the power of the radiation for Myriad System 2001 Mask Aligner) with 20 seconds pause in between
2. Develop the wafer in 1:3 AZ300 developer solution for 30 minutes replacing the solution after 15 minutes.
3. Rinse with DI water

III. Hard bake

Hard bake the wafer on a hot plate for 4 hours at 190°C with a ramp of 10°C/hr. The reflow of the resist is visible after the hard bake.

4.2 Manufacturing Quake valve using laser cutting

The drawing file provided as input to the laser cutter essentially had orthogonal lines of different thicknesses for the flow and control channels. A range of channel widths (60-100um for vector cuts and 120-400um for raster) were produced through experimentation and the profiles measured using a profilometer (Bruker DektakXT). Vector cuts of width 60 um and less were too narrow to be accurately measured by the stylus tip of the profilometer (2um). A channel designed to be 65umx67um was found to be of approximate depth 80um and width 100um. The resistance offered by this channel was high enough to cause a significant pressure drop when a pressure of up to 10 psi was applied at one end and measured at the other end. The pressure measured at the outlet remained at 0 psi. When bonded to a PDMS membrane of thickness 50um using the APTES method and a second channel (118umx265um) bonded on top to form a valve structure, no deflections were observed in the valve area when pressure was applied to the inlets. To obtain lower resistance, wider channels were made by using raster mode of cutting. The smallest valve area for which deflections were observed was 400umx600um.

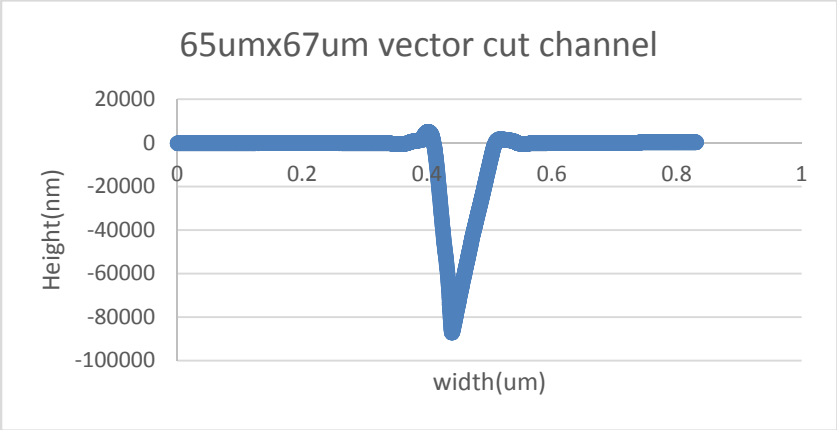

Figure 28: Profile shows almost triangular cross-section of channel with a difference in width and depth of 30um and 15um respectively from designed value

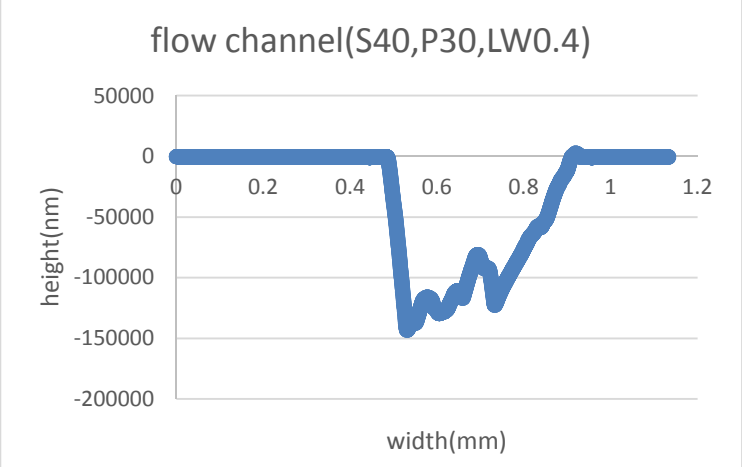

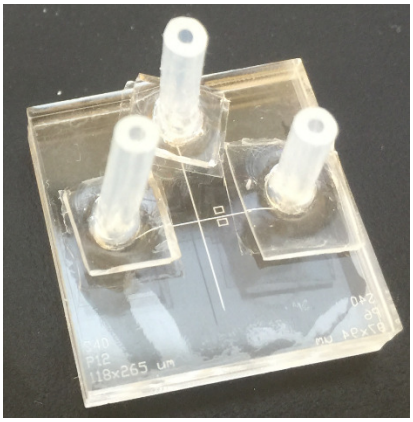

Figure 29: Raster cut flow channel profile (left) of final device (right)

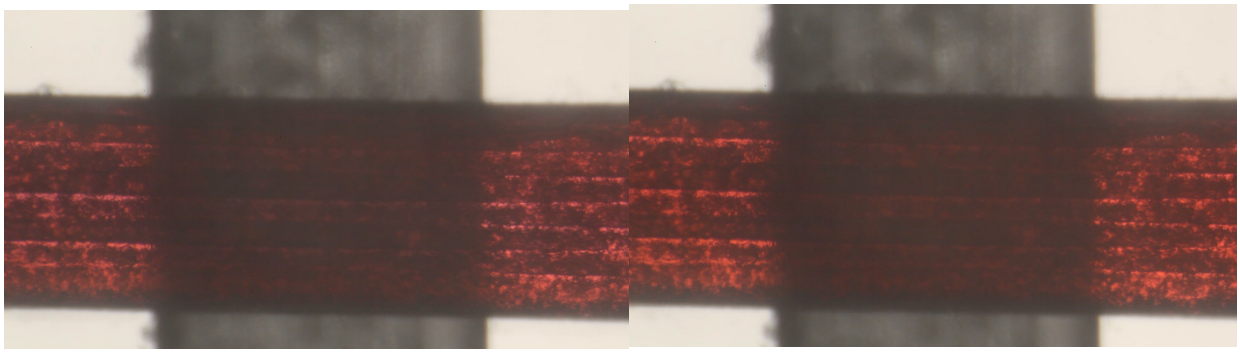

Figure 30: Closed (left) and open (right) states of the valve when switched between 8.5psi and 0psi of control pressure and 3 psi flow pressure of red-colored DI water. The contrast in the colors indicates a difference between the two states.

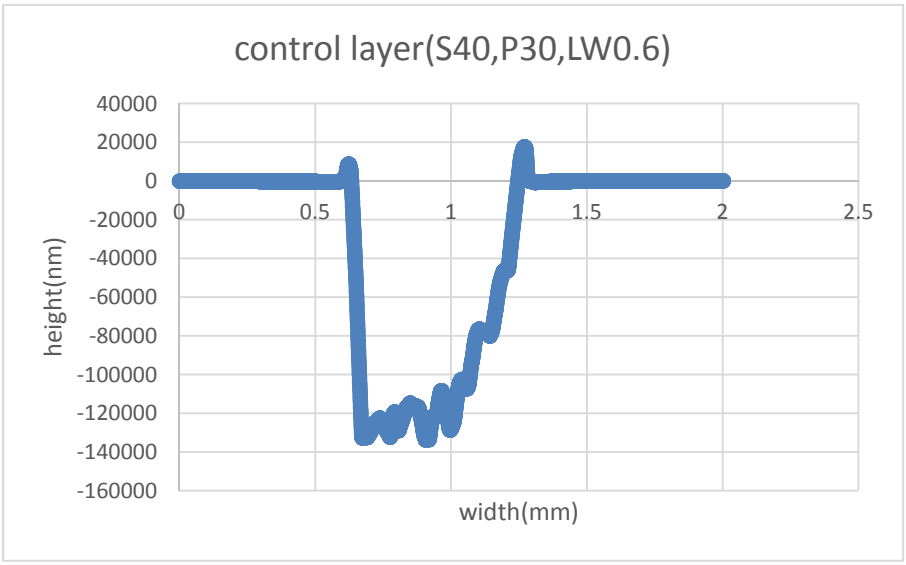

Figure 31: Raster cut control channel of valve of width 600um and maximum depth 133um

Dyed deionized (DI) water was flowed through the channel and pressure applied to the control channel for clear observation of the valve area since the roughness of the surface created difficulties in observing through the microscope with air as the flow medium.

As Fig.30 illustrates, when dyed DI water is passed through the flow channel, the opening and closing of the valve can be seen, although the closing is not complete at 8.5psi control pressure. As the roughness in the flow channel surface is close to 60 um, a complete closure may not be possible in case of liquid medium, in spite of taking into account the elasticity of thin PDMS membranes (30um or less).

To measure the characteristics of the flow channel at different degrees of closure, a pressure gauge was connected to the outlet of the channel. With a constant air flow pressure applied at the input and control pressure varied from 0-14 psi, the output pressure was measured and plotted in Fig.33. It shows that with air as a medium, it is possible to close the channel completely at low flow pressures. These valves could be used to make larger pneumatic logic circuits.

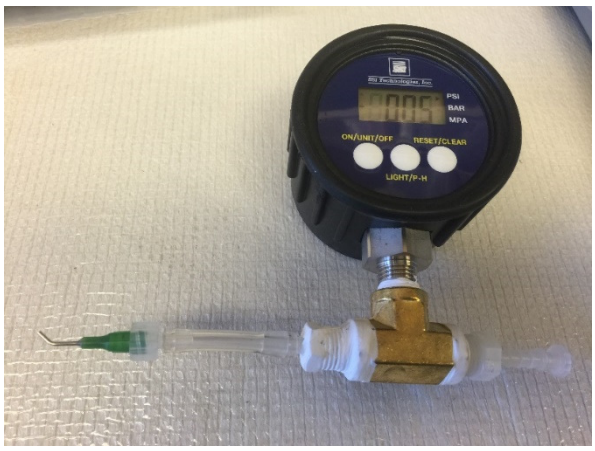

Figure 32: SSI Technologies gauge with precision 0.01 psi to measure air pressure

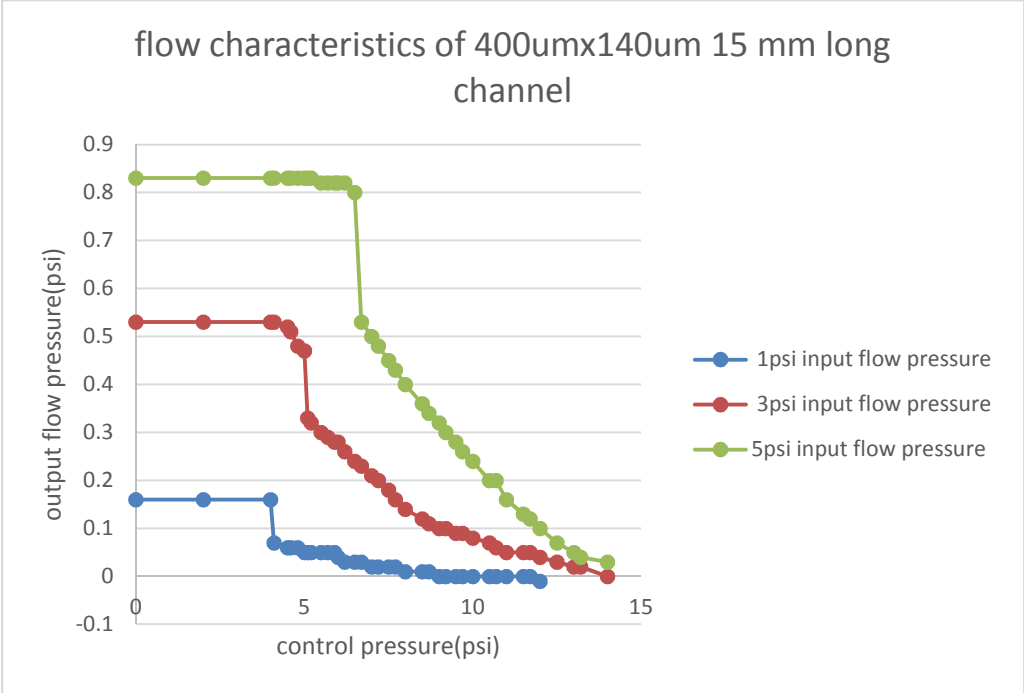

Figure 33: Valve open to close pressure change of flow channel output as control pressure is increased.

Calculation of Channel Resistances[24]:

The pneumatic resistance of a channel depends on its geometry and can be expressed as:

1. For a circular cross-section:

$$R_p = \frac{8*\mu*L}{\pi*r^4}$$ where L is the total length and r is the radius ..... **(1)**

2. For a rectangular cross-section:

$$R_p = \frac{12*\mu*L}{w*h^3(1-\frac{0.63h}{w})}$$ where w is the width, h is the height and h<w ..... **(2)**

The flow channel of the Quake valve whose profile is depicted in Fig. 29 is approximately rectangular and h<w. Therefore, we can estimate the channel resistance using equation 2 in order to quantify the loss of pressure with changing cross section as pressure is applied in the flow channel.

The channel resistance calculations are shown below:

For L=15000um,w=400um,h=115um, μ=18.27uPa*s, [open channel]

$R_p = 7x10^9$ Pa.s m^{-3}

For L=15000um,w=400um,h=57.5um, μ=18.27uPa*s, [half-open channel]

$R_p = 47x10^9$ Pa.s m^{-3}

Correlating these values with Fig. 33 we can estimate that a control pressure of approximately 12 psi is required in order to close the channel to half its height and then an additional 4 to 5 psi to close it completely.

4.3 Manufacturing Quake valve using hot embossing

Molds of the Quake valve design represented by the flow and control layer channels in the CAD files of figures 26 and 27 were first made on silicon wafers. The flow layer mold was fabricated using AZ-50XT photoresist as rounded-roof channels were required and for the control layer, the photlithography process for SU-8 2075 photoresist was followed as detailed in section 4.1.2.

The Carver press was used with embossing parameters as determined in Chapter 3 to emboss the valve layers. Embossed channel dimensions had a good fidelity to mold dimensions. Bonding of the PMMA layers to PDMS of thickness 50um (spun on Mylar) was carried out to form the valve as shown in Fig.36. Many iterations of bonding were carried out as several challenges were faced, including inconsistent bonding and occlusion of the membrane to the flow channel roof. The low aspect ratios responsible for the latter effect were attributed to the uneven pressures applied during the embossing. This was later found to be a drawback of the Carver press due to which modifications to the embossing set-up were experimented with.

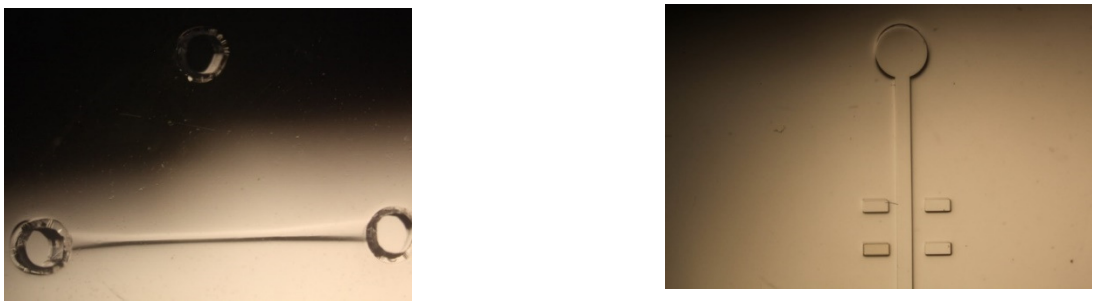

Figure 34: Embossed (left) (110°C, 250lbs) flow channel of dimension 300um(W)x35um(H) with holes drilled for inlets; Embossed (right) control channel (113°C, 270lbs) of dimension 500um(W)x47um(H)

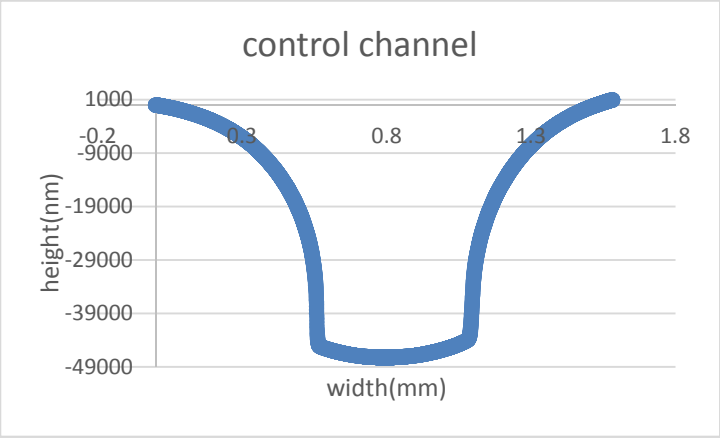

Figure 35: Control channel profile indicating sloping sidewalls that affect bonding area with flow channel

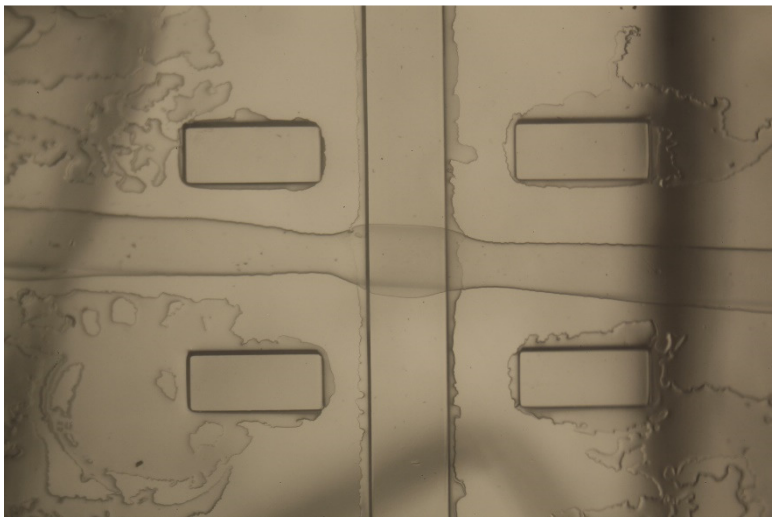

Figure 36: Bonded Quake valve with membrane of thickness 50um

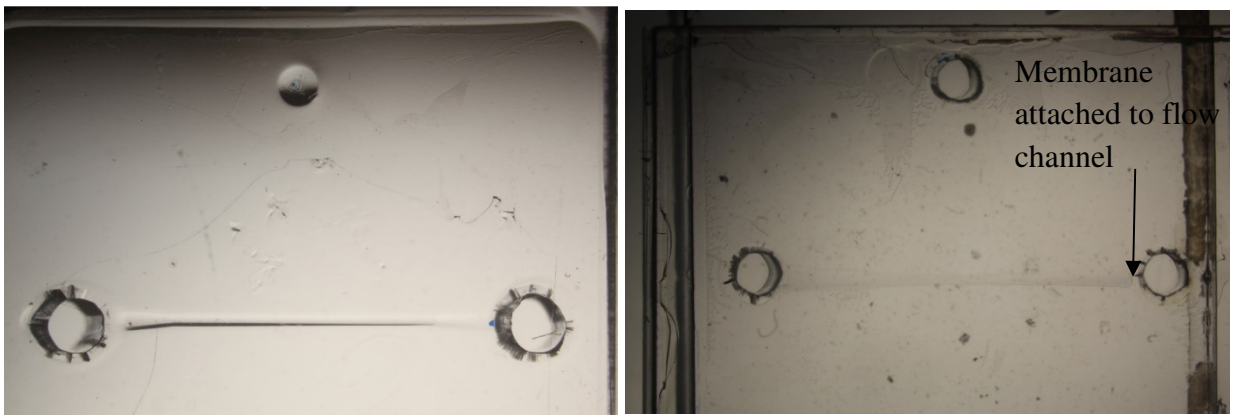

Figure 37: Partial bonding (left) and occlusion (right) of the flow channel blocking air flow

In Fig.37 the bond between the PDMS and PMMA is weak, leaving sections un-bonded. Occlusion of the flow channel causes the bonded pieces to be discarded as they cannot be used for making complete devices with the remaining PMMA layer.

4.3.1 Increasing the uniformity of embossed features

The occlusion of channels and low fidelity of reproduction of channel heights was attributed to the uneven application of pressure on the substrate-mold sandwich by the upper platen of the Carver press. In order to ensure better outcomes of the hot embossing process, a compressible material inserted below the wafer that would compensate for the unevenness was considered. A square rubber piece of thickness 6mm (greater than or equal to twice the substrate thickness) was identified and a thin aluminum plate of thickness 1mm was placed on top of it for the purpose of support for the mold wafer of thickness 200um (Fig. 38). The mold-PMMA combination is placed on top of the aluminum and the Teflon sheet is placed last.

This setup increases the time required for the mold to reach T_g. Temperature measurements using a thermocouple inserted under the mold confirmed the approximate temperature so that pressure could be applied at the right time.

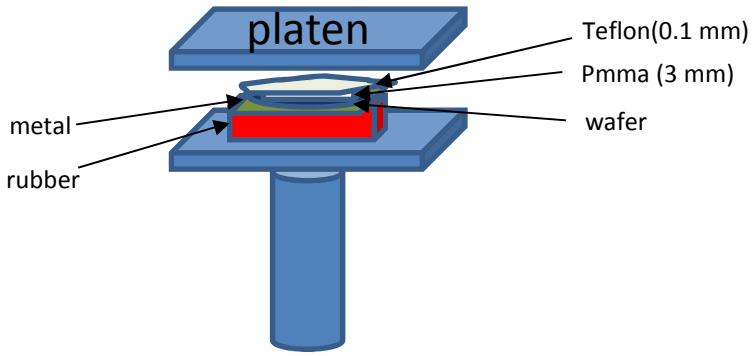

Figure 38: Set-up for improving uniformity of applied pressure on substrate

The outcome of the trials with this setup were dependent on the mold pattern. The density of features of the flow and control layer mold wafers was comparatively less with plenty of space between the different-sized channels. This led to breakage of the mold. In case of the oscillator channels (described in the next chapter), where the density of channels and features are much higher, the molds could be used for several trials without breaking.

4.4 Monolithic membrane normally-closed valve structure

A normally closed valve is a three-layered device consisting of a discontinuity in a channel caused by a feature created on a layer of material (usually glass/polymer termed as the flow layer) on a

membrane (usually PDMS)[25]. The bottom layer, called the control layer, consists of a displacement chamber into which the PDMS gets pulled when a vacuum is applied to open the channel.

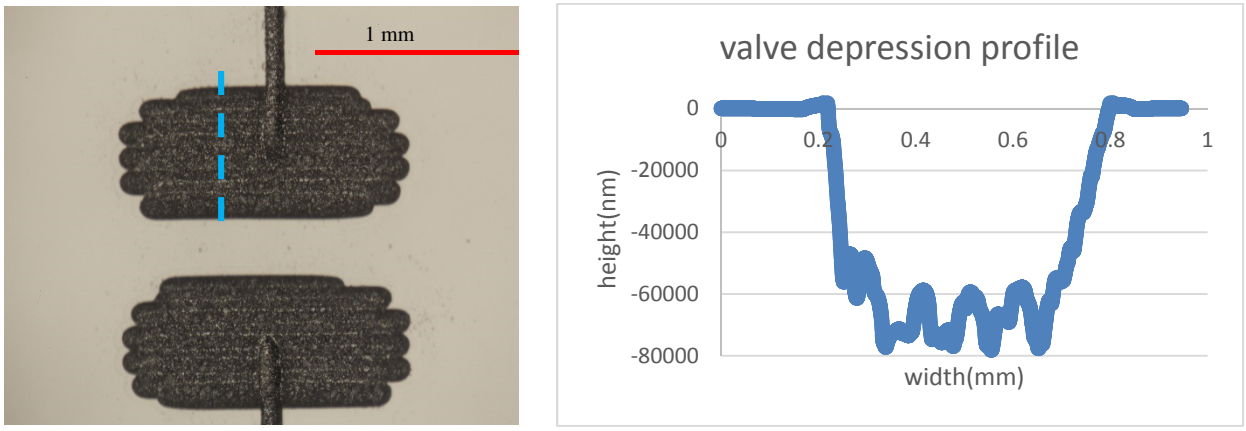

Figure 39: Laser-cut normally closed valve (left) and profile (right) of the valve flow channel depression showing a surface roughness of 20um

The valve is closed (channel sealed) when the pressures at the channel input and control inputs are equal. When vacuum is applied to open the channel, the pressures at the input end and output end are equal.

4.4.1 Laser-cut normally closed valve based inverter

A digital inverter in the electronic realm can be built from an N-type MOSFET and a pull-up resistor as depicted in Fig.40. The microfluidic equivalent of the inverter based on the normally-closed valve is also shown. A high input (vacuum) produces a low output (atmospheric pressure) and vice versa. The closed channel is opened when vacuum is applied at the control input to deform the valve membrane, thus connecting the output to atmospheric pressure. When the control input is at atmospheric pressure, the output is connected to vacuum through the pull-up resistor. The resistor allows for a pressure differential to be sustained between the vacuum source and the output.

An estimation of the pressure drop across the pull-up resistor was obtained by applying a positive pressure at the supply inlet of the inverter and measuring the pressure at the output of the inverter. A digital pressure gauge was used for this purpose. Measurements were taken with the valve open and closed as listed in Table 8. The small output pressure difference of 0.01 psi between open and closed states of the valve indicates that the valve offers a very small resistance.

Table 8: Output pressure levels of inverter at different input/control pressures

Input(psi)	Control (psi)	Output(psi)
8	0	0.01
	-8	0
9	0	0.01
	-8	0.01
10	0	0.02
	-8	0.01
11	0	0.03
	-8	0.02

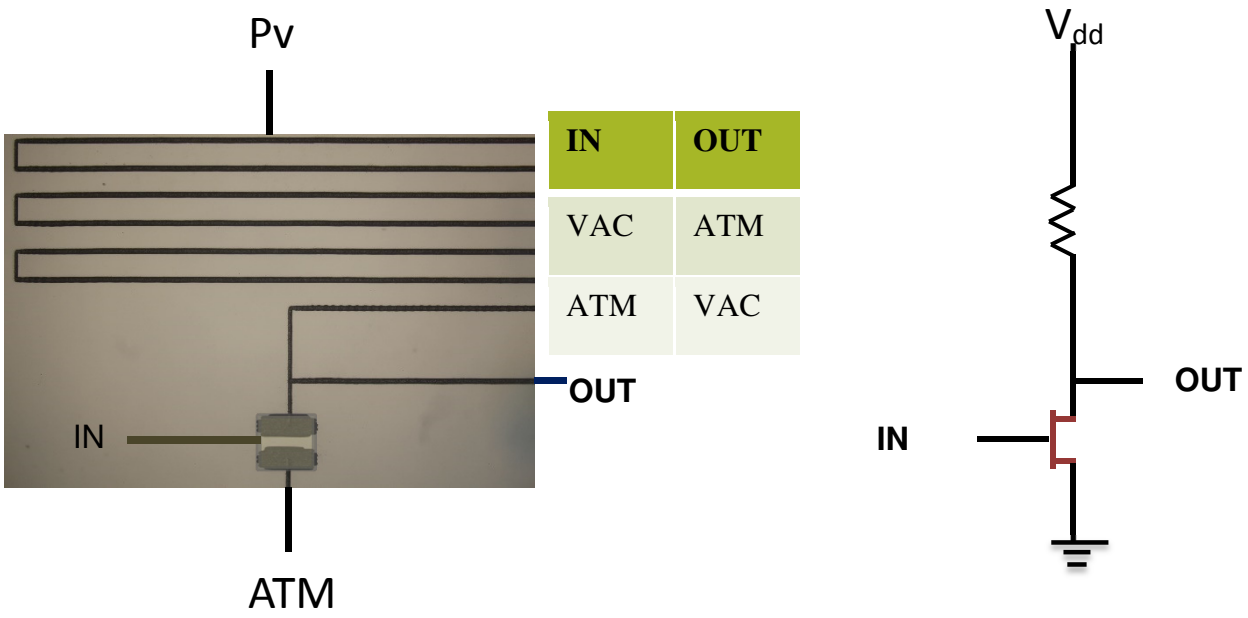

Figure 40: Laser-cut inverter on PMMA (left) with logic output table and equivalent NMOS inverter (right)

Using this inverter structure, pneumatic oscillator circuits are constructed as described in the next chapter.

5. Pneumatic ring oscillator circuit

A timing reference is required for any sequential logic circuit (eg.,counter). The oscillator is a circuit generating a clock signal that can be used to drive the rest of the logic on a chip. Oscillators can be constructed in different ways. This chapter focuses on describing the microfluidic oscillator circuit design based on the classical ring of inverters configuration.

5.1 Basic configuration and design parameters determining frequency of oscillation

An electronic ring oscillator consists of an odd number of inverters connected in a feedback loop. A 3-stage design is the basic configuration as shown in Fig.41. The oscillations are initiated by noise in the system which gets amplified with each propagation around the loop until the output exhibits a swing approximately equal to the supply voltage. Frequency of oscillation is determined by the time delay of each stage. In general, for a number of stages N of inverters and a time delay T_D of each stage,

$$\text{Frequency of oscillation } F_{osc} = \frac{1}{2*N*T_D}$$

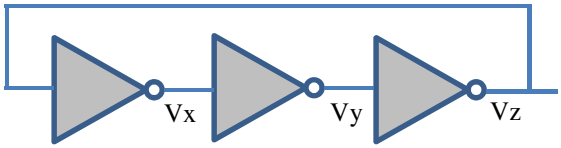

Figure 41: Schematic of 3-stage ring oscillator with an inverter supply voltage of V_{DD}

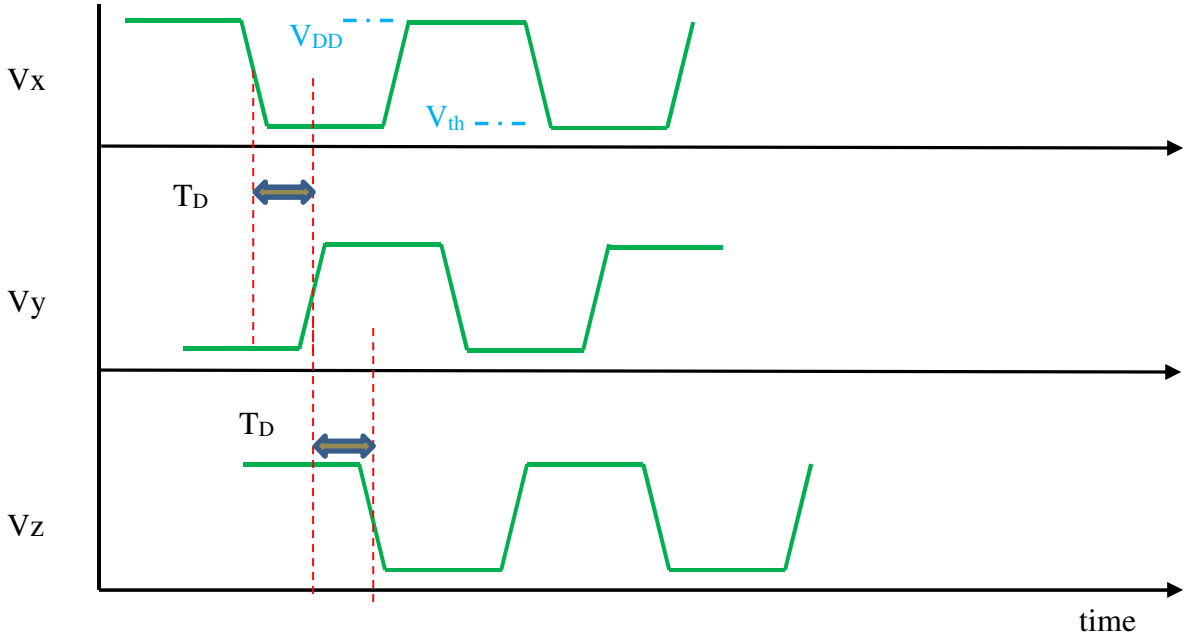

Figure 42: Timing diagram for ring oscillator

5.2 Implementing ring oscillator with Quake valve based inverters

As explained in section 4.1, the Quake valve is an open-at-rest valve that is closed by applying pressure in the control channel. An inverter based on this valve is the microfluidic equivalent of an electronic P-type MOSFET as shown in Fig.43. The pressure outlet connected to the output port of each inverter (either through a resistor or without one) can be the atmosphere or a pressure value less than P_s depending on the pressure differential required between P_s and the output. Connecting three such inverters in a ring configuration will make an oscillator. A condition for valve control pressure of each inverter stage that needs to be fulfilled in order for such an oscillator to function is

$$P_{control} >= P_{flow} + \text{actuation pressure}$$

This is not satisfied with normal Quake valves as the output pressure of each stage that acts as the control pressure for the next stage valve will not be greater than the supply pressure P_s. Additional engineering is required in order to produce the gain. Weaver et al.[26] designed such a pressure-gain open-at-rest valve by embedding a disc in the membrane allowing for force summation and thereby pressure amplification.

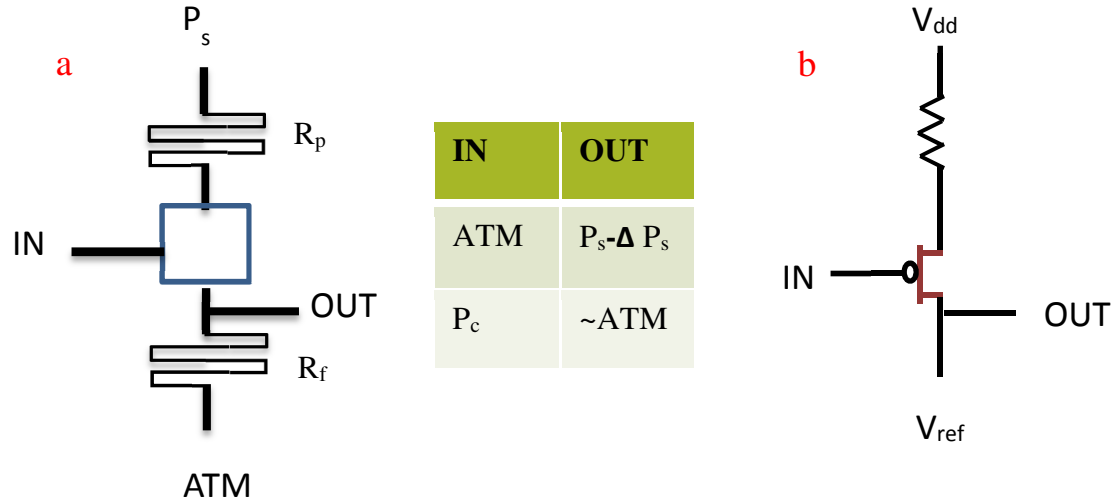

IN	OUT
ATM	P_s-Δ P_s
P_c	~ATM

Figure 43: Inverter (a) based on Quake valve and corresponding logic states of operation. The pressure drop ΔPs is the drop across the resistor Rp plus the drop across the open valve resistance. When a control pressure Pc > Ps- ΔPs is applied, the output pressure is equal to atmosphere when R_f is negligible. The equivalent PMOS inverter is shown in (b).

Although the inverter implemented with the Quake valve cannot make a functional oscillator, for the purpose of analyzing manufacturability, a ring structure as shown in Fig.44 was designed and fabricated in PMMA using different techniques.

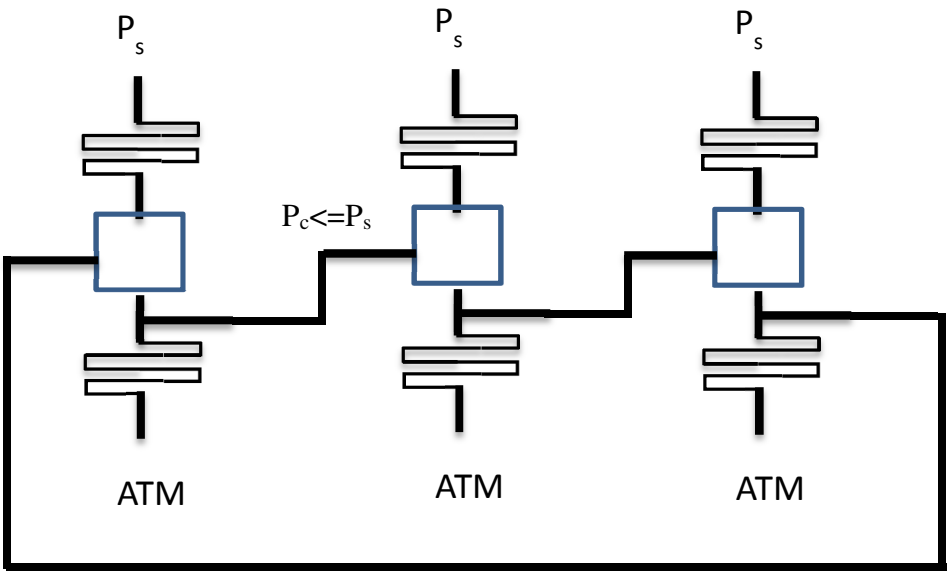

Figure 44: Three stage ring oscillator connected such that output of each stage feeds the control input of the next stage.

5.3 Manufacturing Quake valve based oscillator using hot embossing

For analyzing the ring oscillator architecture with Quake valve inverters, molds for the flow and control layer were made on 3 inch silicon wafers with AZ-50XT and SU-8 resist using the patterns in Fig.45 and 46. Two sizes of channels and valve cross-sectional areas were implemented: 300umx300um and 500umx500um. A capacitor was also incorporated in the feedback loop for one of the designs. Using the hot embossing parameters discussed in Chapter 3, PMMA replicas of flow and control layer were embossed and profiled.

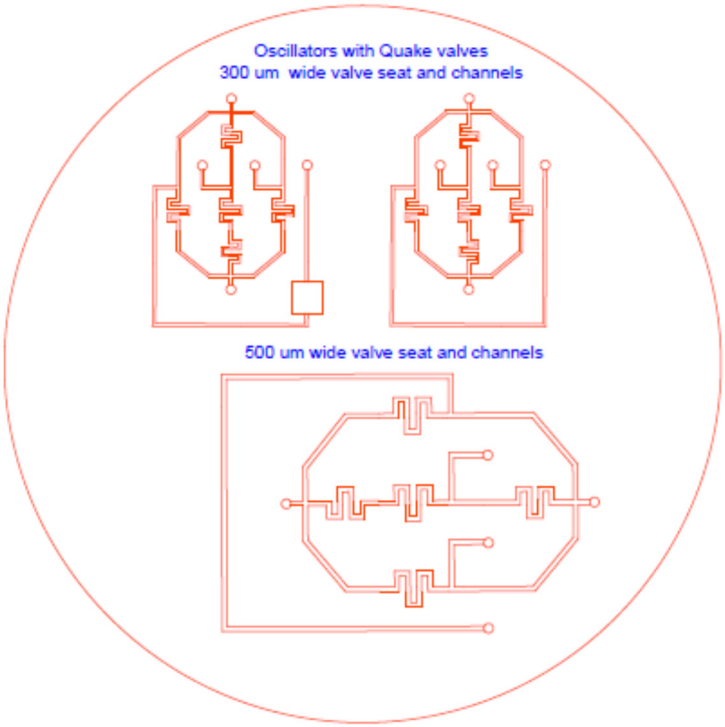

Figure 45: AutoCAD diagram of flow layer of Quake valve inverter based oscillators

Figure 46: AutoCAD diagram of control layer of Quake valve inverter based oscillators

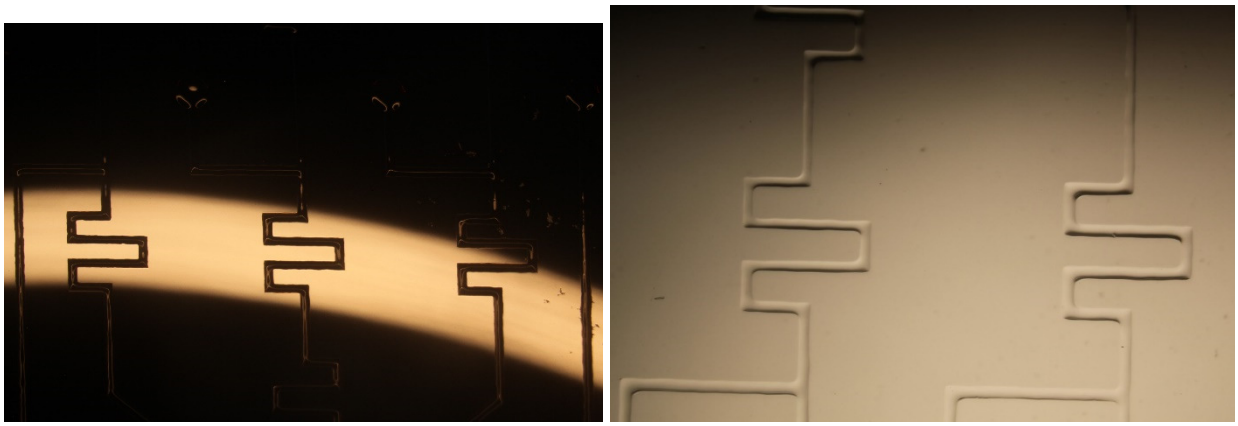

Figure 47: AZ-50XT mold on wafer (left) of oscillator with corresponding embossed pattern on PMMA (right)

Figure 48 indicates that the profile is not uniform across the area of the resistor channels. This is a factor that can affect the resistance and hence the performance of the final device. Figures 49 and 50 show the profiles of the mold and embossed PMMA using the modified setup of the platens. A difference of 3um between the peak heights of the channels along with imperceptible roughness of the PMMA sidewalls demonstrate high fidelity with the mold.

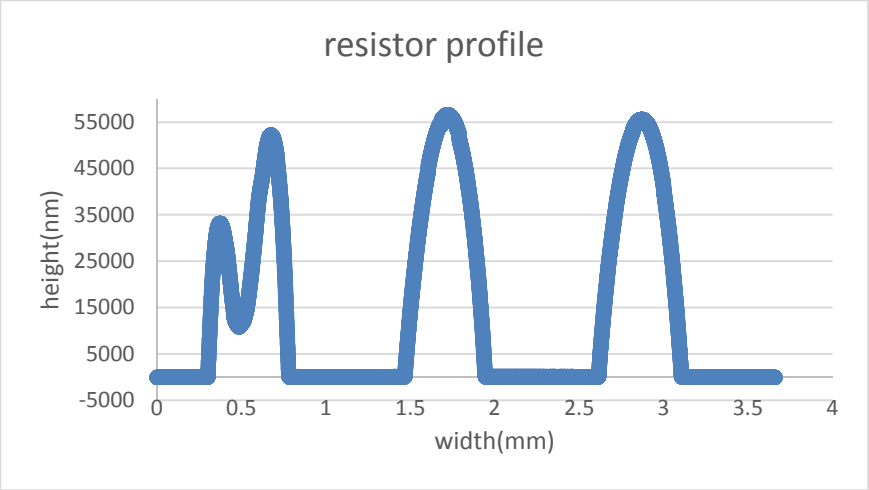

Figure 48: Three sections of resistor channel showing deformation of one section leading to modification of actual resistance

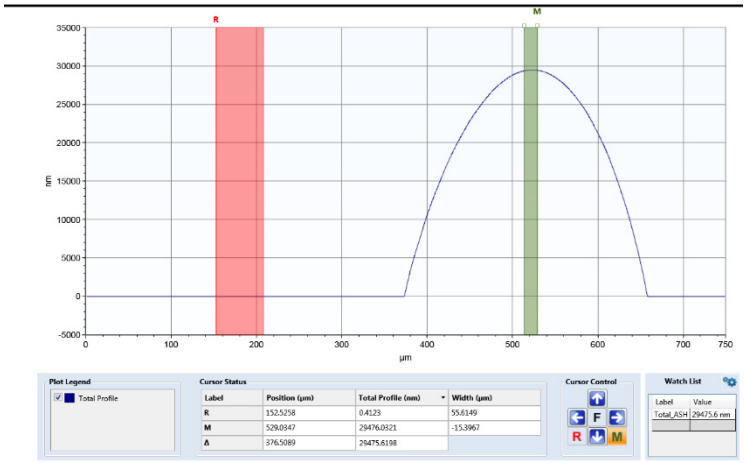

Figure 49: AZ Master mold smaller oscillator flow layer channel profile drawn in Vision64. Rounded roof is reproduced and a peak height of 29.4 um is measured.

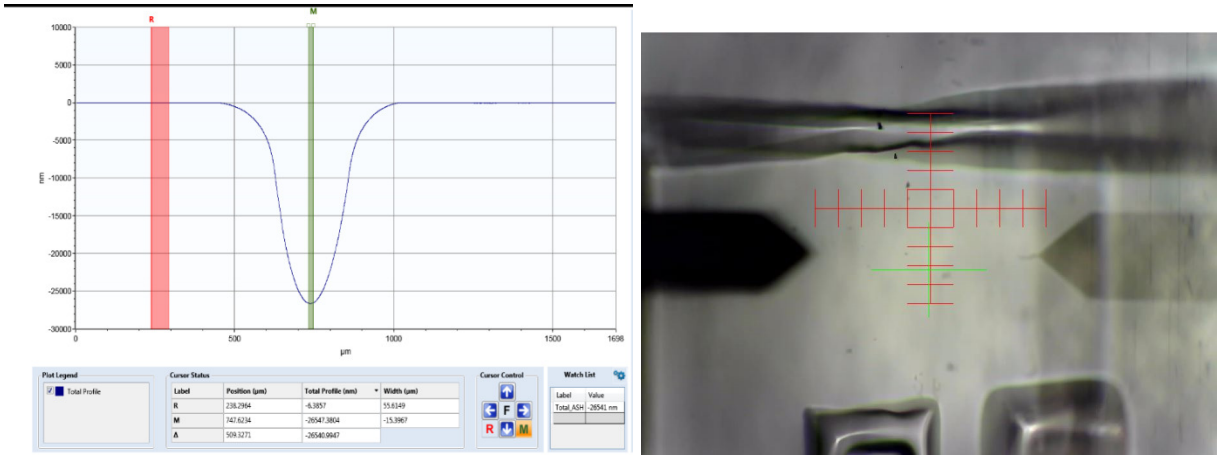

Figure 50: Embossed PMMA smaller oscillator flow layer channel profile drawn in Vision64 at platen temperature 175 °C and 300 lbs force. Peak height is 26.5um.

5.4 Implementing ring oscillator with normally-closed valve based inverters

The equivalent microfluidic circuit implementation consists of three stages of closed-at-rest membrane valve based inverters[27]. In each inverter, the pull-up resistor causes a pressure differential between the vacuum source and the output. Connecting the output of one stage to the next stage's input as shown in Fig. 51 allows for a continuous switching of the states between vacuum and atmosphere. These oscillations will continue as long as the vacuum supply is constant. Time constant of the circuit is proportional to the pneumatic resistance (R) of the pull-up resistor multiplied by the pneumatic capacitance (C) of the valve (which is dependent on the volume of the valve chamber). Hence by controlling these two parameters, the frequency of oscillations can be tuned.

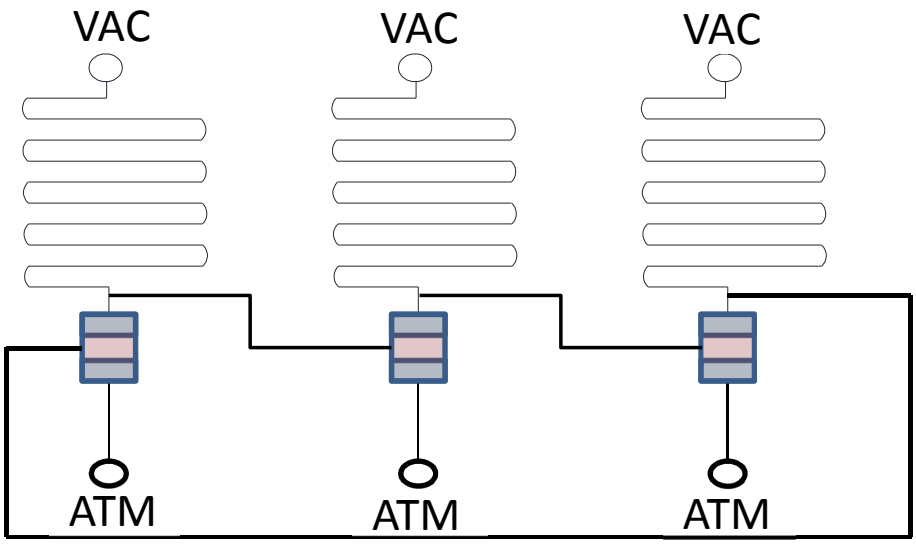

Figure 51: Ring oscillator using three stages of normally closed valve based inverter with vacuum supply and atmosphere ground

5.4.1 Theoretical Model for Compressible Flow

In order to understand the pneumatic ring oscillator operation, the dynamics of a single valve as it switches between the open and close states need to be analyzed as illustrated in Fig.52 and 53. The two parameters that control the frequency of switching are the threshold pressure to open the valve and close the valve.

Let us consider initially that valve 1 and 2 are closed. The source vacuum pulls at valve 2's membrane with a pressure depending on the fluidic resistance Rp. Once the threshold pressure to open the valve is reached, the valve is opened and air is pulled into the valve from the atmosphere. This air flows into the next stage (valve 3) to close the valve once the threshold pressure to close is reached. The flow is governed by Poiseuille's equation for compressible

fluids where it is expressed as a ratio of the change in volume to the change in time. For a compressible fluid in a tube of resistance R, the flow $Q(t)$ is given by:

$$Q(t) = \frac{dV}{dt} = \left(\frac{P1-P2}{R}\right)\left(\frac{P1+P2}{2*P2}\right)$$

Where P1 is the inlet pressure,

P2 is the outlet pressure

R is the resistance of the channel,

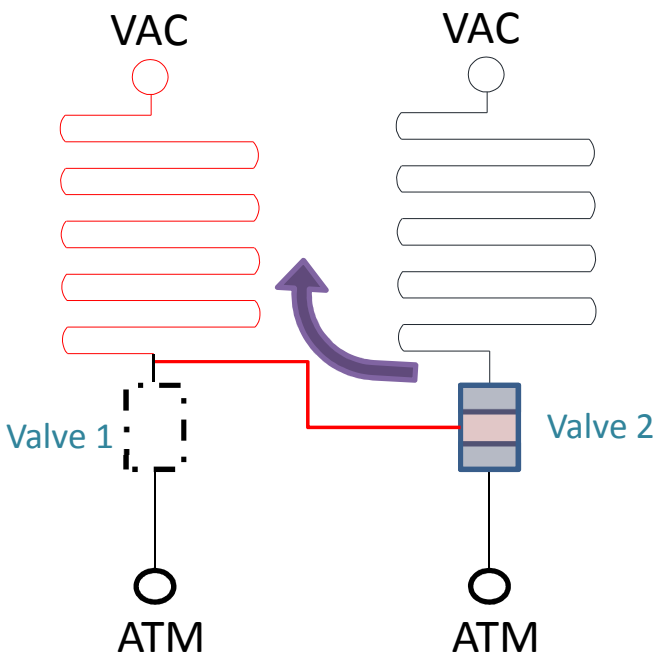

Figure 52: Closed-to-open transition of valve indicates path through the pull-up resistor of previous stage

In our case, P1=vacuum pressure=Ps, P2=chamber pressure = Pvc(t)and R=Rp. Hence the equation becomes:

$$Q(t) = \frac{dV}{dt} = \left(\frac{Ps-Pvc(t)}{Rp}\right)\left(\frac{Ps+Pvc(t)}{2*Pvc(t)}\right)$$

Using this relation, the time period required to open and close the valve can be determined. In general, the time period

$$\tau \propto (R*V)/P$$

where R is the resistance path of the air flow

V is the volume of the valve chamber

P is the pressure applied

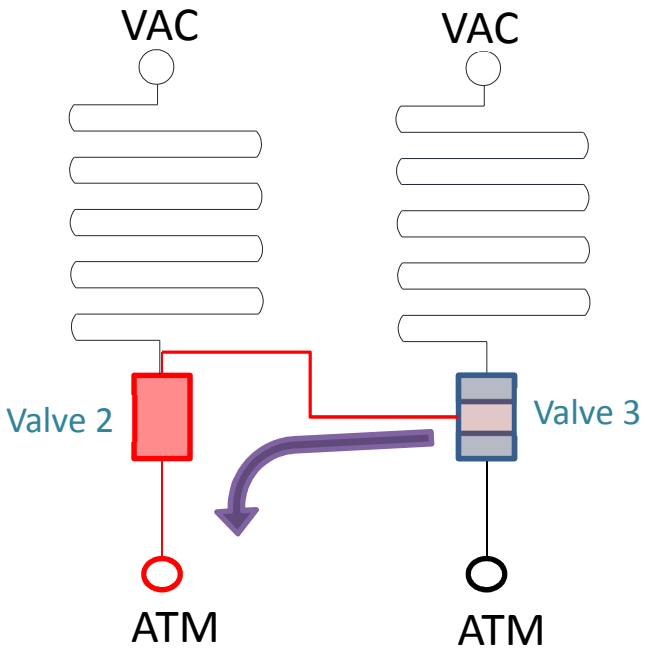

Figure 53: Open-to-closed transition of valve indicates path through the open valve of previous stage

Ring oscillator circuits constructed using the normally closed valve were manufactured using the CNC milling technique described in the next chapter. Working oscillator circuits using laser engraving are explained in Chapter 7.

6. CNC milling of pneumatic oscillators

Precision micromachining as a technique for prototyping microfluidic devices has been discussed in Chapter 1. Micromilling directly on plastic substrates has been studied[28] and optimal operation parameters such as spindle speed, feed rate, depth of cut and effect of coolant analyzed. Most of these setups consisted of specialized milling machines that cost above $10000 depending on the accuracy and resolution of the cuts required.

In the search for an inexpensive option, the Othermill V2 (Other Machine Co, Berkeley, CA) was evaluated for fabricating my designs.

6.1 Othermill CNC milling machine

The basic workflow for milling is to prepare a CAD file of the design and then use a computer-aided manufacturing (CAM) tool to generate the G-code file. G-code is a standard numerical control programming language which provides instructions to the machine controller. Otherplan is a proprietary open software of Other Machine Co. which allows the user to enter settings for the stock and observe the tool milling graphically as it occurs in real-time.

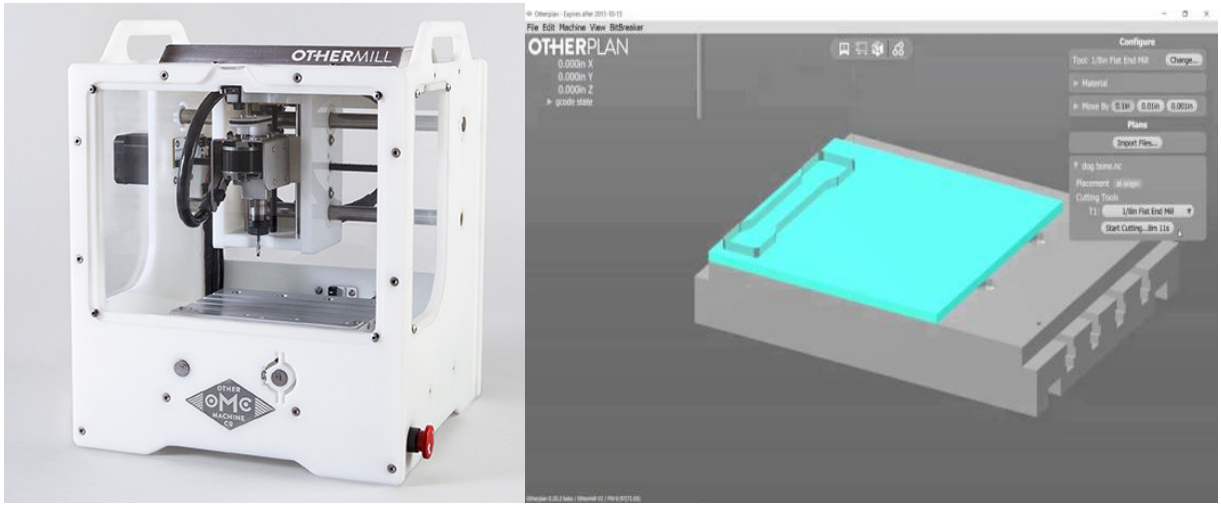

Figure 54: Othermill CNC milling machine (left) and the Otherplan software(right) used to control the milling flow and provide stock dimensions-ref. Othermill website

Table 9 lists the main features of Othermill. The smallest recommended end mill size is 254um, which is also the smallest size available from Othermill. Accordingly, I set a constraint of 260 um for the smallest channels in my designs. Technically, mills of size as low as 25um can be procured from other vendors and used with the Othermill but they are very susceptible to breakage. Additionally, the milling needs to be optimized for the machine as Other Machine Co. has not provided any basic settings as they have with other end mill sizes.

End mills of different types can be used with the Othermill. Flat end mills, used for cutting flat-sided 3D shapes and for detail work, were chosen for my oscillator design to maximize precision of cut channels. Recommended feed and speed settings for acrylic and HDPE plastic for 1/64”

and 1/100” sizes respectively are listed in Table 10 (1/100” settings were not available for acrylic). These are the two tools I needed for my design. The 1/100” end mill broke very easily with these settings necessitating fine-tuning of the values.

Table 9: Othermill V2 specifications

Feature	Value
Overall dimensions	**12.75x12x12.875in**
Working volume with spoilboard	**5.5x4.5x1.35in**
Spindle speed	**10500-16400 rpm**
Accuracy	**<0.003” per 6” linear travel**
Max resolution	**0.001 in 25 microns**
Smallest recommended end mill size	**0.25mm**

Table 10: Acrylic and HDPE feed and speed rates for 1/64” and 1/100” end mill sizes

Setting	Value for 1/64” flat end mill	Value for 1/100” flat end mill
Feed rate	**600-1500 mm/min**	**600-1500 mm/min**
Plunge rate	**40-381 mm/min**	**40-500 mm/min**
Spindle speed	**12000-16400 rpm**	**12000-16400 rpm**
Max pass depth	**0.02-0.25mm**	**0.08-0.13mm**

6.2 Procedure for milling a design using Othermill

The CAD design was prepared in Autodesk Inventor Professional 2017 and the file exported in step (Standard for the Exchange of Product) format. Autodesk Fusion 360 is a product development software wherein the CAD, CAM and CAE tools are available in a single platform. The step file is imported into Fusion and using the CAM menu, a setup for the toolpath is created.

2D pocket: 2D pocket is an option under the 2D menu that provides for generating a toolpath parallel to the selected geometry. This option was found to be adequate for the feature dimensions of my design, the pneumatic ring oscillator. The tool selection, geometry of cuts, heights, pass progression and linking of paths can be set for the toolpath as shown in Fig.66. Settings for the stock size and orientation need to be entered and the toolpath can then be generated for each end mill used in the design. The g-code file obtained is opened in Otherplan to commence the milling process.

Fixing the stock: It is important to fix the material to be milled firmly and as flat as possible to the bed of the Othermill in order to avoid any movement during the cutting and hence inaccuracies. Strips of double-sided tape are placed across the back side of the acrylic evenly such that there is no overlap. The stock is then pressed on the bed and the milling started.

Cutting different feature sizes: The g-codes for a design are run according to tool size. As an example, for my design, the 1/64” tool is inserted and the corresponding g-code executed. After the tool path is completed, the tool is removed and the 1/100” tool fixed in place. Its g-code is then executed.

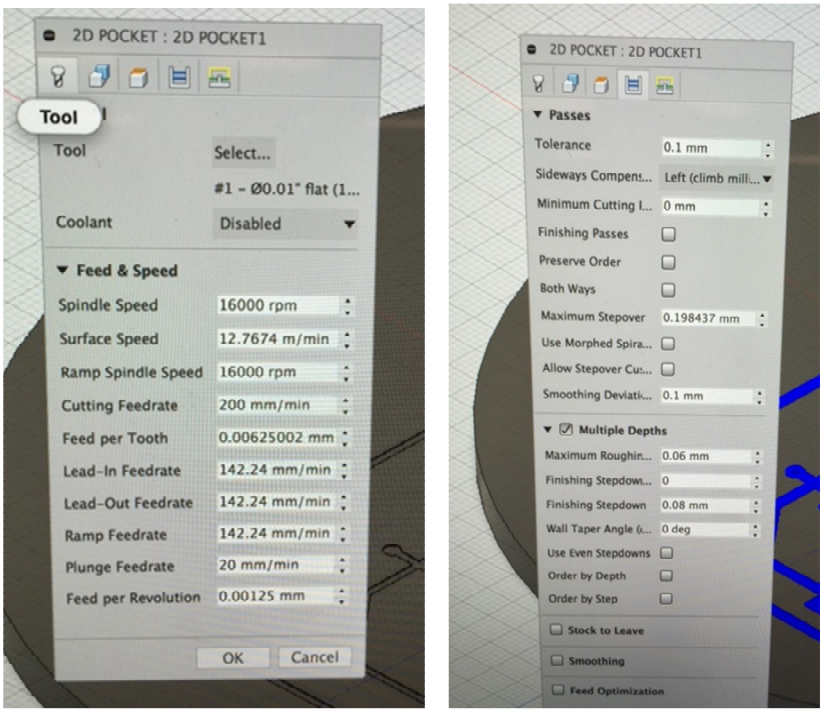

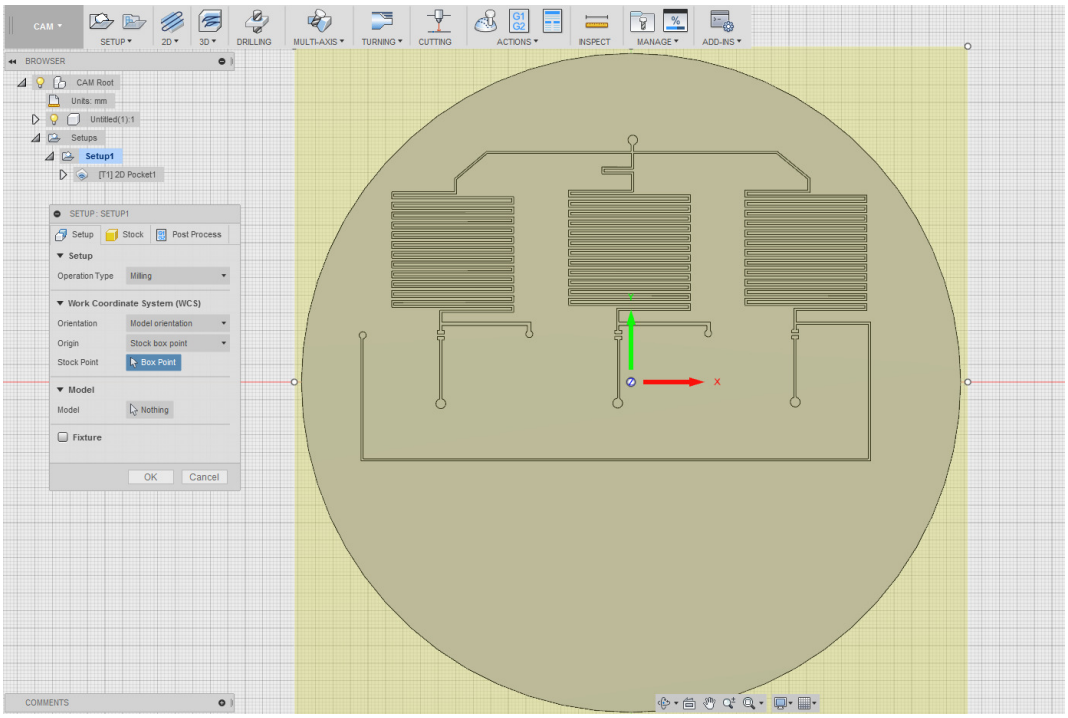

Figure 55: Fusion 360 CAM 2D pocket setup (top) and stock setup (bottom)

The pocket settings that produced minimal breakage of end mills and burrs at the edges of the milled channels are:

Spindle speed: 16500 rpm

Feed cutting rate: 142 mm/min

Plunge rate: 15-20 mm/min

Passes (stepdown): 0.08mm

6.3 Milling of Quake valve inverter based ring oscillator

The 3D designs of the flow and control layers of the Quake valve inverter based ring oscillator shown in Fig.56 were milled and the channels profiled. The dimensions of the milled features demonstrated close conformance to the designed values in some areas of the PMMA but deviated in other areas. Figure 57 shows that a 300um wide channel of designed depth 60um had a measured depth of 45um. The difference in heights between the resistor and outer channels are as small as 5um. Within a single channel, the roughness was approximately between 5-10um. The 500um wide channel design had channels of heights in the range 60-67um. The widths of the embossed channels in both cases were within 20um of the designed values.

Assembly: The flow layer was bonded to PDMS spun on Mylar(thickness ~50um) using the APTES procedure and then assembled with the control layer through one more step of bonding to create a device.

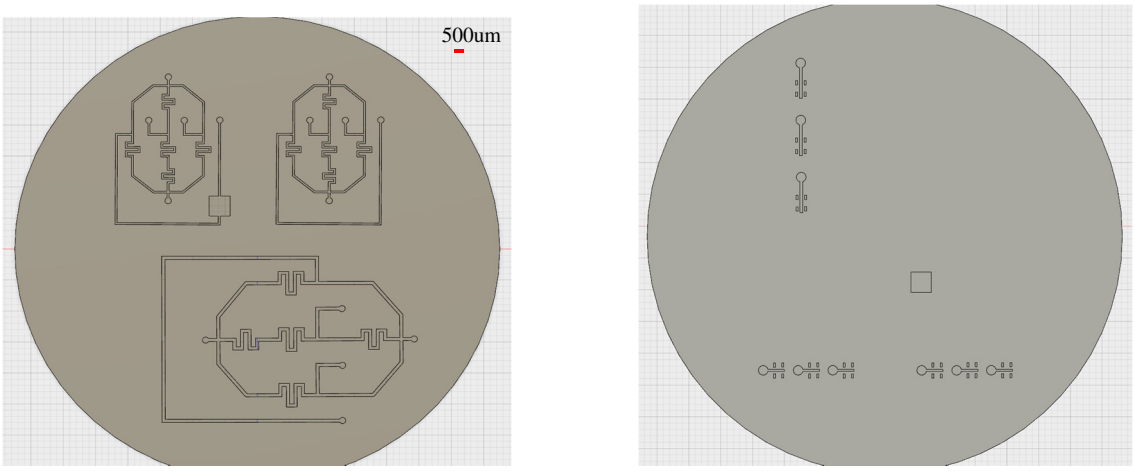

Figure 56: 3D CAD layout of oscillator flow layer (left) and control layer (right) for 300um width channel design and 500 um width channel design

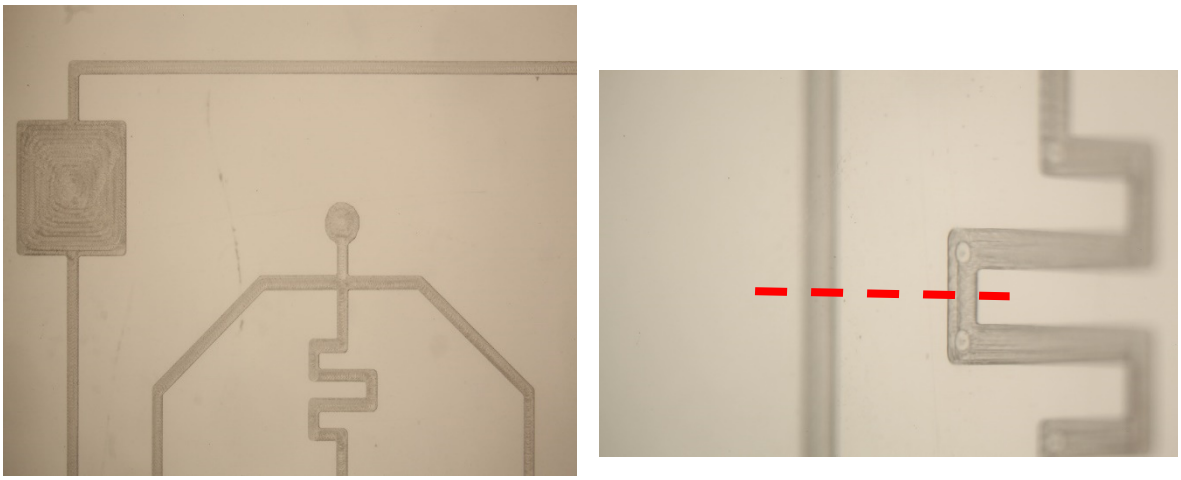

Figure 57: Milled 300um channel oscillator with capacitor in feedback circuit (top) along with height profile of resistor and outer channel (bottom).

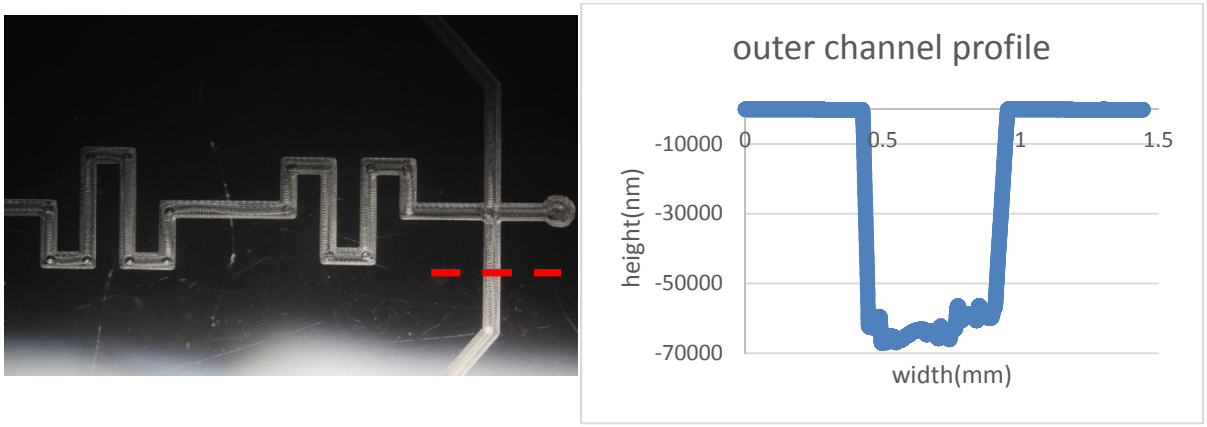

Figure 58: Milled 500um channel oscillator (left) along with height profile of outer channel (right).

6.4 Milling of normally closed valve based ring oscillator

The 3D design of the ring oscillator based on the normally closed valve was generated in Inventor as shown in Fig.59 with square-shaped valve flow channels and a pull-up resistor of length roughly 25 times higher than the pull-down resistor length. The valves were of total size 1mm(width)x1.4mm(length) with the seat 1mmx0.4mm and resistor channels were of width 300um. Resistor channel depth was set to 60-100um and valve depths were set to 60um. The 1/64" tool bit was used to mill the valve seats with the rest of the features milled using the 1/100" tool. As depicted in Fig.61, the dimensions of the milled valve depression compare to the designed dimensions with a resolution of 0.02mm in the x-y plane and 5um in the z-plane. The surface roughness is of the order of 3um.

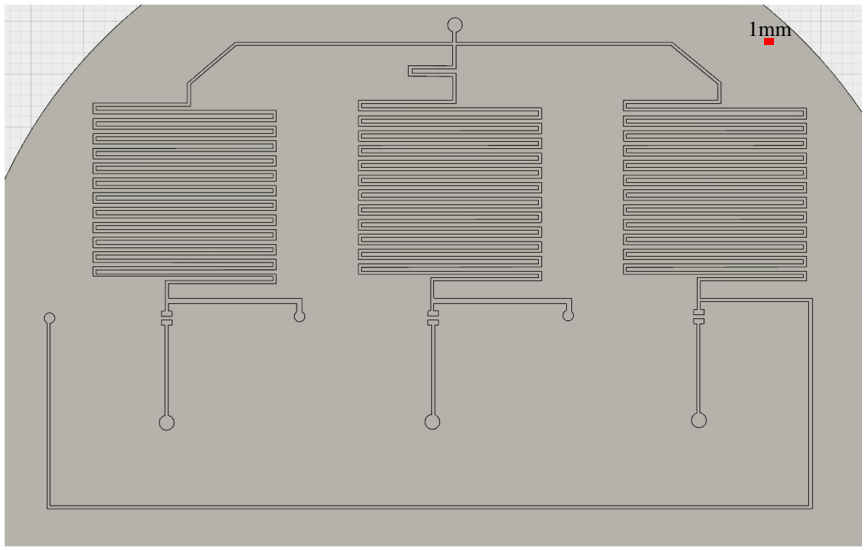

Figure 59: Inventor 3D diagram of 3-stage normally-closed valve based ring oscillator

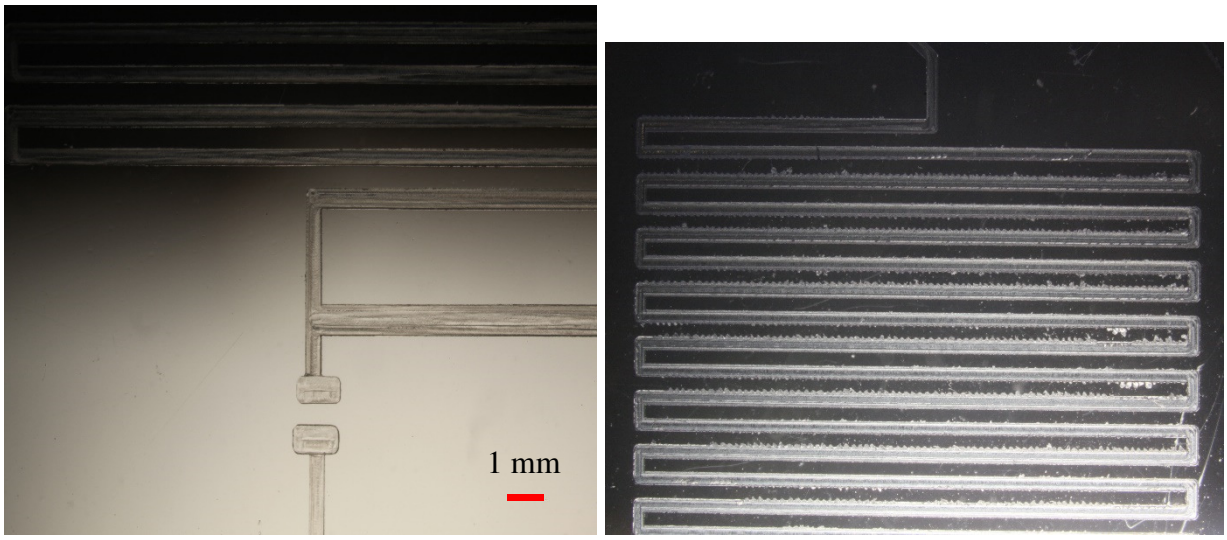

Figure 60: Milled valve chambers (left) and resistor network with burrs at edges of channels (right).

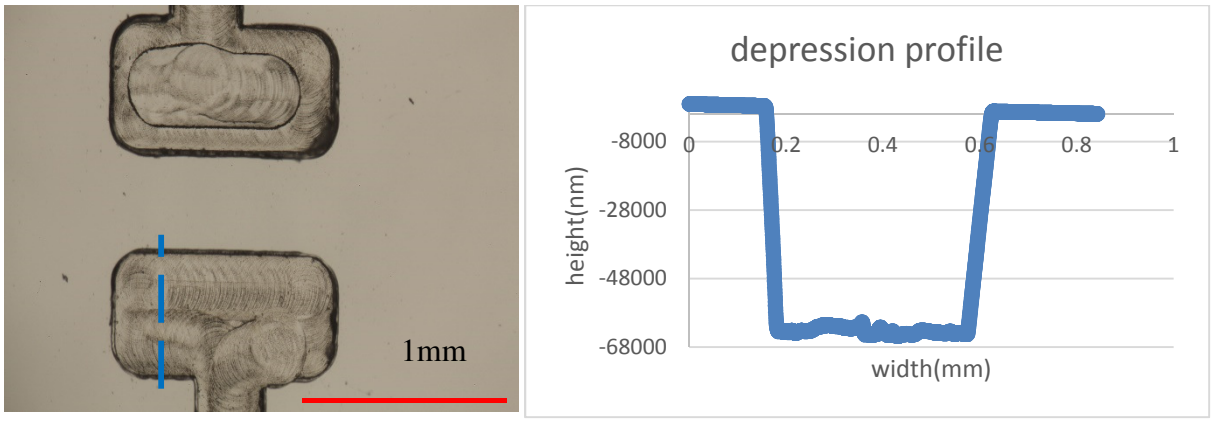

Figure 61: Milled square valve chamber (left) along with height profile (right).

Assembly: The flow layer was bonded to PDMS spun on Mylar (thickness ~250um) and then assembled with the control layer through one more step of bonding to create a device.

6.5 Surface roughness

In general, surface roughness decreases with decrease in feed rate and increase in spindle speed. Surface roughness measurements made with profilometer traces showed that the surface of the channels milled had roughness of the order of 3-10um across various samples.

Burrs can be seen on the edges of the channels (Fig.60). There are different approaches to reducing burrs and increasing the quality of the finish:

1. Climb down milling: The workpiece moves in the same direction as the rotating cutting teeth at the point of contact in comparison to conventional milling where it moves against the teeth. This option is not available in Othermill and hence could not be exercised.
2. Sharp tools: Sharp tools produce lower levels of friction than dull tools and keep material ductility and hence burr generation low. As a helpful guideline, it is important that the spindle speed not be too high or the feed rate too low. The feed rate was decided in my milling sessions after breakage of 3-5 1/100" tools after using higher feed rates. The maximum spindle rate used as suggested by Other Machine Co. produced a low surface roughness and hence was justified.
3. Avoiding tool exits: The toolpath should be adjusted to avoid exits. Although this option was chosen for my designs, it didn't affect burr generation.

6.6 Challenges in milling

Despite the several advantages of micromilling, there were many challenges in manufacturing good quality devices of suitable dimensions:

1. Bonding with PDMS membrane: The burrs on the edges of the channel inhibited the uniformity of the bonding. In particular, the area containing the resistors was completely affected with the membrane not attaching to any part of the PMMA substrate in the resistor network.

2. Smaller end mills: Smaller end mills used for smaller feature sizes (1/100”) had the drawback of being very susceptible to breakage and considerably increasing machining time (by an order of 3 times).
3. Accuracy of depths: Milling feature depths less than 100um is a low yield process with cell cast acrylic stock where the stock thickness can vary by 50-100um across an area of 3 inch x 3 inch. Normally, accurate control of surface planarity can be accomplished by planarizing the surface of the PMMA stock before machining. In addition, the end mill should preferably be aligned to the stock surface by performing a rigorous calibration process. This involves calculating the exact offset between the tool and the substrate and fine alignment by making multiple cuts and measuring the length of the cuts.

CNC milling is a technique capable of producing features of dimensions with a small error margin with respect to designed values. Although the surface roughness of the order of a few microns is acceptable for logic circuit devices, the burrs are an impediment to the bonding process with PDMS. Fine-tuning of the milling parameters such as spindle speed, feed rate, etc. help in developing a marginally better outcome. The maximum improvement is brought about by the use of smaller end mills but these are prone to breakage and also increase the time required to machine the material.

Due to the above described disadvantages, CNC milling was not experimented with any further to manufacture the oscillators. Laser engraving is explored in detail in the next chapter.

7. Manufacturing oscillator layers with laser engraving

Laser engraving was introduced as a technique to manufacture valve layers in PMMA in Chapter 2. In the next sections, the fabrication, assembly and characterization of the ring oscillator using laser engraving is discussed.

7.1 Fabrication with laser engraving

The oscillator flow and control layer line diagrams for laser engraving were designed in AutoCAD 2016 with some differences from the CNC milled design of the oscillator using normally closed valves:

1. Vias were reduced from three to one for the flow channel to control channel connections. The potential for introducing errors in punching the via holes on PDMS was thus minimized.
2. The pull-up resistor length was reduced by more than two times as observations of valve operation under the microscope for the previous design showed that the close-to-open transition of the valve was too slow.

The channel and valve flow/control chamber depths were designed for 60um and raster cuts were used to engrave the channels. Resistors were 250um in width and valve dimensions remained 1mm(W)x1.4mm(L).

Channel profiling: The features on the device layers were profiled using the Dektak profilometer. As all the cuts were raster, the channel bottom surfaces were rough with heights differing by as much as 30um for the valve chambers representing adjacent passes of the laser on the PMMA. The resistor channel roughness was a maximum of 42um leading to an average height of 54um (Fig. 62).

Assembly: The assembly was performed in three steps-

Step 1: A 254um thick PDMS membrane (Rogers HT-6240) was bonded to one PMMA piece (Astari-Niagara Acrycast) using the APTES process.
Step 2: Via holes were punched in the PDMS-PMMA piece in the vacuum line and feedback line.
Step3: The other PMMA device layer was bonded to this piece using the APTES process after visual alignment of the layers.

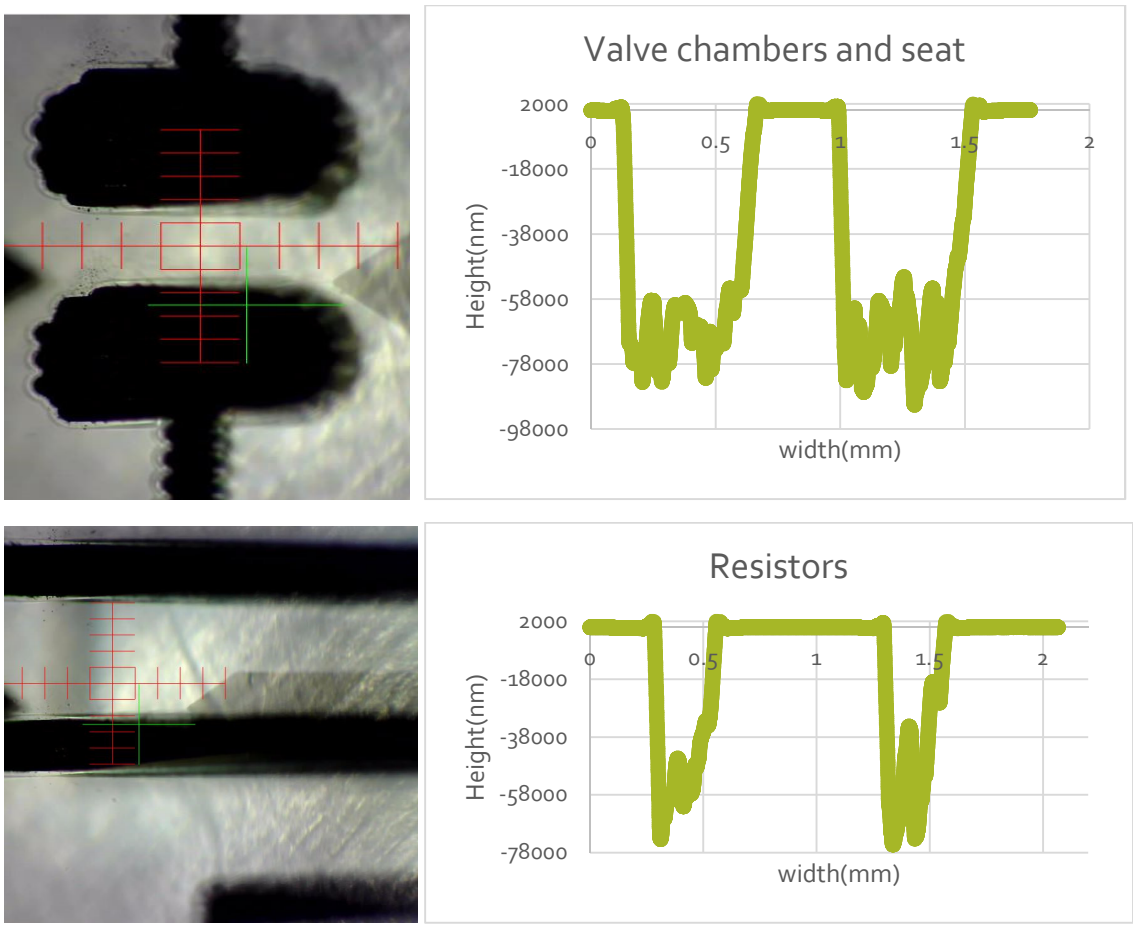

Figure 62: Valve chambers (top) and resistor network (bottom) along with their respective profiles.

7.2 Procedure for APTES treatment

The APTES treatment used for bonding the PDMS to the PMMA layers is the same as outlined before in Chapter 2 but some additional steps for the normally closed valves are required:

1. After cleaning the PMMA piece with IPA and DI water, the valve seats need to be excluded from the APTES treatment. Kapton tape applied over the valve area proved to be sufficient for this purpose.
2. After APTES treatment, the kapton tape is removed and the area that was covered by tape cleaned with a cotton-tipped applicator soaked in IPA.

Figure 63 illustrates the step-by-step process for PMMA-PDMS bonding. In the clamping step, the PMMA and PDMS are placed in conformal contact and sandwiched between two square aluminum plates of thickness 5mm. The plates were used to maximize the uniformity of pressure distribution. Three inch (Kant Twist) clamps were then tightened around the plates (number of clamps depending on device area) and then the clamped structure placed in the oven at 70°C. After a minimum of two hours, the clamped

structure can be taken out of the oven and allowed to cool for 20 minutes. The clamps are removed and the finished device extracted.

Step 1: Apply kapton tape to cleaned PMMA valve seats

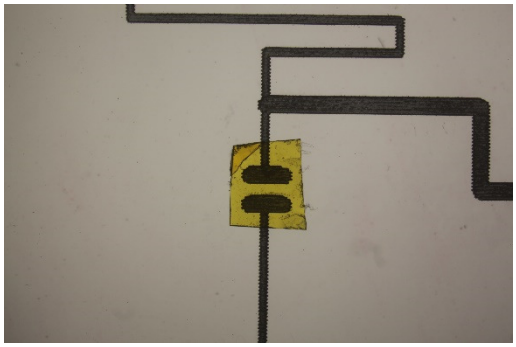

Step 2: PMMA Surface Modification

Step 3: PMMA surface treatment with 3-APTES heated to 85°C

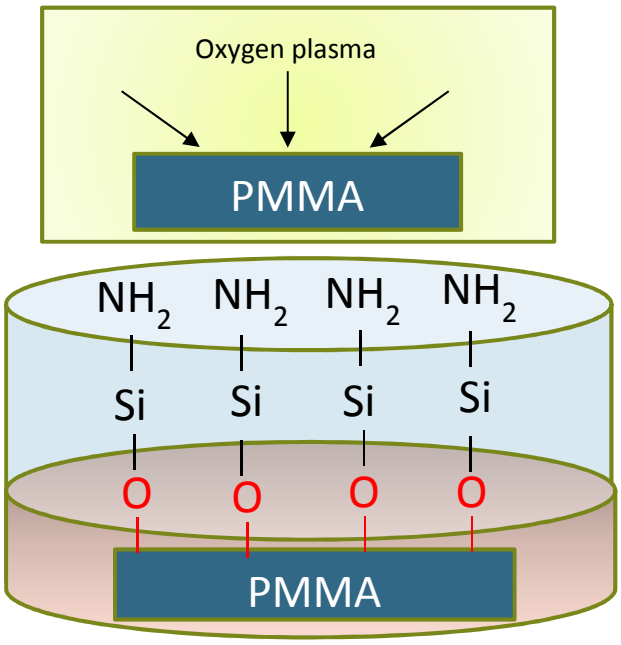

Step 4: Rinse with water

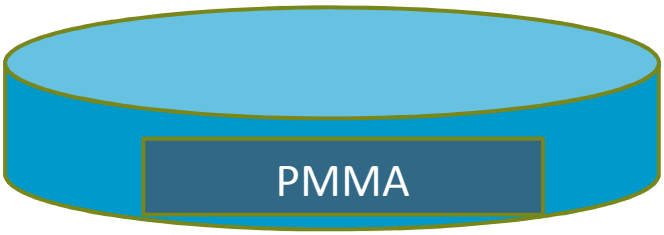

Step 5: After drying with N2 gun, remove kapton tape

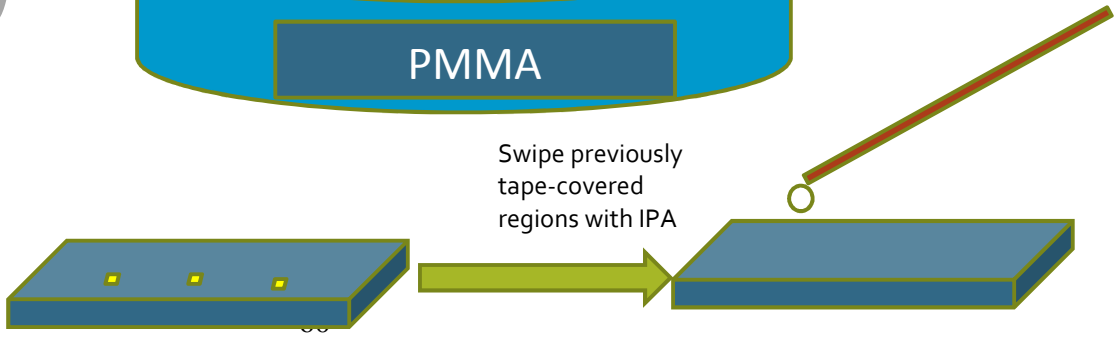

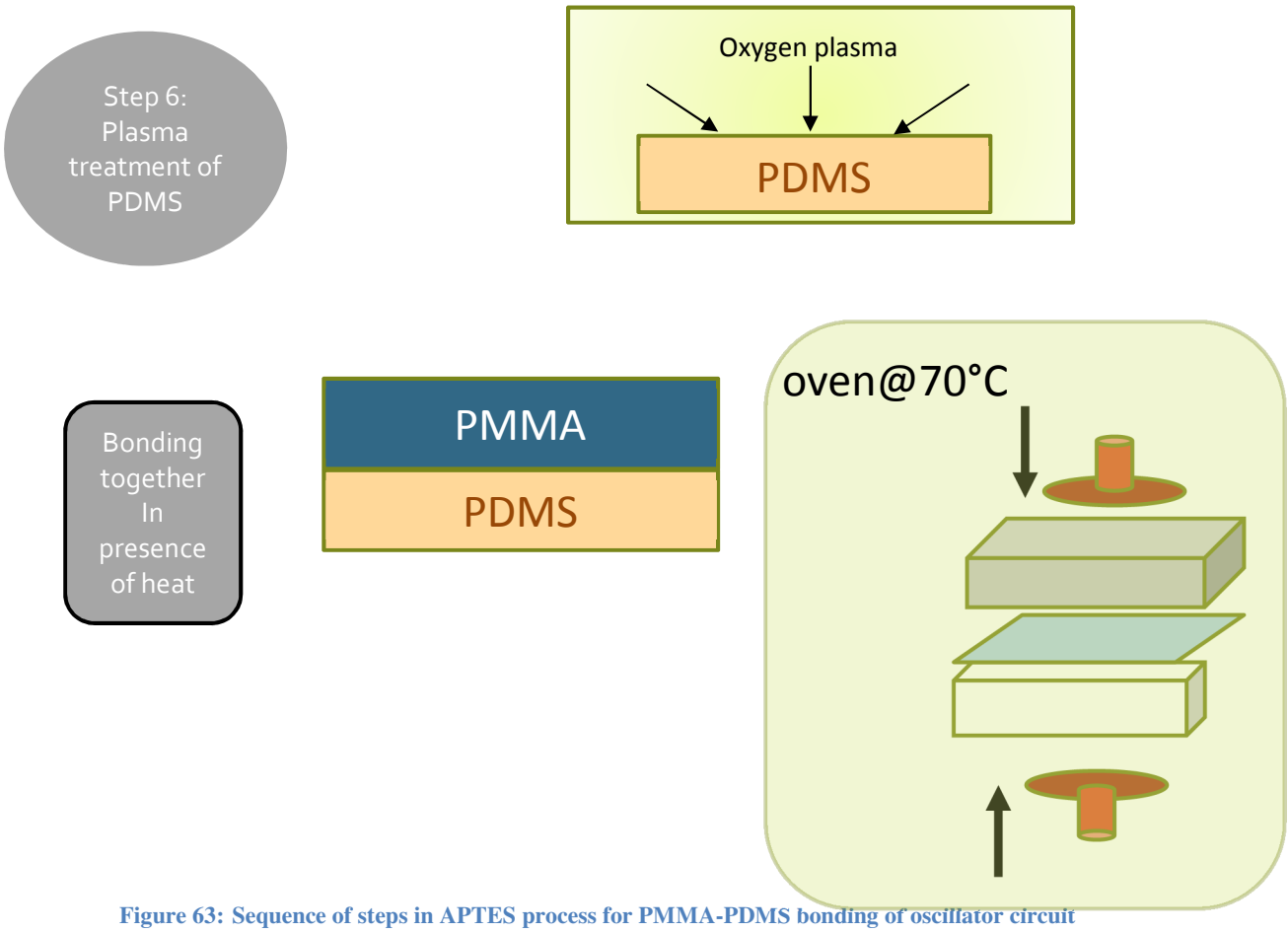

Figure 63: Sequence of steps in APTES process for PMMA-PDMS bonding of oscillator circuit

Figure 64 shows a complete ring oscillator device. For the vacuum inlet on the device, silicone tubes (Cole Parmer, 1.14mm inner diameter) bonded to PDMS were used. These were attached to the vacuum inlet using a silicon-silicone adhesive (Adhesive Applications, Inc. S1001-1DC11) tape to carry out testing and analysis of the device operation.

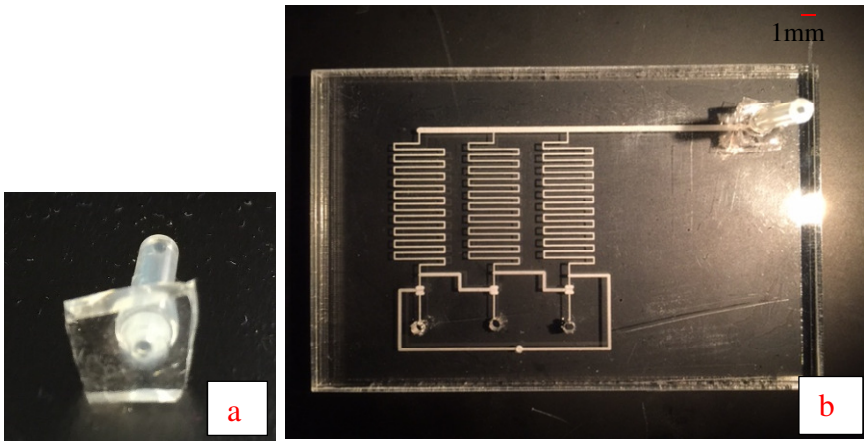

Figure 64: Inlet tubes(a) and (b) Ring oscillator cut on 1/8"thick PMMA with a laser setting of Speed 40,Power 18 for channel depths of 60um

7.3 Analysis of oscillator performance

The oscillator frequency characteristics were analyzed both with vacuum magnitude variation and a syringe as a source. By clamping a syringe and studying the frequency change with time, a measure of device utility for portable applications can be determined.

For frequency measurements, a movie of the valve oscillations (top view) was taken with a Canon EOS 5D Mark II camera (30 fps) under a microscope (Nikon SMZ1500) and split into frames using VLC media player (ver. 2.1.5). The frames were analyzed for periodicity as follows:

1. The frames were opened in ImageJ software and local contrast option applied to enhance the contour of the membrane as seen from the top of the valve.
2. Valve seat width is a known value and is set as a scale for ImageJ measurements.
3. At a fixed location from the edge of the valve seat in the x direction (marked 'd' in Fig. 65), the distance between the contour of the membrane position and one side of the valve seat is measured as indicated with the red line.
4. The measurement of step 3 is performed for subsequent frames until a repetition of distance values is observed.
5. The difference between the frame numbers having the closest distance values provides the time period and hence frequency.

   As Fig. 65 illustrates, the time period of that particular device oscillation is 6/30 (0.2) seconds corresponding to a frequency of 5 Hz.

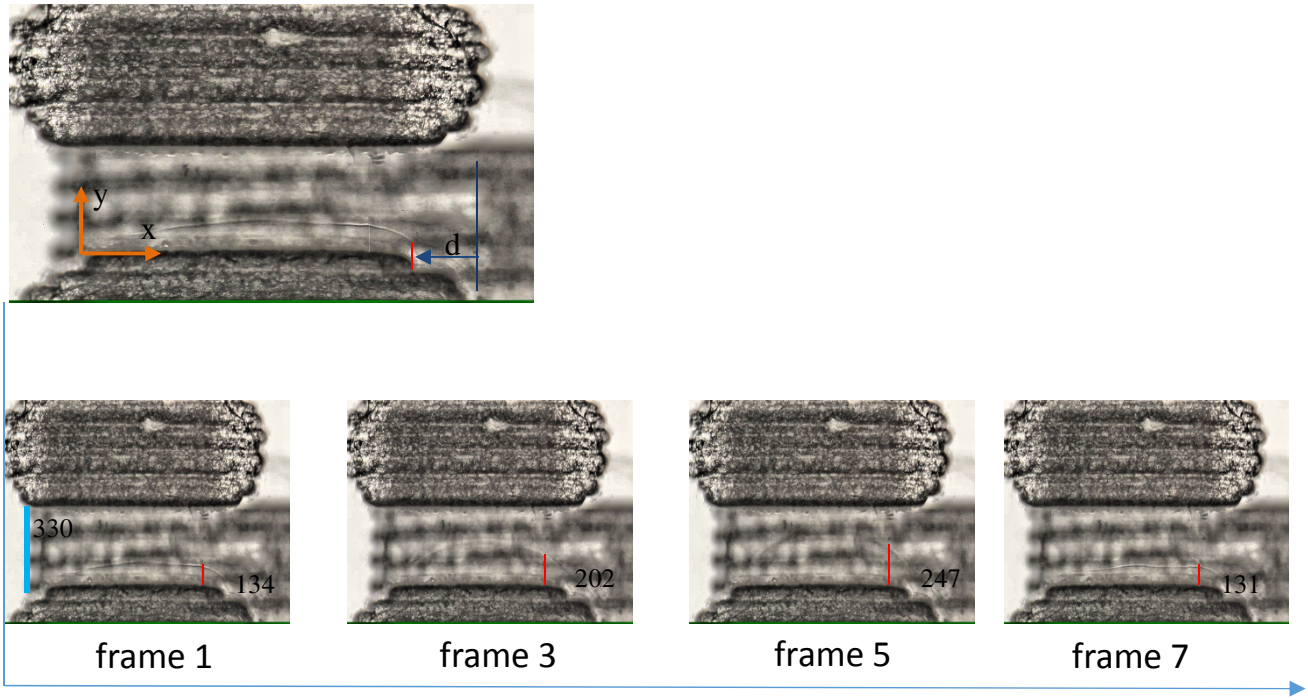

Figure 65: Frames 7 and 1 have the closest distance values and indicate that the membrane positions are the same. Between frame 1 and 7, the membrane contour against the PMMA top layer shows a rising pattern and then falls off at frame 7 to the same position as in frame 1.

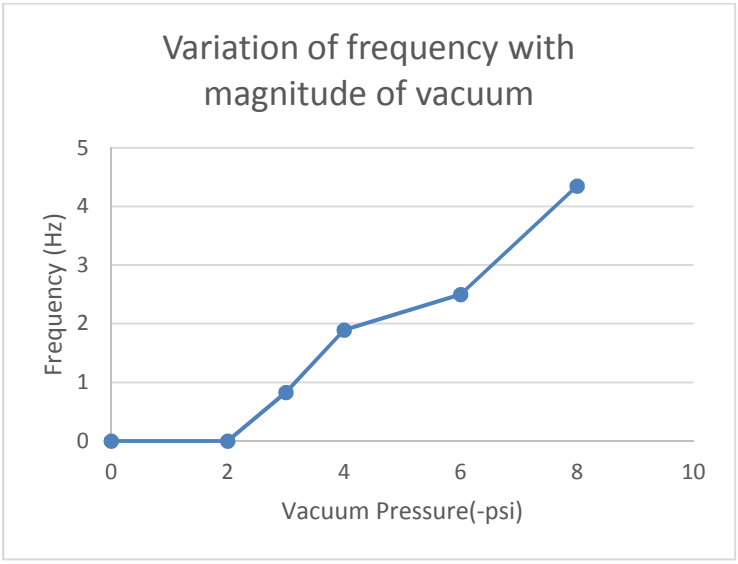

Figure 66: Elveflow pressure controller (left) for applying constant vacuum supply and (right) frequency of oscillations varying with magnitude of vacuum applied

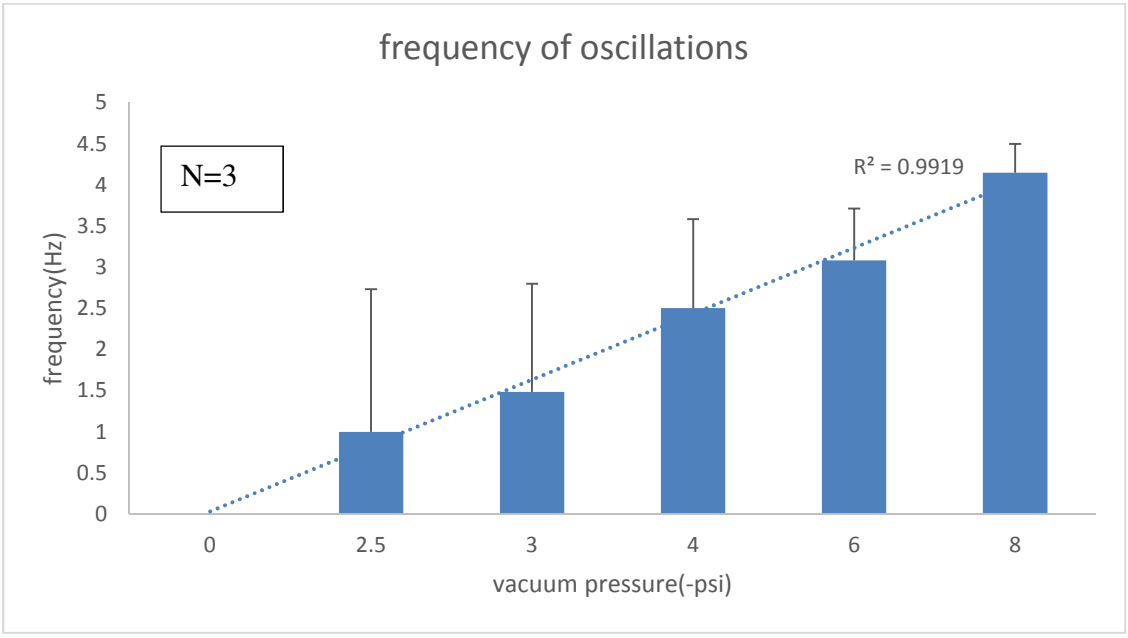

Figure 67: Frequency of oscillations varying with magnitude of constant vacuum pressure applied for N=3 devices. A linear increase of frequency is observed.

Figure 67 illustrates a linear increase of frequency with vacuum magnitude. A maximum variation of frequency across devices at lower pressures of -3 and -2.5 psi has been observed. The lowest variation occurs at the highest vacuum pressure applied, -8 psi.

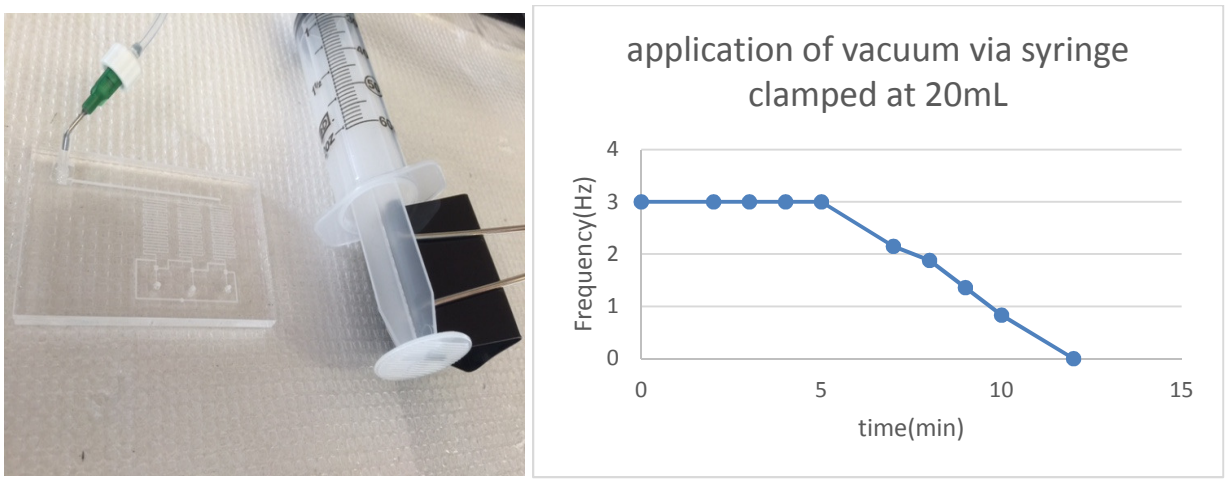

Figure 68: Pulled 60mL syringe clamped at a position (left) for applying vacuum and (right) change of frequency with time

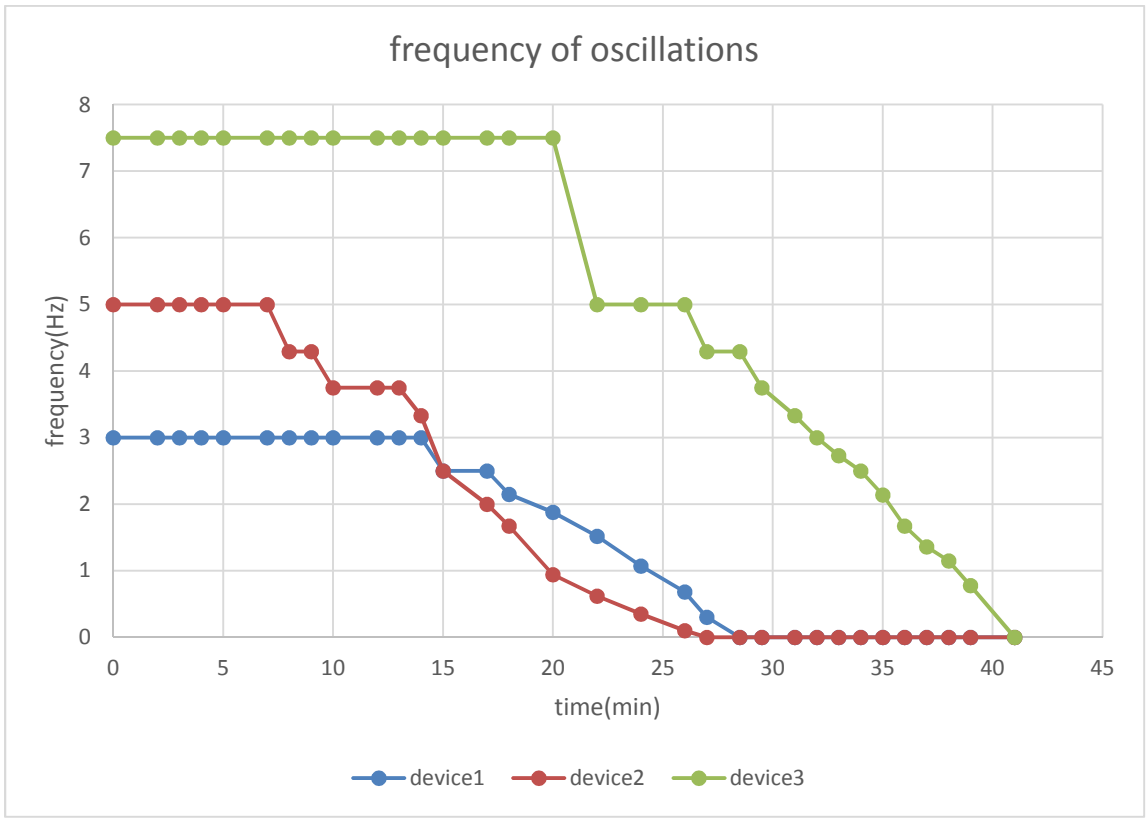

Figure 69: Change of frequency with time for three devices powered by a 60mL syringe clamped to 80% of its volume

As the results show, the average frequency of oscillations is 4.15 Hz at -8 psi of pressure and oscillations cease to be generated below -2 psi. The frequency decreases linearly with applied vacuum. Application of vacuum by means of a pulled syringe clamped at different positions generated oscillations that can be sustained for an average of 13 minutes at an average frequency of 5 Hz. After the initial stable frequency period, as the syringe fills with air (due to the valve

sucking in air from the atmosphere), the frequency decreases until the oscillations cease completely. To test the frequency shift of oscillations over time, a constant vacuum pressure was applied over a period of a few hours with frequency measured at one hour intervals. As Fig.70 illustrates, after 2 hours, the frequency of oscillations increases by 0.75 Hz and remains at that value till 5 hours. This is to be expected due to the change in adhesion of the PDMS membrane to the valve seat over time. The resulting lowering of the threshold pressure for opening the valve results in higher frequencies of oscillations.

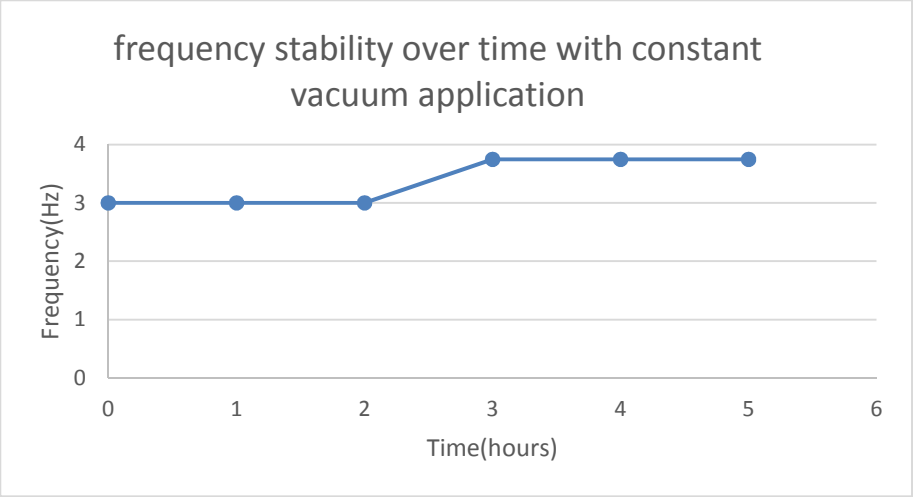

Figure 70: Frequency stability over a period of 5 hours with a constant vacuum applied through Elveflow apparatus

7.4 Oscillator-driven circuits

A circuit was designed wherein the ring oscillator stages were used to drive three valves in series as shown in Fig.71. The two PMMA layers were fabricated by laser engraving, bonded with PDMS and assembled using the same method.

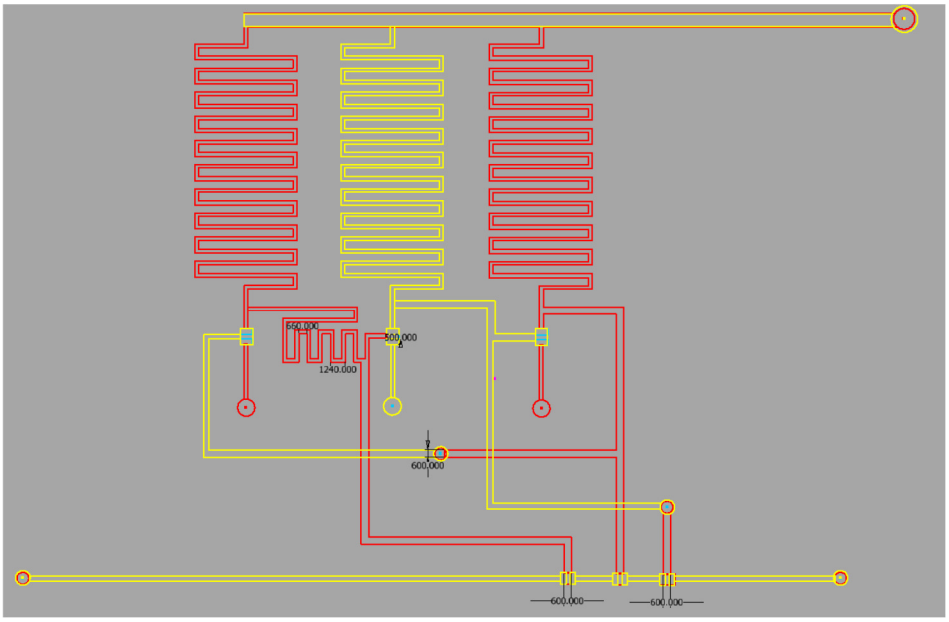

Figure 71: Oscillator driving out-of-phase three valves in series

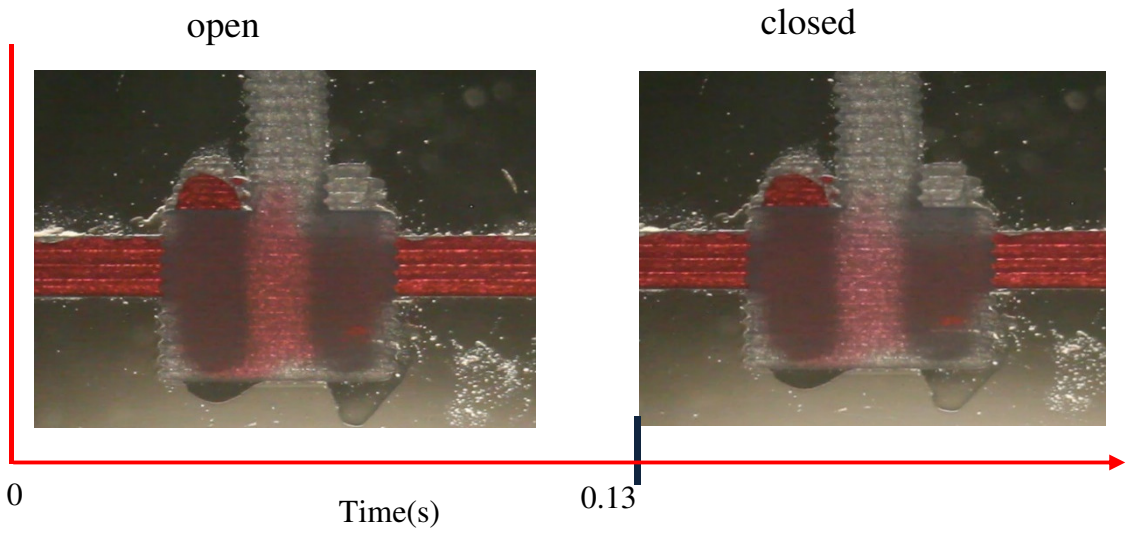

Figure 72: Open and closed states of the valve with red-dyed DI water flowing through the flow channel

Figure 72 shows the center driven valve with red-dyed DI water flowing through it. The frequency of oscillations for the valve was 5 Hz and remained stable at this value for a duration of 5 hours.

7.5 Conclusions

The fabricated oscillator circuit has demonstrated both long-term stability of frequency and robustness of operation. A syringe is sufficient to drive the oscillator for a considerable period of time which demonstrates the applicability in portable microfluidic devices.

Manufacturing the device layers with laser engraving is an efficient approach in terms of time and setup as it takes approximately 10-20 minutes to complete the cutting process. No additional adjustments or calibration is required as in CNC milling or hot embossing and uniformity of features across pieces is an advantage for large-scale manufacturing.

The oscillator can be used to drive additional circuits as illustrated through the out-of-phase three-valve device and hence can be a component of self-driven control logic for fluidic devices.

8. Future Research Work

8.1 Introduction

Plastic microfluidic logic circuits can be manufactured using a variety of manufacturing techniques as we have seen. The first part of this research focused on commonly used methods such as hot embossing and CNC milling for creating pneumatic valves and oscillators with PMMA. Hot embossing, although suitable for small-area devices such as single valves, proved non-viable for larger areas (oscillators) with the setup used due to non-repeatability of pattern reproduction and hence low throughput. CNC milling produced features that had low surface roughness but burrs generated on the edges of channels proved to be a hindrance to bonding with PDMS membranes.

The second part of the research discussed the design and manufacturing of ring oscillators with the laser engraving technique. In addition to characterizing the oscillators for frequency and stability with time, oscillator-driven circuits were also demonstrated. The suitability of the devices for portable applications were proven by the results of the syringe experiments.

The next sections discuss the future path for improvements and building complex devices.

8.2 Adhesive-tape based bonding of PDMS to PMMA

The bonding of PDMS to PMMA via APTES treatment of PMMA is a process that has proven reliable. However, there are a number of steps in addition to time required to carry out the procedure. Each valve seat has to be masked with tape before the treatment. For circuits with a large number of valves, this is a time-consuming procedure. Sticking of the PDMS to the valve seat despite masking is another problem that has been observed in assembling devices. Using an adhesive tape to stick the PDMS to the PMMA could reduce both time and probability of unintended sticking in areas.

8.3 Thinner PDMS membranes

The membrane thicknesses in the oscillator devices were 254um. Although this particular thickness is more readily available and hence preferable for ease of fabrication, thinner membranes can produce higher frequency of oscillations, thereby expanding the application areas for the device. Figure 73 shows an oscillator attempted with a PDMS membrane 125um thick (Interstate Specialty Products). Bonding was a challenge in obtaining functioning devices as the PDMS did not bond consistently across the area containing features. A heat press to apply uniform pressure could produce successful devices. This needs to be explored further.

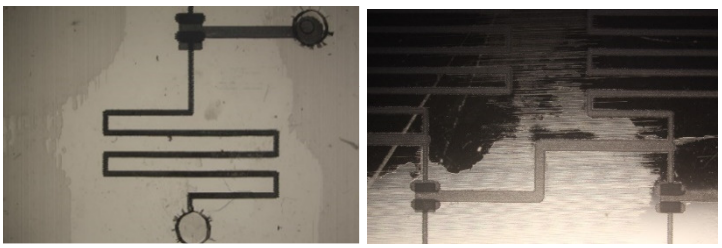

Figure 73: Oscillator assembled with 125um membrane shows gaps where bonding did not occur between PDMS and PMMA

8.4 Complex logic circuits with smaller valves and higher density of features

Valves used in the oscillator designs were of dimension 1mmx1.4mm. By designing smaller valves and placing the resistor channels closer together, complex, compact devices can be produced. Higher frequency of oscillations can also be attained in this manner, allowing it to be used for applications where fast switching of fluids are required. An example of control logic implemented to switch between analytes/reagents for an assay is illustrated in Fig.74. By encompassing the entire functionality and processes within a small area, a portable lab-on-a chip can thus be realized.

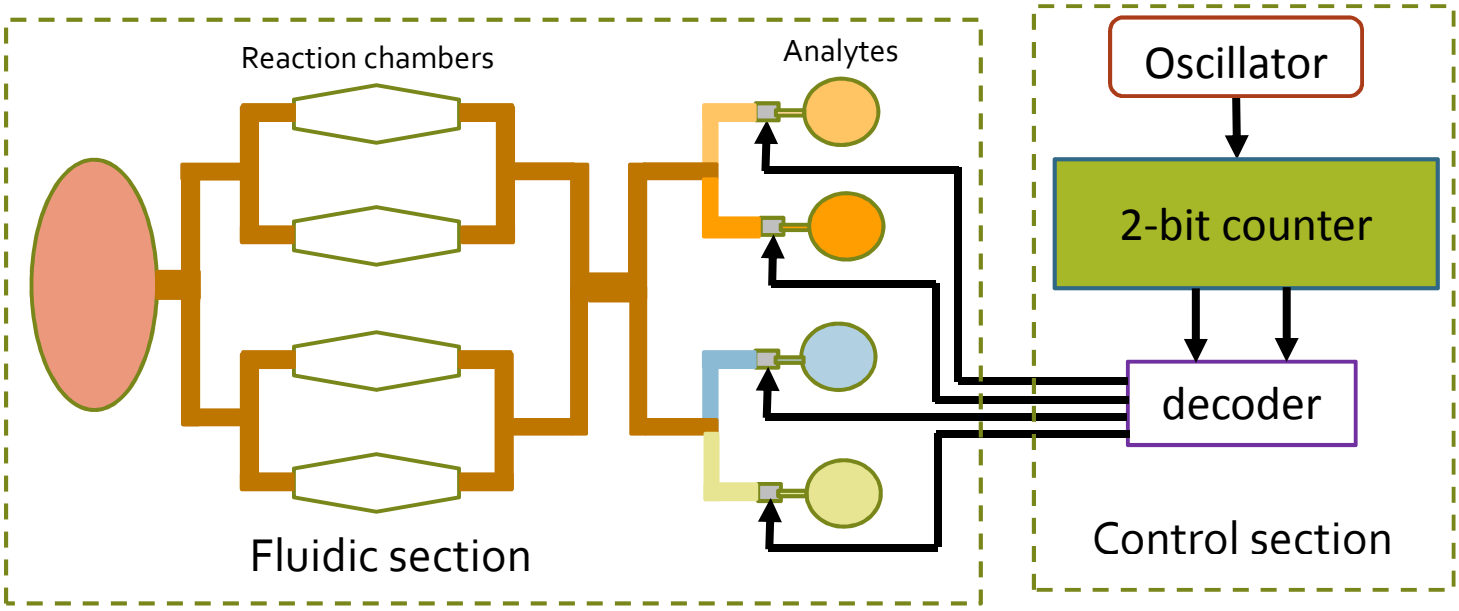

Figure 74: Schematic of an assay with fluidic section and control section on a single chip.

References

1. Bharat Bhushan, *Handbook of Nanotechnology* **3rd edition**, Springer
2. Erik C. Jenson, William H. Grover, and Richard A. Mathies, *J. Microelectromech*, **2007**, Vo. 16,No.6, 1380
3. D.J. Lipomi, R.V. Martinez,L. Cademartiri,G.M. Whitesides, *Polymer Science: A Comprehensive Reference*,**7**, 212-214
4. Adriana San-Miguel,Hang Lu, *Microfluidics as a tool for C. elegans research*, **2013**
5. M. Worgull et al, *Microsyst Technol 14*, **2008,** 767-773
6. H. Becker,U. Heim, *Sensors and Actuators*, Vol 83, **2000,** 130-135
7. P.F.O'Neill et al.,*Biomicrofluidics,***2014,**052112-3
8. Bethany C. Gross,Jayda L. Erkal,Sarah Y. Lockwood, et al, *Anal. Chem.*, **2014**, 86, 3240–3253.
9. Toshimitsu Kanai,et al. *Chem.Eng. J.*, **2016**, 290, 400-404.
10. Wonjae Lee,Donghoon KwonWoong Choi,Gyoo Yeol Jung,Anthony K. Au, Albert Folch & Sangmin Jeon, *Sci. Reports*, **2015**, 5, 7717.
11. Can Yang,Xiao-Hong Yin and Guang-Ming Cheng, *J. Micromech. Microeng.*, **2013**, 23,093001.
12. David J. Guckenberger et al, *Lab on a Chip*, **2015**, 15, 2364.
13. Milena Koleva, *Technical University of Gabrovo*
14. Wenhua Zhang,et al., *Lab on a Chip*, **2009**, 9,3088-3094
15. Yolanda H. Tennico,Myra T. Koesdjojo,Saki Kondo,David T. Mandrell,Vincent T. Remcho, *Sensors and Actuators*, **2010**,799-804.
16. Hsih Yin Tan et al., *Sensors and Actuators*, **2010,**151,133-139.
17. Kangil Kim,Sin Wook Park and Sang Sik Yang, *BioChip J.*, **2010**, 4(2), 148-154.
18. Linzhi Tang and Nae Yoon Lee, *Lab on a Chip*, **2010**, 10, 1274–1280.
19. Xiuhua Sun et al., *J Chromatogr A.,***2007,**1162(2),162-166
20. Mazher I. Mohammed et al., *J. Micromech. Microeng*, 2016, 27, 015021.
21. Alireza Shamsi et al, *Microsyst Technol*, 2014, 20,1925-1931
22. A. Mathur et al, *Current Appl. Physics*, 2009, 9, 1199–1202.
23. *Lab on a Chip*, **2012:** http://www.rsc.org/suppdata/lc/c2/c2lc40699c/c2lc40699c.pdf
24. Henrik Bruus, *Microscale Acoustofluidics*, **2014**,1-28.
25. William H. Grover et al., *Lab on a Chip*, **2006,**6,623-631.
26. James A. Weaver et al, *Nature Physics,* **2010,**6,218-223.
27. Philip N. Duncan, Transon V. Nguyen and Elliot E. Hui, *PNAS*, **2013,**110,18104-18109.
28. Pin-Chuan Chen et al., *Int J Adv Manuf Tech*, **2014,**1623-1630.